

CHARACTERIZATION OF MONO, BINARY, AND TERNARY SPHERE PACKING

A Thesis

Submitted to the College of Engineering
Of Nahrain University in Partial Fulfillment
of the Requirements for the Degree of
Master of Science
in
Chemical Engineering

by

HANAA RIYADH SALAH

(B.Sc. in Chemical Engineering 2004)

Jamadi el-thani

1427

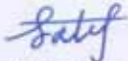
June

2007

Certification

I certify that this thesis entitled "**Characterization of mono, binary, and ternary sphere packing**", was prepared by **Hanaa Riyadh Salah**, under my supervision at Nahrain University/College of Engineering in partial fulfillment of the requirements for the degree of Master of Science in Chemical Engineering.

Signature:



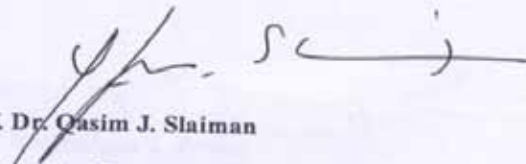
Name:

Dr. Mohammed N. Latif
(Supervisor)

Date:

1 / 7 / 2007

Signature:



Name:

Prof. Dr. Qasim J. Slaiman
(Head of Department)

Date:

1 / 7 / 2007

Certificate

We certify, as an examining committee. That we have read the thesis entitled "Characterization of mono, binary, and ternary sphere packing", examined the student **Hanaa Riyadh Salah** in its content and found it meets the standard of thesis for the degree of Master of Science in Chemical Engineering.

Signature:

Name: **Dr. Mohammed N. Latif**
(Supervisor)

Date: 10 / 17 / 2007

Signature:

Name: **Dr. Basim O. Hasan**
(Member)

Date: 10 / 17 / 2007

Signature:

Name: **Dr. Maha R. Abdul-Amir**
(Member)

Date: 16 / 17 / 2007

Signature:

Name: **Prof. Dr. Mahmoud Omar Adullah**
(Chairman)

Date: 11 / 17 / 2007

Approval of the College of Engineering

Signature:

Name: **Prof. Dr. Muhsin J. Jweeg**
(Acting Dean)

Date: 23 / 17 / 2007

Abstract

This work presents the study of single phase fluid flow through a packed bed, where two type of fluids were used (air and water). Spherical glass particles were used as solid phase, the glass spheres were 0.9987, 0.7955, 0.6015, 0.509, 0.4210 cm in diameter.

The bed was 7.64 cm in diameter and 15.15 cm in length. Many variables were studied in this packed bed. These variables included the packing porosity of bed (mono, binary, and ternary), type of fluid flow (water and air) and flow rate of fluid which were represented by Reynolds number, in order to study the effect of these variables on the pressure drop and friction factor.

The range of Reynolds number used in this work for air flow through packed bed is 8.5- 707 and for water is 43-1467.

Results showed that the pressure drop through the packed bed is highly sensitive to the packing porosity and inversely proportional to it, at maximum porosity (0.4508) the values of pressure drop range 6.1-25.8 Pa for air and 205.6-13900.7 Pa for water are less than those at minimum porosity (0.3766), the pressure drop range value 15.5-596.6 Pa for air and 546-35815.6 Pa for water.

The friction factor for binary size particles is less than those for mono size particles for the approximately near values of porosity, because the surface area of binary size particles is less than it for mono size particles, as the surface area increases the values of Reynolds number decreases which lead to increases the values of friction factor.

At high flow rate (turbulent region) the friction factor-Reynolds number curves is approximately straight (at turbulent region the Reynolds number have insignificant effect on friction factor values).

Also it was found that the friction factor increases with decreasing Reynolds number.

The friction factor was expressed as a function of Reynolds number. It was found that the general equation, which governs the mono, binary and ternary is:

A. for air flow through packed bed.

$$\frac{R_1}{\rho u_1^2} = 3.21 \text{Re}^{-1} + 0.65 \text{Re}^{-0.1}$$

with a correlation coefficient of 0.9172 and a percentage of average of error 5.3964%.

B. for water flow through packed bed.

$$\frac{R_1}{\rho u_1^2} = 4.97 \text{Re}^{-1} + 0.57 \text{Re}^{-0.1}$$

with a correlation coefficient of 0.8286 and a percentage of average of error 6.7618%.

List of Contents

Contents	Page
Abstract	I
List of Contents	III
Notations	VII
List of Tables	IX
List of Figures	XI
Chapter One : Introduction	
1.1 Introduction	1
Chapter Two : Literature survey	
2.1 The flow of fluid through porous media	3
2.2 Packing	4
2.3 Packed column	6
2.4 Packed Bed	7
2.5 Variables affecting flow through granular bed	8
2.5.1 The size and shape of the particles	8
2.5.2 The walls effects	10
2.5.3 The porosity of the bed	12
2.5.4 The surface roughness of the particles	14
2.5.5 The orientation of the particles	14
2.6 Prediction of voidage distribution	15

2.7 Velocity measurement	16
2.8 Specific surface	17
2.9 Friction factor	18
2.10 The surface roughness effect on friction factor	21
2.11 Pressure drop through packed bed	22
2.12 The relation between depth of bed and pressure drop	24
2.13 Theory	25
2.14 Fluid flow through randomly packed columns	27

Chapter Three : Experimental Work

3.1 Aim of the work	34
3.2 Description of materials	34
3.3 Description of apparatus used for packed bed	35
3.3.1 For air flow through packed bed	35
3.3.2 For air flow through packed bed	36
3.4 Experimental procedure	36
3.4.1 Air flow	36
3.4.1 Water flow	37
3.5 Test method	37
3.5.1 True particle density	37
3.5.2 Bulk density	39
3.5.3 Bed porosity	39

Chapter Four : Results

4.1 Packing of mono sizes particles	44
4.1.1 Air flow	44
4.1.2 Water flow	45
2.2 Packing of binary size particles	46
2.2.1 Air flow	47
4.2.2 Water flow	49
4.3 Packing of ternary size particles	51
4.3.1 Air flow	51
4.3.2 Water flow	53

Chapter Five : Discussion

5.1 Packing of mono size particles	56
5.1.1 Air flow	56
5.1.2 Water flow	60
5.2 Packing of binary size particles	64
5.2.1 Air flow	64
5.2.2 Water flow	70
5.3 Packing of ternary size particles	76
5.3.1 Air flow	76
5.3.2 Water flow	82

Chapter Six : Conclusions and Recommendations

6.1 Conclusions	89
6.2 Recommendations for future work	90
References	91
Appendices	

Notations

Symbols	Notations
A	= The bed cross-sectional area (m^2)
a	= Representation of packing and fluid characteristics at laminar flow
b	= Representation of packing and fluid characteristics at turbulent flow
D	= Diameter of cylinder (m)
d_m	= Equivalent diameter of the pore channels (m)
d_p	= Diameter of the particle (m)
d_{pav}	= Average particles size (m)
D_p	= Diameter of equivalent volume sphere (m)
d_t	= Diameter of tube (m)
f	= Modified friction factor
f_w	= Correlation factor
k'	= Dimensionless constant whose value depends on the structure of the bed
k''	= Carman Kozeny constant
L	= The height of packing in the bed (m)
L'	= Length of channel (m)
Δp	= Pressure drop through packed bed ($\text{kg}/\text{m}\cdot\text{s}^2$)
Q	= Flow rate (m^3/hr)
q	= Number of components in the mixture

$\frac{R_1}{\rho u_1^2}$	=	Modified friction factor
Re_1	=	Modified Reynolds number
S	=	Specific surface area of the particles (m^2/m^3)
S_B	=	Specific surface area of the bed (m^2/m^3)
S_c	=	Surface of the container per unit volume of bed (m^2/m^3)
u	=	Superficial velocity (m/s)
u_1	=	Average velocity through the pore channels (m/s).
X_i	=	Proportion of the component i in the mixture

Greek Symbols

ε	=	Porosity
ρ_b	=	Bulk density (g/cm^3)
ρ_t	=	True density (g/cm^3)
ρ_{tm}	=	True density of mixture (g/cm^3)
ρ_{ii}	=	True density of component i
ρ	=	Density of fluid (kg/m^3)
μ	=	Fluid viscosity ($kg/m.s$)
Φ_s	=	Sphericity
λ	=	orientation factor
α	=	Angle which the normal solid-liquid interface makes with the stream direction.

List of Tables

Table	Title	Page
2-1	Sphericity of different shape materials	10
2-2	Experimental design of ternary mixture	26
3-1	The physical properties of fluid	34
3-2	The true density of spherical particle	38
4-1	Result of experiment for spherical particles with $d_p = 0.9987$ cm and $\varepsilon = 0.4508$	44
4-2	Result of experiment for spherical particles with $d_p = 0.421$ cm and $\varepsilon = 0.3888$	45
4-3	Result of experiment for spherical particles with $d_p = 0.9987$ cm and $\varepsilon = 0.4508$	45
4-4	Result of experiment for spherical particles with $d_p = 0.509$ cm and $\varepsilon = 0.3931$	46
4-5	Result of experiment for spherical particles with $d_p = 0.9987, 0.7955$ cm and $\varepsilon = 0.4232$	47
4-6	Result of experiment for spherical particles with $d_p = 0.9987, 0.421$ cm and $\varepsilon = 0.3822$	47
4-7	Result of experiment for spherical particles with $d_p = 0.7955, 0.421$ cm and $\varepsilon = 0.3965$	48
4-8	Result of experiment for spherical particles with $d_p = 0.509, 0.421$ cm and $\varepsilon = 0.3933$	48
4-9	Result of experiment for spherical particles with $d_p = 0.9987, 0.7955$ cm and $\varepsilon = 0.4232$	49

4-10	Result of experiment for spherical particles with $d_p = 0.9987, 0.421$ cm and $\varepsilon=0.3822$	49
4-11	Result of experiment for spherical particles with $d_p = 0.7955, 0.421$ cm and $\varepsilon=0.3965$	50
4-12	Result of experiment for spherical particles with $d_p = 0.509, 0.421$ cm and $\varepsilon=0.3933$	50
4-13	Result of experiment for spherical particles with $d_p = 0.9987, 0.509, 0.421$ cm and $\varepsilon=0.3838$	51
4-14	Result of experiment for spherical particles with $d_p = 0.7955, 0.6015, 0.509$ cm and $\varepsilon=0.3985$	52
4-15	Result of experiment for spherical particles with $d_p = 0.7955, 0.6015, 0.421$ cm and $\varepsilon=0.3984$	52
4-16	Result of experiment for spherical particles with $d_p = 0.7955, 0.509, 0.421$ cm and $\varepsilon=0.3836$	53
4-17	Result of experiment for spherical particles with $d_p = 0.9987, 0.509, 0.421$ cm and $\varepsilon=0.3838$	53
4-18	Result of experiment for spherical particles with $d_p = 0.7955, 0.6015, 0.509$ cm and $\varepsilon=0.3985$	54
4-19	Result of experiment for spherical particles with $d_p = 0.7955, 0.6015, 0.421$ cm and $\varepsilon=0.3984$	54
4-20	Result of experiment for spherical particles with $d_p = 0.7955, 0.509, 0.421$ cm and $\varepsilon=0.38365$	55

List of figures

Figure	Title	Page
2-1	The relation between porosity of bed and size of container	9
2-2	The wall effect	11
2-3	The possible arrangement of sphere particles in the bed	13
2-4	Typical radial voidage distributions	16
2-5	Friction factor versus Reynolds number	19
2-6	Relation between depth of bed and pressure drop	24
2-7	Flow through pipe	27
3-1	A schematic diagram of the apparatus	41
3-2	Photograph picture for air flow through packed bed	42
3-3	Photograph picture for water flow through packed bed	43
5-1	Friction factor versus Reynolds number for spherical particles with $d_p=0.9987$ cm and $\epsilon=0.4505$ (Table 4-1)	56
5-2	Friction factor versus Reynolds number for spherical particles with $d_p=0.7955$ cm and $\epsilon=0.4349$ (Appendix A-1)	57
5-3	Friction factor versus Reynolds number for spherical particles with $d_p=0.6015$ cm and $\epsilon=0.4249$ (Appendix A-2)	57
5-4	Friction factor versus Reynolds number for spherical particles With $d_p=0.509$ cm and $\epsilon=0.3931$ (Appendix A-3)	58
5-5	Friction factor versus Reynolds number for spherical particles With $d_p=0.421$ cm and $\epsilon=0.3888$ (Table 4-2)	58
5-6	Friction factor versus Reynolds number for spherical particles with $d_p=0.9987$ cm and $\epsilon=0.4505$ (Table 4-3)	60

5-7	Friction factor versus Reynolds number for spherical particles with $d_p=0.7955$ cm and $\varepsilon=0.4349$ (Appendix A-4)	61
5-8	Friction factor versus Reynolds number for spherical particles with $d_p=0.6015$ cm and $\varepsilon=0.0.4249$ (Appendix A-5)	61
5-9	Friction factor versus Reynolds number for spherical particles With $d_p=0.509$ cm and $\varepsilon=0.3931$ (Appendix A-6)	62
5-10	Friction factor versus Reynolds number for spherical particles With $d_p=0.421$ cm and $\varepsilon=0.3888$ (Table 4-4)	62
5-11	Friction factor versus Reynolds number for spherical particles With $d_p= 0.9987, 0.7955$ cm and $\varepsilon=0.4232$ (Table 4-5)	64
5-12	Friction factor versus Reynolds number for spherical particles With $d_p= 0.9987, 0.6015$ cm and $\varepsilon=0.4186$ (Appendix B-1)	65
5-13	Friction factor versus Reynolds number for spherical particles with $d_p= 0.9987, 0.509$ cm and $\varepsilon=0.4171$ (Appendix B-2)	65
5-14	Friction factor versus Reynolds number for spherical particles With $d_p= 0.9987, 0.421$ cm and $\varepsilon=0.3822$ (Table 4-6)	66
5-15	Friction factor versus Reynolds number for spherical particles with $d_p= 0.7955, 0.6015$ cm and $\varepsilon=0.4173$ (Appendix B-3)	66
5-16	Friction factor versus Reynolds number for spherical particles with $d_p= 0.7955, 0.509$ cm and $\varepsilon=0.4166$ (Appendix B-4)	67
5-17	Friction factor versus Reynolds number for spherical particles With $d_p= 0.7955, 0.421$ cm and $\varepsilon=0.3965$ (Table 4-7)	67
5-18	Friction factor versus Reynolds number for spherical particles With $d_p= 0.6015, 0.509$ cm and $\varepsilon=0.4186$ (Appendix B-5)	68

5-19	Friction factor versus Reynolds number for spherical particles With $d_p = 0.6015, 0.421$ cm and $\varepsilon = 0.409$ (Appendix B-6)	68
5-20	Friction factor versus Reynolds number for spherical particles with $d_p = 0.509, 0.421$ cm and $\varepsilon = 0.3933$ (Table 4-8)	69
5-21	Friction factor versus Reynolds number for spherical particles with $d_p = 0.9987, 0.7955$ cm and $\varepsilon = 0.4232$ (Table 4-9)	70
5-22	Friction factor versus Reynolds number for spherical particles with $d_p = 0.9987, 0.6015$ cm and $\varepsilon = 0.4186$ (Appendix B-7)	71
5-23	Friction factor versus Reynolds number for spherical particles with $d_p = 0.9987, 0.509$ cm and $\varepsilon = 0.4171$ (Appendix B-8)	71
5-24	Friction factor versus Reynolds number for spherical particles With $d_p = 0.9987, 0.421$ cm and $\varepsilon = 0.3822$ (Table 4-10)	72
5-25	Friction factor versus Reynolds number for spherical particles with $d_p = 0.7955, 0.6015$ cm and $\varepsilon = 0.4173$ (Appendix B-9)	72
5-26	Friction factor versus Reynolds number for spherical particles with $d_p = 0.7955, 0.509$ cm and $\varepsilon = 0.4166$ (Appendix B-10)	73
5-27	Friction factor versus Reynolds number for spherical particles with $d_p = 0.7955, 0.421$ cm and $\varepsilon = 0.3965$ (Table 4-11)	73
5-28	Friction factor versus Reynolds number for spherical particles with $d_p = 0.6015, 0.509$ cm and $\varepsilon = 0.4121$ (Appendix B-11)	74
5-29	Friction factor versus Reynolds number for spherical particles with $d_p = 0.6015, 0.421$ cm and $\varepsilon = 0.409$ (Appendix B-12)	74
5-30	Friction factor versus Reynolds number for spherical particles with $d_p = 0.509, 0.421$ cm and $\varepsilon = 0.3933$ (Table 4-12)	75

5-31	Friction factor versus Reynolds number for spherical particles with $d_p = 0.9987, 0.7955, 0.6015$ cm and $\varepsilon = 0.427$ (Appendix C-1)	76
5-32	Friction factor versus Reynolds number for spherical particles with $d_p = 0.9987, 0.7955, 0.509$ cm and $\varepsilon = 0.4019$ (Appendix C-4)	77
5-33	Friction factor versus Reynolds number for spherical particles with $d_p = 0.9987, 0.7955, 0.421$ cm and $\varepsilon = 0.386$ (Appendix C-3)	77
5-34	Friction factor versus Reynolds number for spherical particles with $d_p = 0.9987, 0.6015, 0.509$ cm and $\varepsilon = 0.3998$ (Appendix C-4)	78
5-35	Friction factor versus Reynolds number for spherical particles with $d_p = 0.9987, 0.6015, 0.421$ cm and $\varepsilon = 0.3906$ (Appendix C-5)	78
5-36	Friction factor versus Reynolds number for spherical particles With $d_p = 0.9987, 0.509, 0.421$ cm and $\varepsilon = 0.3838$ (Table 4-13)	79
5-37	Friction factor versus Reynolds number for spherical particles with $d_p = 0.7955, 0.6015, 0.509$ cm and $\varepsilon = 0.3985$ (Table 4-14)	79
5-38	Friction factor versus Reynolds number for spherical particles With $d_p = 0.7955, 0.6015, 0.421$ cm and $\varepsilon = 0.3984$ (Table 4-15)	80
5-39	Friction factor versus Reynolds number for spherical particles with $d_p = 0.7955, 0.509, 0.421$ cm and $\varepsilon = 0.3836$ (Table 4-16)	80
5-40	Friction factor versus Reynolds number for spherical particles with $d_p = 0.6015, 0.509, 0.421$ cm and $\varepsilon = 0.3766$ (Appendix C-6)	81
5-41	Friction factor versus Reynolds number for spherical particles with $d_p = 0.998, 0.7955, 0.6015$ cm and $\varepsilon = 0.4276$ (Appendix C-7)	82
5-42	Friction factor versus Reynolds number for spherical particles with $d_p = 0.9987, 0.7955, 0.509$ cm and $\varepsilon = 0.4019$ (Appendix C-8)	83

5-43	Friction factor versus Reynolds number for spherical particles with $d_p = 0.9987, 0.7955, 0.421$ cm and $\varepsilon=0.386$ (Appendix C-9)	83
5-44	Friction factor versus Reynolds number for spherical particles with $d_p = 0.9987, 0.6015, 0.509$ cm and $\varepsilon=0.3998$ (Appendix C-10)	84
5-45	Friction factor versus Reynolds number for spherical particles with $d_p = 0.9987, 0.6015, 0.421$ cm and $\varepsilon=0.3906$ (Appendix C-11)	84
5-46	Friction factor versus Reynolds number for spherical particles with $d_p = 0.9987, 0.509, 0.421$ cm and $\varepsilon=0.3838$ (Table 4-17)	85
5-47	Friction factor versus Reynolds number for spherical particles with $d_p = 0.7955, 0.6015, 0.509$ cm and $\varepsilon=0.3985$ (Table 4-18)	85
5-48	Friction factor versus Reynolds number for spherical particles With $d_p = 0.7955, 0.6015, 0.421$ cm and $\varepsilon=0.3983$ (Table 4-19)	86
5-49	Friction factor versus Reynolds number for spherical particles with $d_p = 0.7955, 0.509, 0.421$ cm and $\varepsilon=0.3836$ (Table 4-20)	86
5-50	Friction factor versus Reynolds number for spherical particles with $d_p = 0.6015, 0.509, 0.421$ cm and $\varepsilon=0.3766$ (Appendix C-12)	87

Chapter one

Introduction

1.1 Introduction

Fluid flow through packed bed has many important applications in chemical and other process engineering fields which are used for fixed-catalytic reactor, adsorption of a solute, gas absorption, combustion, drying, filter bed, wastewater treatment and the flow of crude oil in petroleum reservoir [1].

A typical packed bed is a cylindrical column that is filled with a suitable packing material [2]. The packing material may be sphere, cylinders, irregular particles or various kinds of commercial packing [3]. It should have a large void volume to allow flow of fluid without excessive pressure drop and it should be chemically inert to fluids being processed [4].

One of the problems concerning the flow of fluids through beds of particles is the manner in which the particles are packed and the distribution of voids within the packed bed [5].

The particles packed together to form a structure which depends on a large number of parameters many of which are difficult to measure, or even to define. These include the shape and size distribution of particles, the way the packing has put together and the various forces exerted on it afterwards [6].

It is important to obtaining uniform fluid distribution in such beds to minimizing operating costs and optimizing plant performance. Since to some extent a packed bed acts as its own distributor the importance of obtaining uniform fluid distribution has increased as aspect ratios (bed height to diameter) decrease [7].

The advantage of using a packed column rather than just tank or other reaction vessel is that the packing affords a large surface area per unit volume of mass transfer [2].

The flow of fluid through bed composed of stationary granular particles is a frequent occurrence in the chemical industry and therefore expressions are needed to predict pressure drop across beds due to the resistance caused by the presence of the particles [8].pressure drop measurement is important when designing the pump for the fluid, in order to decrease costs of the system [9].

The flow around submerged objects in fluid (liquid or gas) causes the molecules to bounce into each other and thereby release of energy. This interaction could be considered as a friction between the molecules [1].

The aim of this work is to:

- I. Study the effect of particle size distribution on the bed porosity.
- II. Determine the pressure drop and friction factor for single phase fluid flow (air and water) through column packed with different sizes of glass bed.
- III. Study the effect of bed porosity on the pressure drop and friction factor through the packed bed.
- IV. Study the effect of working fluid (air or water) on the pressure drop and friction factor through the packed bed.
- V. Propose an empirical correlation between friction factor and Reynolds number for air and water flow through bed of spheres.

Chapter two

Literature survey

2.1 The flow of fluid through porous media

The flow of fluid through beds composed either of irregular shaped material or of packings of regular geometrical form has attracted considerable attention from many investigators [10]. **Kozeny in 1927 [11], Carman in 1938 [12], Blank in 1962 [13] and Green and Ampts in 1962 [14]**, studied the flow of air through columns packed with spherical materials [11, 12, 13, 14].

Schoenborn and Dougherty in 1944 [15], studied the flow of air, water and oil through beds of various commercial ring and saddle packing [15].

The flow of one or two fluids through packed beds have many important engineering applications such as adsorption (one phase flow through the bed), distillation (flow of two countercurrent fluids), and/or trickle bed reactor (flow of two co-current fluids) [16].

Many materials (ex. soil, sand, packed catalyst beds) consist of a large number of particles packed closely together. In between the solid particles there is open space, giving rise to pores through which fluid can flow. Porous media do not have to consist of many particles to be porous; it could simply be composed of a single continuous solid body that has many pores (or holes) in it. Because of the irregular packing, tortuous nature of the pores it is exceedingly difficult to fluid flow through such materials [17].

In many industrial operations, a fluid phase flow through a particulate-solid phase. Examples include filtration, mass transfer in packed columns, chemical reactions using solid catalysts, and flow of crude oil in petroleum

reservoir. In many cases, the solid phase is stationary, as it is in a packed distillation column. In other cases the bed moves countercurrent to the gas stream, as it does in some catalytic reactors. In some cases, the fluid velocity is great enough that the momentum transferred from the fluid to the solid particles balances the opposing gravitational force on the particles and the bed expands in to fluid like phase; in other applications, the fluid phase carries the solid phase with it, as it does in pneumatic conveying [4].

In a packed bed the flow path is made up of many parallel and interconnecting channels. The channels are not of fixed diameter, but widen and narrow repeatedly.

The flow through large open channels will be at higher velocity than flow through parallel narrow constricted channels, because the pressure drop per meter of bed length must be constant regardless of the channels under consideration. For this reason, the transition from laminar to turbulent flow will occur at a much lower bulk flow rate in open passages than it will in restricted channels. Moreover, at the convergence of two channels, eddy currents and turbulence will be promoted because of the inequality of velocity in the two channels. The flow behavior in expanded or fluidized beds will be very similar to that for packed beds, except that the flow passages will be more open almost continuously inter connected [4].

2.2 Packing

The packing of particles is of great interest in a variety of scientific and technological areas. These include, for example, production of concrete, coal technology, packed columns [18].

The packing is built under gravity, particle by particle. Each particle is dropped at a randomly chosen position above the already placed spheres, and

rolls down over them until it reaches a stable position with respect to gravity [19].

The method of packing into the column must be considered because, if the phases (fluid and solid) do not contact everywhere within the column, the packing is not completely effective [4].

Many types of packing materials have been used, ranging from simple, readily available solids such as stones or broken bottles to expensive complex geometric shapes. In general, the packing material should have the following characteristics [4]:

1. It should have a large void volume. This will allow to fluid to flow without excessive pressure drop.
2. It should be relatively inexpensive (represent low cost).
3. It should be corrosion resistant.
4. It should have structural strength to permit easy handling and installation.
5. It should be chemically inert to fluids being processed.

Packing porosity is one of the fundamental properties of a bed of particulate materials. Several workers have found that the fractional void volume of a bed of mixed solid particles varies with the size distribution of the materials [20] and the manner of particles is dropped into column. If it is dropped from short distance above the packing, then a reproducible packing is obtained which may be called the normal packing for that material. To obtain beds with voids less than normal packing the particles may be dropped into the column from greater heights above the bed [10].

Many of investigators have described the fractional void volume of a bed of solid particles. It is well-known an empirical fact that the packing porosity varies with the size distribution of the materials involved. From a

theoretical point of view, on the other hand, much work have been devoted to the regular packing of solid spheres, and a few investigators such as **Furnas in 1931 [21]**, **Westman and Hugill in 1930 [22]**, have examined the mixture of a bed of solid particles of different sizes [23]. **Graton and Fraser in 1947 [24]** studied the packing of spheres led to the much-quoted limits of porosity for regular packing of single-size spheres. **Fuller and Thompson in 1987 [25]** studied the influence of distribution of the particle size up on the density of granular material.

2.3 Packed column

A typical packed column is a cylindrical column that is filled with a suitable packing material. The packing material represents the solid stationary phase and the fluid immiscible phase, allowed to pass through, or by it [26].

The cylindrical column can take two forms depending on how the stationary phase is contained in it. In one form, the capillary column, the stationary phase is held as a thin film adhering to the column walls. In the other form, the column contains an inert supporting material (such as porcelain, or various plastics, thin-walled metal rings of steel or aluminum, glass, stone, or other material) carrying the stationary phase and is called the *packed column* [26].

Packed columns are widely used in liquid extraction process scrubbers, absorbers and condensers, reaction chambers, rectifying and fractionating columns drying chambers, fumes or dust extraction plants, catalyst carriers, regenerative heat transfer media and demisting operations [26].

Packed columns are typically employed in operations where a smaller-diameter column is usually cheap and sufficient to handle the fluid flow rates. It is often required to estimate parameters such as pressure drop through

packing and friction factor as a function the volumetric flow rate or superficial velocity to optimally design the equipment [4].

Packed columns may be more economical in processing corrosive liquids because of corrosion- resistance ceramic packing [27].

2.4 Packed bed

The flow of fluid through bed composed of stationary granular particles is a frequent occurrence in the chemical industry and therefore expressions are needed to predict pressure drop across beds due to the resistance caused by the presence of the particles [8].

Packed systems in industry may be divided into the following classes:

1. Fixed beds
 - a. Solid- gas system.
 - b. Solid- liquid systems.
2. Moving beds.
3. Solid- liquid- gas system.

Typical example of solid-gas fixed-bed systems are the catalytic reactors which were used by the Germans in the Fischer-Tropsch synthesis retorting of oil Shale, roasting of ores, combustion of coal and coke in fuel beds, and blast furnace operations.

The most important solid-liquid fixed-bed applications are water filtration, flow of oil through sand strata, coal washing, and leaching.

Moving beds are employed in the FCC (fluidized catalytic cracking) process.

The Solid-liquid-gas system comprises fractionating towers, absorbers, scrubbers, and many other kinds of chemical engineering equipment [28].

2.5 Variables affecting flow through granular bed

The variables affecting resistance to flow through a granular bed can be classified into two basic categories [29]:

- Variables related to the fluid flowing through the bed such as viscosity, density, and rate of fluid flow.
- Variables related to the nature of the bed are numerous and to be considered as size and shape of the particles, the wall effects, porosity of the bed, surface roughness of the particle and orientation of particles.

2.5.1 The size and shape of the particles

To define regular particles such as cubes, cylinders or spheres, the length, width, thickness or diameter are usually used. However it becomes difficult when the particles are irregular. In this case the equivalent particle size is normally used, i.e., the following definitions of the equivalent sphere have been used [29]:

1. A sphere having the same surface area as the particle, the diameter is called the surface diameter.
2. A sphere having the same volume as the particle, the diameter is called the volume diameter.
3. A sphere having the same ratio of surface area to volume as the particle, the diameter is now called the surface- volume diameter.

It is further assumed that the size of the particle is small in comparison with the column size in which the packing is contained [3]; the ratio of the column diameter to the particle diameter should be a minimum of 8:1 to 10:1 to reduce wall effects [30]. Figure. 2-1 shows the relation between porosity of bed and size of container [31].

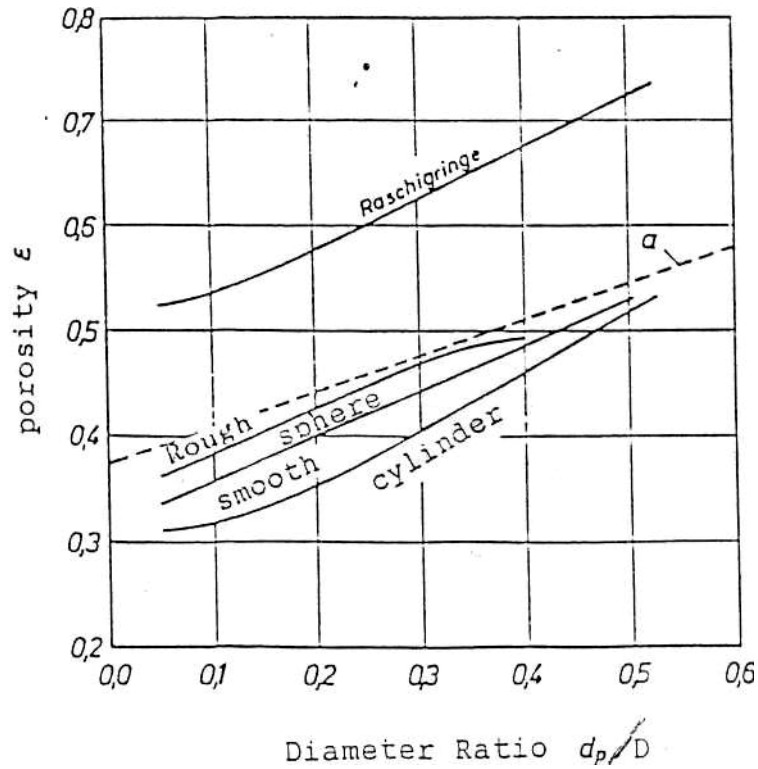


Figure 2-1 The relation between porosity of bed and size of container [31].

Particle shape is usually measured by a factor called the shape factor (ϕ_s). This factor is difficult to ascertain, particularly when dealing with small irregular shapes. It has value of one for spheres and for other shapes is less than one [29]. Table 2-1 shows the shape factor of different shape materials [32].

The sphericity shape factor ϕ_s of a particle is the ratio of the surface area of this sphere to the surface area of particle [30].

$$\phi_s = \frac{S_{sphere}}{S_{particle}} = \frac{\pi d_p^2}{S_{particle}} \quad \dots (2.1)$$

where

d_p is the diameter of a sphere of the same volume as the particle

The shape of the particle has influence on:

1. The range voids that can be obtained, thus cubes and plates have a wide range in voids but with spheres it is difficult to cover more than a very small range in voids [10].
2. The fluid path in beds, for irregular particles the fluid passes in more tortuous than those in similar beds of spheres [29].

Table 2-1 Sphericity of different shape materials [32]

Material	Sphericity	Material	Sphericity
Sphere, cubes, short cylinders ($L=d_p$) Rashing rings ($L=d_p$)	1.0	Ottawa sand	0.95
		Rounded sand	0.83
		Coal dust	0.73
Rashing rings $L=d_{po}^*$, $d_{pi} = 0.5d_{po}^*$ $L=d_{po}$, $d_{pi} = 0.75d_{po}$	0.58	Flint sand	0.65
	0.33	Crushed glass	0.65
Berl saddles	0.3	Mica flakes	0.28
* d_{po} , d_{pi} is the outside and inside diameter of rashing rigs			

2.5.2 The wall effects

The walls retaining a granular packed bed affect the resistance of the bed in two ways [29]:

- (i) The particles adjacent to the walls pack more loosely than those remote from them thus increasing the porosity of the zone near the walls. Fig. 2-2 shows the fluctuation of porosity in a bed of spheres and cylinders [33].
- (ii) They create an additional surface area providing additional resistance of flow.

The effect of the walls is a ratio termed the relative resistance which is the ratio of the resistance to flow of finite bed to the resistance to flow of a infinite bed of the same characteristics [29], so that the actual resistance to flow in a bed of small diameter is less than it would be in an infinite container for the same flow rate per unit area of bed cross-section [8].

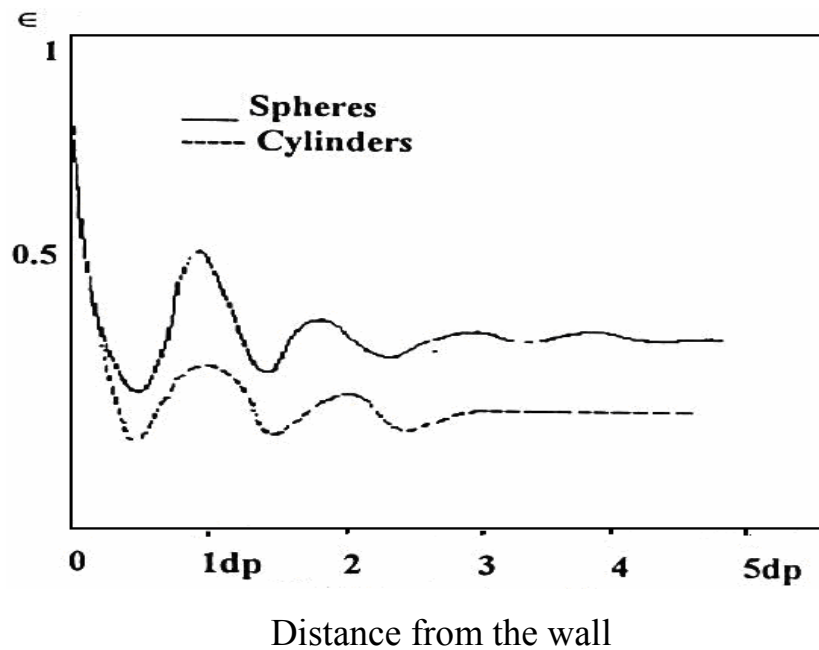


Figure 2-2 The wall effect [33]

To decrease wall effects, the particle diameter should be small in comparison with the column diameter in which the packing is contained [3].

Furnas in 1931[21] studied the wall effect and found that when the ratio of the diameter of the container (D), to that of the particle (d_p), is greater than 10:1, the wall effect can be neglected [34].

Graton and Fraser in 1953 [34] show that the porosity of the bed is greater in the layers next to the wall, which lead to increase the fluid permeability there. **Furnas in 1931 [21]** concluded that the porosity of an

annular ring of thickness $d/2$ from the walls was 30% greater than that of the rest of the bed [31].

Carman and Coulson In 1938 made no correction for the change in porosity near to the wall. They used the mean porosity and for low rates added half the area of the walls to the surface area of the particles [31]. A wall affects correction factor f_w for velocity though the packed bed has been determined experimentally by Coulson as [8].

$$f_w = \left(1 + \frac{1}{2} \frac{S_c}{S}\right)^2 \quad \dots (2.2)$$

where:

S_c = is the surface of the container per unit volume of bed.

S = is the specific surface area of the particles.

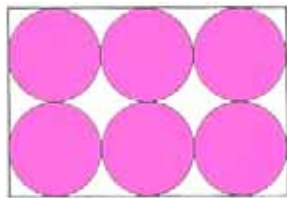
2.5.3 The porosity of the bed

The porosity of the bed (ϵ) is defined as the ratio of the void volume to the total volume of the bed (the volume fraction occupied by the fluid phase). Other names given the porosity include the void fraction, fractional voidage, or simply, voidage [35].

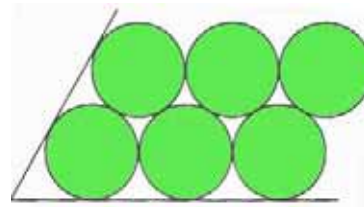
$$porosity(\epsilon) = \frac{V_{void}}{V_{total}} \quad \dots (2.3)$$

The arrangement or packing of the particles plays a role in porosity. There are three possible way of arrangement of particles; cubic, rhombohedra, and Cubic packing with smaller grains. When the particle

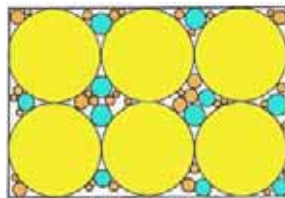
stacked directly on top of each other (cubic packing) the porosity is higher than the particles in a pyramid shape (rhombohedral packing) sitting on top of two other particles. When smaller particles are mixed with larger particles, the smaller particles could fill in the void spaces between the larger particles (Cubic packing with smaller grains filling the void space); this would result in a lower porosity. Fig. 2-3 shows the possible arrangement of particles in the bed of sphere [36, 37].



Cubic packing



Rhombohedral packing



Cubic packing with smaller grains filling the void space

Figure 2-3 The possible arrangement of sphere particles in the bed [36]

Roblee in 1958[38], Benenati and Brosilow in 1982 [39], Pillai and Lerou in 1986[40], had clearly indicted the presence of oscillatory radial variations of the void fraction in packed bed.

The porosity has an effect on the properties of granular medium. In fact there is no doubt that any small change in the porosity of the bed leads to a big change in pressure drop across the bed. **Lava in 1937** found that a 1% decrease in porosity of bed produces about an 8% increase in the pressure drop, whilst **Carmen in 1938** reported a higher value 10% increase in the pressure drop for every 1% decrease in porosity [29].

2.5.4 The surface roughness of the particles

The effects of surface roughness upon the pressure drop have indicated a marked effect in the turbulence range. Roughness dose not affect friction in the laminar region. The flow through empty conduits, where surface roughness was also found to be an important factor in the turbulent region a notable difference between packed bed and empty conduit flow is, however, found in the transition range. In empty vessels, the nature of the flow changes abruptly from laminar to the turbulent at Reynolds number values of about 2100 where, as the transition that occurs in packed tubes is a general one [28]. Surface roughness has two major effects; it increases the resistance of the bed to fluid flow and increases the porosity of the bed [29].

2.5.5 The orientation of the particles

It is apparent that the orientation of the particles composing the bed with respect to the direction of flow has a significant effect which depends on the shape and the arrangement of the particles. **Coulson and Gupta in 1938** reported that for the same porosity the resistance to flow changed with arrangement of the particles relative to each other.

Sullivan and Hertel in 1940 suggested a factor for the orientation and their equation for flow through a packed bed including this factor is:

$$\lambda = (\sin^2 \alpha) \quad \dots (2.4)$$

where:

λ is the orientation factor

α is the angle which the normal to the solid-liquid interface makes with the stream direction.

They presented data for three specific packing; sphere, cylinders perpendicular to the direction of flow and cylinders parallel to the direction of flow. In the case of the spheres, the orientation factor equals 2/3, for cylinders perpendicular to the direction of flow, the factor equals 1/2 and for cylinders parallel to the direction of flow the factor equals 1 [29].

2.6 Prediction of voidage distribution

The characteristics of the flow through packed bed are important in filter design and an understanding of the relationship between void fraction and the flow distribution is essential. Fig. 2-4 shows a typical radial voidage distribution (in a bed of 98 mm in diameter packed with 4 mm spherical beads). It has been shown that, for flow through a fixed bed of uniform particles that there is a maximum velocity approximately one particle diameter from the outer wall of the bed, which decrease sharply toward the wall and more gradually away from it. The fraction of the bed influenced by this velocity profile depends on the ratio of particle size to bed diameter [41].

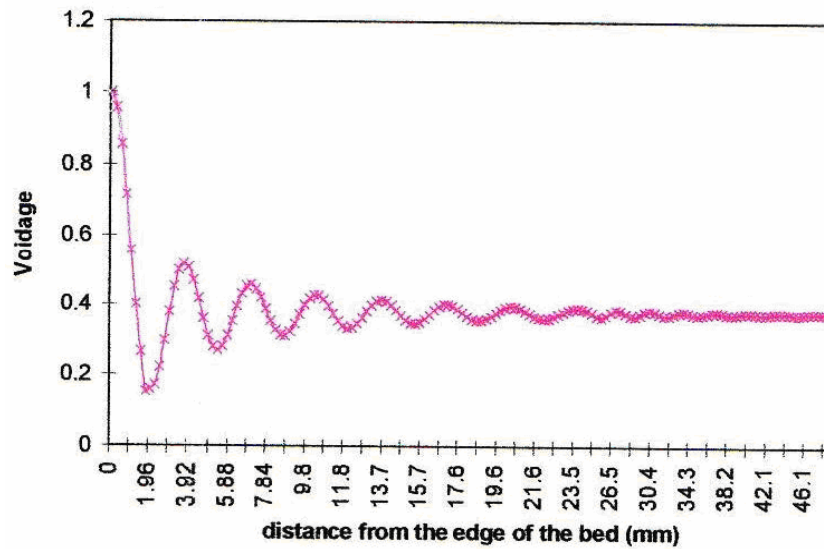


Figure 2-4 Typical radial voidage distributions [41]

The voidage is found to be a minimum about half a particle diameter from the wall of the bed and then follow a damped oscillatory function until it reaches a constant value about 5 particle diameters from the wall, where the packing is random [41].

Large randomly packed beds of uniform spheres tend to pack with an average void fraction of 39% since locally the voidage varies from point to point. Near the wall of the containing vessel the void fraction will be larger than near the center of the bed. Immediately adjacent to the wall the void fraction approach unity and in the center of the bed a minimum voidage observed [39].

2.7 Velocity Measurement

The measurement of velocities within the packing of bed would be virtually impossible. Therefore, the flow rate was studied in the column just downstream from the packing. This meant that the velocities so obtained were superficial values, which based upon the total void and non-void area. The

objective was to determine the average velocity that would exist in the bed at a given radial position based upon the total area rather than the actual void area. Such a measurement is an average velocity because the void fraction varies with distance along the axis of the pipe. In order to attain this objective, the effect of distance of the measuring device from the packing must be examined. If this distance is too large, the observed velocity profiles may be more descriptive of empty column conditions than those existing within the packed bed. If the distance is too small, velocity components perpendicular to the direction of flow may be significant [23].

2.8 Specific surface

The general surface of a bed of particles can often be characterized by the specific area of the bed (S_B) and the fractional voidage of the bed (ϵ). S_B is the surface area presented to the fluid per unit volume of bed when the particles are packed in bed. Its units are $(\text{length})^{-1}$.

S is the specific surface area of the particles and is the surface area of a particle divided by its volume. Its units are again $(\text{length})^{-1}$. For sphere [8, 42]:

$$S = \frac{\text{Surface area}}{\text{volume}} = \frac{\pi d_p^2}{\pi(d_p^3/6)} = \frac{6}{d_p} \quad \dots (2.5)$$

It can be seen that S and S_B are not equal due to the voidage occurring when the particles are packed in to a bed. If contact points occur between particles so that only a very small fraction of surface area is lost by overlapping, then [8, 42]:

$$S_B = S(1-\epsilon) \quad \dots (2.6)$$

For a given shape of particle S increases as the particle size is reduced. [9].

When mixtures of sizes are studied the value of S for sphere of mixed sizes is given by [12].

$$S = 6(1 - \varepsilon) \sum \frac{x_i}{d_{pi}} \quad \dots (2.7)$$

where

x_i is the fractional weight of spherical particle.

d_p is the diameter of spherical particle.

2.9 friction factor

The friction factor is determined for the entire Reynolds number. For $Re < 10$ the flow is laminar, the range $10 < Re < 100$ is commonly referred to as transition whereas flows characterized by $Re > 100$ are considered turbulent [43].

Many studies have been done in correlating data for packed columns at higher fluid velocities where the pressure drop appears to vary with some power of velocity, the exponent ranging between 1 and 2. **Blanke in 1962 [12]**, suggested that this change of relationship between pressure drop and velocity is entirely analogous to that which occurs in ordinary pipes and proposed a friction factor plot similar to that of Stanton. The equation used was that for kinetic effect modified by a friction factor, which is turn, is a function of Reynolds number [44].

$$\Delta p = 2f (\rho u^2 / D_p) \quad \dots (2.8)$$

$$f = \phi(NRe) \quad \dots (2.9)$$

Some workers have included the effect of void fraction by the addition of another factor in equation 2.8. It is usually given in the form $(1-\epsilon)^m/\epsilon^3$ where m is either 1 or 2.

Kozeny in 1927 [11], and Carman in 1938 [12], suggested that the change of relationship between pressure drop, void fraction effect and velocity, and proposed a friction factor for entire Reynolds number by plotting on a logarithmic basis [8].

Fig. 2-5 is a correlation of the friction factor as a function of the Reynolds number for condition of fixed bed operation; the main variables are the velocity, particle diameter, pressure drop per unit length and fraction voids. This method was found to work satisfactorily for constant diameter fractions of the glass spheres.

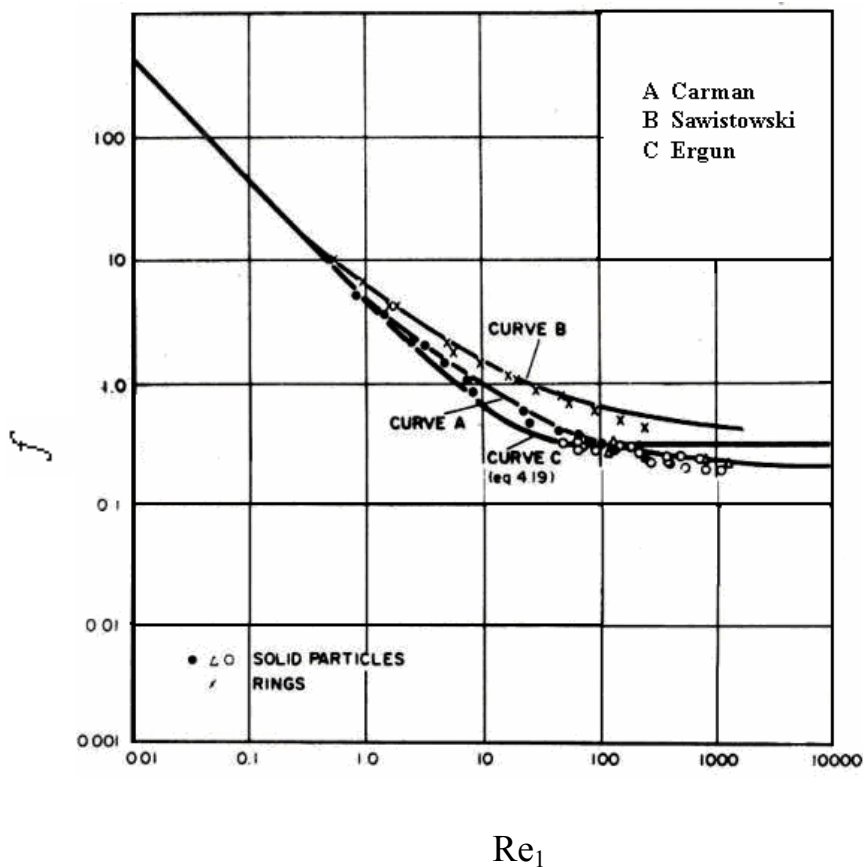


Figure 2-5 Friction factor versus Reynolds number [8]

Carman in 1938 correlated data for flow through randomly packed beds of solid particles by a single curve (curve A, Fig. 2-5), whose general equation was [8]:

$$f = 5 \text{Re}_1^{-1} + 0.4 \text{Re}_1^{-0.1} \quad \dots (2.10)$$

where Re_1 is the modified Reynolds number.

$$\text{Re}_1 = \frac{\rho u}{s(1-\varepsilon)\mu} \quad \dots (2.11)$$

As where ρ , u , s , ε and μ are the density of the fluid, fluid velocity, surface area of particles, porosity of the bed, and the fluid viscosity, respectively.

Ergun in 1952 suggested an equation for flow through ring packings as:

$$f = 4.17 \text{Re}_1^{-1} + 0.29 \quad \dots (2.12)$$

Sawistowski in 1957 has compared the results obtained for flow of fluids through beds of hollow packing. He proposed:

$$f = 5 \text{Re}_1^{-1} + \text{Re}_1^{-0.1} \quad \dots (2.13)$$

Equation 2.12 is plotted as curve B in Fig. 2-5.

As shown in Fig. 2-5, the first terms of equations 2.10, 2.12 and 2.13 predominate at low rates of flow ($Re_1 < 10$) where the losses are mainly attributable to skin friction, and the second terms are small. At high flow rates ($2 < Re_1 < 100$), the second terms become more significant and the slope of the plot gradually changes from -1.0 to about $-\frac{1}{4}$. At higher flow rates ($Re_1 > 100$) the plot is approximately straight. The change from complete streamline flow to complete turbulent flow is very gradual because flow conditions are not the same in all the pores [8].

2.10 The surface roughness effect on friction factor

Attempts to study the effect of surface roughness on the friction factor have shown that the variable has a significant effect but no quantitative method of evaluating the effect has been formulated.

Leva in 1949 carried out important experiments using three different groups of materials. He used glass as smooth particles, clay and Alundum as rough materials, Aloxite and Mgo as rougher materials. He described the degree of roughness of the materials qualitatively (as a result of his tests). This method of description does not help in the development of a quantitative correlation between the relative roughness (ϵ/d) and the friction factor.

Leva expressed equations for the friction factor of these materials as follow, for smooth materials the expression was:

$$f = \frac{1.75}{Re^{0.1}} \quad \dots (2.14)$$

For rough materials his expression was:

$$f = \frac{2.625}{\text{Re}^{0.1}} \quad \dots (2.15)$$

whilst for rougher materials the expression was:

$$f = \frac{4.0}{\text{Re}^{0.1}} \quad \dots (2.16)$$

These expressions do not include the relative roughness (ϵ/d) and can only therefore be used for the materials that were used. Leva concluded (from previous expressions) that the degree of surface roughness had no effect on the slope of the $\log f - \log \text{Re}$ curve between the limits of Re from 130 to 7000 which covered the range was used [29].

2.11 Pressure Drop through packed bed

The pressure drop of fluid flow through the packed bed is an important issue. It is affected by several factors such as fluid flow rate, fluid viscosity and density, bed geometry, particle size and size distributions. A partial relationship was found between these variables and the pressure drop which was proportional to fluid velocity at low rates, and proportional to the square of the velocity at high flow rates. Reynolds was the first to formulate the resistance by friction on the motion of fluid as the sum of these two conditions [8, 45]:

$$\frac{\Delta p}{L} = a u + b \rho u^2 \quad \dots (2.17)$$

where a and b are representative of packing and fluid properties

Carman and Kozeny derived an expression for pressure drop under viscous flow as [46]:

$$\frac{\Delta p}{L} = \frac{150 (1-\varepsilon)^2 u \mu}{\varepsilon^3 \phi_s^2 d_p^2} \quad \dots (2.18)$$

Burke and Plummer derived an expression for change in pressure at turbulent flow resulting from kinetic energy loss as [46]:

$$\frac{\Delta p}{L} = \frac{1.75(1-\varepsilon)\rho u^2}{\varepsilon^3 \phi_s d_p} \quad \dots (2.19)$$

Ergun found that the total pressure drop is the sum of the viscous forces and the kinetic forces and created a general relationship based on the two equations above (equations 2.18 and 2.19) as [46]:

$$\frac{\Delta p}{L} = \frac{150 (1-\varepsilon)^2 u \mu}{\varepsilon^3 \phi_s^2 d_p^2} + \frac{1.75 (1-\varepsilon)\rho u^2}{\varepsilon^3 \phi_s d_p} \quad \dots (2.20)$$

where ΔP , ε , ρ , d_p , ϕ_s , u , L , and μ are the pressure drop, void fraction of the bed, density of the fluid, particle diameter, sphericity of the particle, fluid velocity, height of the bed, and the fluid viscosity respectively.

For packing contain different particle size, the average particle size can be calculated as the mass average, as defined in equation 2.21[47].

$$d_{pav} = \frac{1}{\sum_{i=1}^n \frac{x_i}{d_{pi}}} \quad \dots (2.21)$$

where

x_i is the fractional weight of spherical particle.

d_{pi} is the diameter of spherical particle.

2.12 The Relation between depth of bed and pressure drop

From the readings of the manometers, Colson found that the differences in pressure over varying depths of the packing were obtained directly. Some results for beds of spherical particles ($d_p = 5/32''$ and $5/16''$), plates ($1/16''$) and cylinders ($1/8''$) are shown graphically in Fig. 2-6. The experimental points are seen to lie on straight lines indicating a linear relation between pressure drop (Δp) and depth of bed (L) [10].

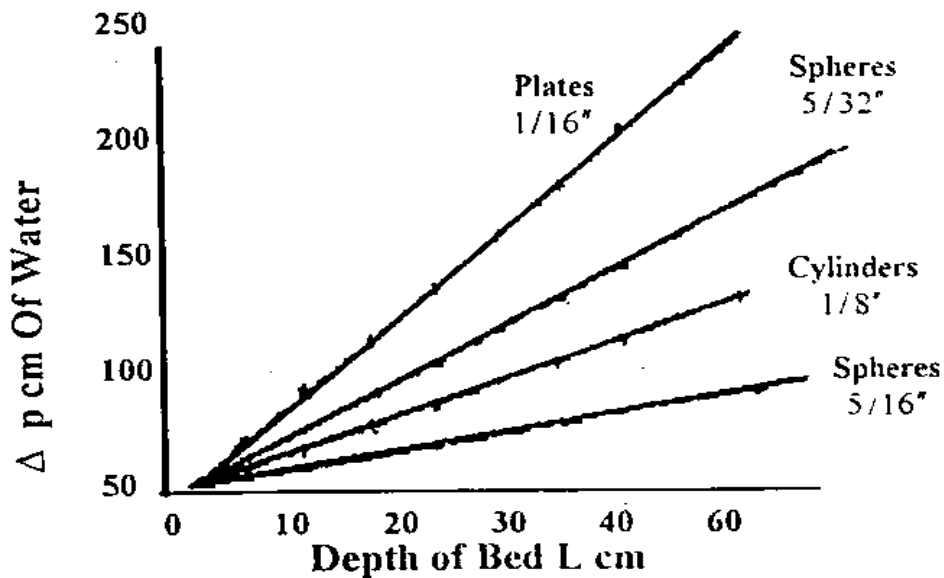


Figure 2-6 Relation between depth of bed and pressure drop [10]

2.13 Theory

The porosity of any mixture in a given particulate system depends on the proportions of the components present, but not on the total amount of the mixture. Let q be the number of components and x_i the proportion of the component in the mixture, so that

$$x_i \geq 0 \quad (i=1,2,\dots,q) \quad \dots (2.22)$$

$$x_1 + x_2 + \dots + x_q = 1 \quad \dots (2.23)$$

The porosity of the particulate mixtures, as response, is the function of all the proportions, which was assumed can be adequately represented by a polynomial in x_i .

In the simplex- centroid design, $2^q - 1$ measurements are taken, one on each of the following. The q pure components, the $\binom{q}{2}$ binary mixtures with equal proportions, the $\binom{q}{3}$ ternary mixtures with equal proportions. This corresponds to the points (x_1, x_2, \dots, x_q) of the simplex Eq 2.23 by making the following permutations:

$$\binom{q}{1} \text{ Of } (1, 0, \dots, 0)$$

$$\binom{q}{2} \text{ Of } (1/2, 1/2, 0, \dots, 0)$$

$$\binom{q}{3} \text{ Of } (1/3, 1/3, 1/3, 0, \dots, 0)$$

Thus, the design consists of the centroid of the simplex Eq.2.23 and the centroids of all the lower-dimensional simplexes it contains.

Table 2-2 gives the simplex-centroid design for ternary mixture [48].

Table 2-2 Experimental design for ternary mixture [48]

Test No.	Xw1	Xw2	Xw3	Xw4	Xw5
1	1	0	0	0	0
2	0	1	0	0	0
3	0	0	1	0	0
4	0	0	0	1	0
5	0	0	0	0	1
6	1/2	1/2	0	0	0
7	1/2	0	1/2	0	0
8	1/2	0	0	1/2	0
9	1/2	0	0	0	1/2
10	0	1/2	1/2	0	0
11	0	1/2	0	1/2	0
12	0	1/2	0	0	1/2
13	0	0	1/2	1/2	0
14	0	0	1/2	0	1/2
15	0	0	0	1/2	1/2
16	1/3	1/3	1/3	0	0
17	1/3	1/3	0	1/3	0
18	1/3	1/3	0	0	1/3
19	1/3	0	1/3	0	1/3
20	1/3	0	0	1/3	1/3
21	1/3	0	1/3	1/3	0
22	0	1/3	1/3	1/3	0
23	0	1/3	1/3	0	1/3
24	0	1/3	0	1/3	1/3
25	0	0	1/3	1/3	1/3

2.14 Fluid flow through randomly packed columns

Many attempts have been made to obtain general expressions for pressure drop and mean velocity for flow through packing in terms of voidage and specific surface, as these quantities are often known or can be measured. Alternatively, measurements of the pressure drop, velocity, and voidage provide a convenient way of measuring the surface area of some particulate materials [9].

A horizontal pipe with a concentric element marked ABCD is shown in Fig. 2-7.

The forces acting are the normal pressures over the ends and shear forces over the curved sides.

$$\text{Force over AB} = p \pi s^2 \quad \dots (2.24)$$

$$\text{Force over CD} = - \left(p + \frac{dp}{dl} \delta l \right) \pi s^2 \quad \dots (2.25)$$

$$\text{Force over curved surface} = 2\pi s \delta l R_y \quad \dots (2.26)$$

$$\text{Where the shear stress } R_y = \mu \frac{du_x}{ds} \left(= -\mu \frac{du_x}{dy} \right) \quad \dots (2.27)$$

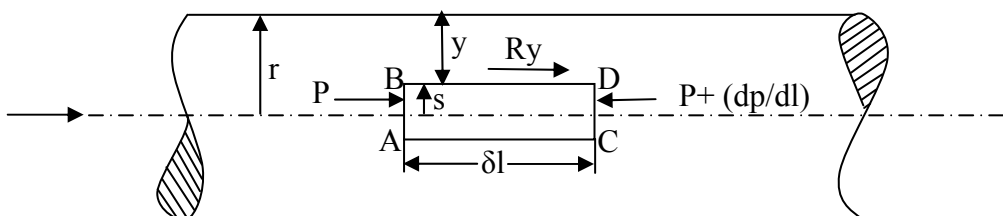


Figure 2-7 Flow through pipe

Taking force balance:

$$p \pi s^2 - \left(p + \frac{dp}{dl} \delta l \right) \pi s^2 + 2 \pi s \delta l \mu \frac{du_x}{ds} = 0 \quad \dots (2.28)$$

$$\left(- \frac{dp}{dl} \right) s + 2 \mu \frac{du_x}{ds} = 0 \quad \dots (2.29)$$

From equation 2.27

$$\frac{du_x}{dy} = - \frac{du_x}{ds} \quad \dots (2.30)$$

And hence in equation 2.29

$$\frac{du_x}{dy} = \left(- \frac{dp}{dl} \right) \frac{s}{2 \mu} \quad \dots (2.31)$$

And the shear stress at the wall is given by

$$\left(\frac{du_x}{dy} \right)_{y=0} = \left(- \frac{dp}{dl} \right) \frac{r}{2 \mu} = \left(- \frac{dp}{dl} \right) \frac{d}{4 \mu} \quad \dots (2.32)$$

The velocity at any distance s from the axis of the pipe can now be found by integrating equation 2.29.

Thus:

$$u_x = \frac{1}{2\mu} \frac{dp}{dl} \frac{s^2}{2} + \text{Constant} \quad \dots (2.33)$$

At the wall of the pipe (where $s=r$) the velocity u_x must be zero to satisfy the condition of zero wall slip. Substituting the value $u_x=0$ when $s=r$

$$\text{Constant} = \frac{1}{2\mu} \left(-\frac{dp}{dl} \right) \frac{r^2}{2} \quad \dots (2.34)$$

And therefore

$$u_x = \frac{1}{4\mu} \left(-\frac{dp}{dl} \right) (r^2 - s^2) \quad \dots (2.35)$$

Thus the velocity over the cross-section varies in parabolic manner with distance from the axis of the pipe. The velocity of the flow is seen to be a maximum when $s=0$ i.e. Thus the maximum velocity, at the pipe axis, is given by u_{cl} where [49].

$$u_{\max} = u_{cl} = \frac{1}{4\mu} \left(-\frac{dp}{dl} \right) r^2 = \left(-\frac{dp}{dl} \right) \frac{d^2}{16\mu} \quad \dots (2.36)$$

where $u = \frac{u_{\max}}{2}$

$$u = \frac{-\Delta p d_t^2}{32 L \mu} \quad \dots (2.37)$$

If the free space in the bed is assumed to consist of a series of tortuous channels, equation 2.37 for flow through a bed may be rewritten

$$\text{as: } u_1 = \frac{d_m^2 (-\Delta p)}{k' \mu L'} \quad \dots (2.38)$$

In a cube of side x , the volume of free space is ϵx^3 so that the mean cross-sectional area for flow is the free volume divided by the height, or ϵx^2 . The volume flow rate through this cube is $u x^2$, so that the average linear velocity through the porous u_1 , is given by

$$u_1 = \frac{u x^2}{\epsilon x^2} = \frac{u}{\epsilon} \quad \dots (2.39)$$

Although equation 2.39 is reasonably true for random packing it does not apply to all regular packing. Thus with a bed of sphere arranged in cubic packing, $\epsilon = 0.476$, but the fractional free area varies continuously, from 0.215 in a plane across the diameters to unity between successive layers.

The equivalent diameter of pore space d_m that could be taken as:

$$d_m = \frac{\epsilon}{S_B} = \frac{\epsilon}{S(1-\epsilon)} \quad \dots (2.40)$$

Then taking $u_1 = \frac{u}{\varepsilon}$ and $L' = L$ equation 2.38 become

$$u = \frac{\varepsilon^3 (-\Delta p)}{k'' S_B \mu L} \quad \dots (2.41)$$

Equation 2.41 applies to stream flow condition, but Carman and others have extended the analogy with pipe flow to cover both streamline and turbulent flow conditions through packed bed. In this treatment a modified Reynolds number Re_1 , is plotted against a modified friction factor $\frac{R_1}{\rho u_1^2}$.

The modified Reynolds number Re_1 is obtained by taking the same velocity and characteristic linear dimension d_m as were used in deriving equation 2.41 thus:

$$Re_1 = \frac{u \varepsilon \rho}{S \varepsilon (1 - \varepsilon) \mu}$$

$$Re_1 = \frac{u \rho}{S (1 - \varepsilon) \mu} \quad \dots (2.42)$$

The friction factor, can be plotted against the modified Reynolds number, is $\frac{R_1}{\rho u_1^2}$, where R_1 is the component of the drag force per unit area of particle surface in the direction of motion. R_1 can be related to the properties of the bed and pressure gradient as follows.

Consider the forces acting on the fluid in a bed of unit cross-sectional area and thickness L . The volume of particle in the bed is $L(1-\varepsilon)$ and therefore the total surface is $SL(1-\varepsilon)$. Thus the resistance force = $R_1SL(1-\varepsilon)$. This force acting on the fluid must be equal to that produced by the pressure difference of Δp across the bed. Then, since the free cross-section of fluid is equal to ε .

$$(-\Delta p)\varepsilon = R_1 S L(1-\varepsilon) \quad \dots(2.43)$$

$$R_1 = \frac{\varepsilon(-\Delta p)}{S(1-\varepsilon)L} \quad \dots (2.44)$$

Thus

$$\frac{R_1}{\rho u_1^2} = \frac{\varepsilon^3(-\Delta p)}{S(1-\varepsilon)L \rho u^2} \quad \dots (2.45)$$

Carman [12] found that when $\frac{R_1}{\rho u_1^2}$ was plotted against Re_1 using logarithmic coordinates, gave a general equation of the form:

$$\frac{R_1}{\rho u_1^2} = 5 Re^{-1} + 0.4 Re^{-0.1} \quad \dots (2.46)$$

Sawistowski [50] compared the results obtained for flow of fluids through beds of packing and noted that equation 2.46 gave a consistently low result. He proposed the equation:

$$\frac{R_1}{\rho u_1^2} = 5 \text{Re}^{-1} + \text{Re}^{-0.1} \quad \dots (2.47)$$

Ergun [51] has obtained a good semi-empirical correlation for friction factor. He proposed the equation [27]:

$$\frac{R_1}{\rho u_1^2} = 4.17 \text{Re}^{-1} + 0.29 \quad \dots (2.48)$$

Chapter Three

Experimental Work

3.1 Aim of this work

The aim of this work is to study a single phase fluid flow through packed bed, by using air and water as a fluid, and to study the affected flow rate, packing porosity, packing particle size distribution (mono, binary, ternary) and type of fluid (either air or water) on the pressure drop and friction factor through packed bed.

3.2 Description of materials.

In this work five sizes of spherical glass particles were used. The spherical particles diameters were 0.99, 0.79, 0.6, 0.51 and 0.42cm. The true densities of these particles were 2.56, 2.51, 2.55, 2.54, and 2.47g/cm³ respectively.

The fluids used were air and water and their properties were taken at laboratory temperature of 32C° for air and 31C° for water. The physical properties (density and viscosity) are shown in table 3-1.

Table 3-1 The physical properties of fluids [32].

Type of fluid	Density (kg/m ³)	Viscosity (kg/m.s)
water	995.647	0.8*10 ⁻³
air	1.1582	1.88*10 ⁻⁵

3.3 Description of apparatus used for packed bed.

A schematic diagram of the apparatus used is shown in Fig.3-1, and photograph pictures for air and water flow are shown in figures 3-2 and 3-3 respectively.

The packed bed column was made of Pyrex glass tube (Q.V.F) 7.64 cm inside diameter and 15.15 cm height. The Q.V.F glass contains two taps at the inlet and outlet of the column. The taps used for measuring the pressure drop are placed flush to the inside surface to determine the static pressure actually. The first one was placed downstream at a distance 1 cm from the sieve entrance region and the second tap was placed at distance 1 cm from the top sieve of the column (the sieve used to avoid the bed expands into fluid like phase). The distance between the inlet and outlet to the column and the sieve was to avoid the turbulence at the bed. The column was mounted vertically and held by iron flanges.

The fluids used were air and water and each of them having its following apparatus.

3.3.1. For air flow through packed bed:

1. Air flow is produced by a compressor to the packed column. The compressor contained a vane rotary type driven by AC motor. The compressor was used to supply the air to packed bed at constant pressure.
2. A storage tank was used to receive air from the compressor and provide it to the rotameter.

3. A rotameter was used for measuring air flow rate, and the flow rate up to 16 cubic meters per hour.
4. The U-tube manometer (with ethanol) was used for measuring the pressure drop through packed column.

3.3.2 for water flow through packed bed:

1. A centrifugal pump of power (1.5kW) was used for pumping water from storage tank to the rotameter.
2. A glass (Q.V.F) storage tank of 100 liter (0.1 m³ volume) was used to provide water for pumping.
3. A rotameter was used for measuring water flow rate, and the flow rate up to 5 cubic meters per hour.
4. The inclined-tube (with mercury) was used for measuring the pressure drop through packed column.

3.4 Experimental Procedure

The particles were poured into the column until it was filled and the bed porosity was determined using equation 3.1.

$$\varepsilon = 1 - \frac{\rho_b}{\rho_t} \quad \dots (3.1)$$

Where:

ρ_b is the bulk density (g/cm³).

ρ_t is the true density of particles (g/cm³).

3.4.1. Air flow

The fluid used was air provided by the compressor and its flow rates up to 16 cubic meters per hour. It was controlled by means of a control valve at the inlet of the rotameter. The average velocity of the air was obtained from rotameter using equation 3.2.

$$u = \frac{Q}{A} \quad \dots (3.2)$$

Where

Q is the flow rate of fluid (m³/hr).

A is the bed cross-sectional area (m²).

The rotameter valve was opened for air flow. The rotameter float was ensured to achieve steady state, and the pressure drop across the bed was measured using u-tube manometer. The friction factor was obtained from pressure drop using equation 2.45.

$$\frac{R_1}{\rho u_1^2} = \frac{\varepsilon^3 (-\Delta p)}{S(1-\varepsilon)L \rho u^2}$$

3.4.2. Water flow

The working fluid used was water provided by the pump, and its flow rates up to 5 cubic meters per hour controlled by means of a control valve at the inlet of the rotameter. The rotameter valve was opened until the bed was covered with water and the column became free from bubbles. The pressure drop across the bed was measured using inclined-tube manometer. The friction factor was obtained from pressure drop using equation 2.45.

3.5 Test Method

3.5.1. True particle density

The true densities of particles were determined using shifted water method. To obtain the volume of samples, a known weight of particles was immersed in a graduated cylinder (with capacity of 500 ml) filled with water. The weight of container was measured using a sensitive balance first when the container filled with water only and second when it contains the particle besides the water. In both cases, water level inside the container was carefully maintained at its permissible full mark level. Using the following equation, true density of particles was determined [31].

$$\rho_t = \frac{w_1 \times \rho_w}{w_2 - w_3 + w_1} \quad \dots (3.3)$$

Where:

ρ_w = water density at laboratory temperature (g/cm^3)

w_1 = solid particles weight (g).

w_2 = mass of cylinder filled with water (g).

w_3 = mass of cylinder with water and particles (g).

Each measurement was repeated three times for each test bead to determine the true density value using the above method as shown in table 3-2.

Table 3-2 The true density of spherical particles.

Particle type	Diameter (cm)	ρ_t (g/cm ³)
1	0.9987	2.5597
2	0.7955	2.515
3	0.6015	2.5555
4	0.509	2.5405
5	0.421	2.4736

3.5.2 Bulk density

This index is defined by the following expression [37]:

$$\text{bulk density } (\rho_b) = \frac{\text{mass of the bed}}{\text{volume of bed}} \quad \dots (3.4)$$

For a cylindrical bed

$$\text{Volume} = \frac{\pi}{4} D^2 L$$

Where:

D=inside diameter of the cylinder (cm).

L=length of the particle in the bed (cm).

3.5.3 Bed porosity

The porosity of the bed was determined using the following equation

$$\varepsilon = 1 - \frac{\rho_b}{\rho_t} \quad \dots (3.5)$$

where

ρ_t is the true density of particle(g/cm^3).

ρ_b is the apparent bulk density(g/cm^3).

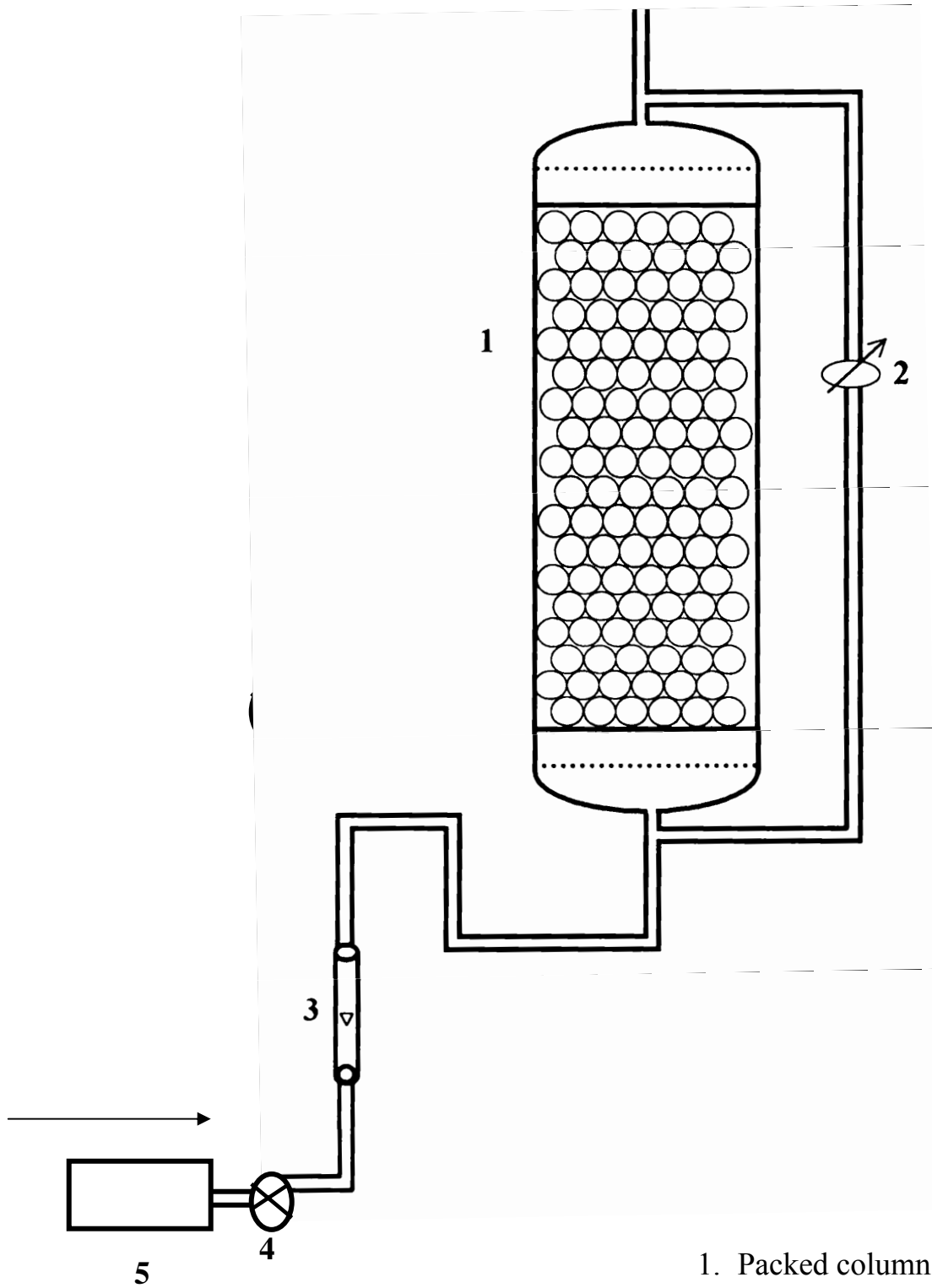
For mixture of particles, the mixture true density (ρ_{tm}) can be determined from the following equation [37].

$$\rho_{tm} = \frac{1}{\sum_{i=1}^m \frac{x_i}{\rho_{ti}}} \quad \dots (3.6)$$

As where

x_i is the mass percent of component i.

ρ_{ti} is the true density of component i(g/cm^3).



1. Packed column.
2. Differential Manometer.
3. Rotameter.
4. Control valve.
5. Compressor or pump.

Figure 3-1 A schematic diagram of the apparatus

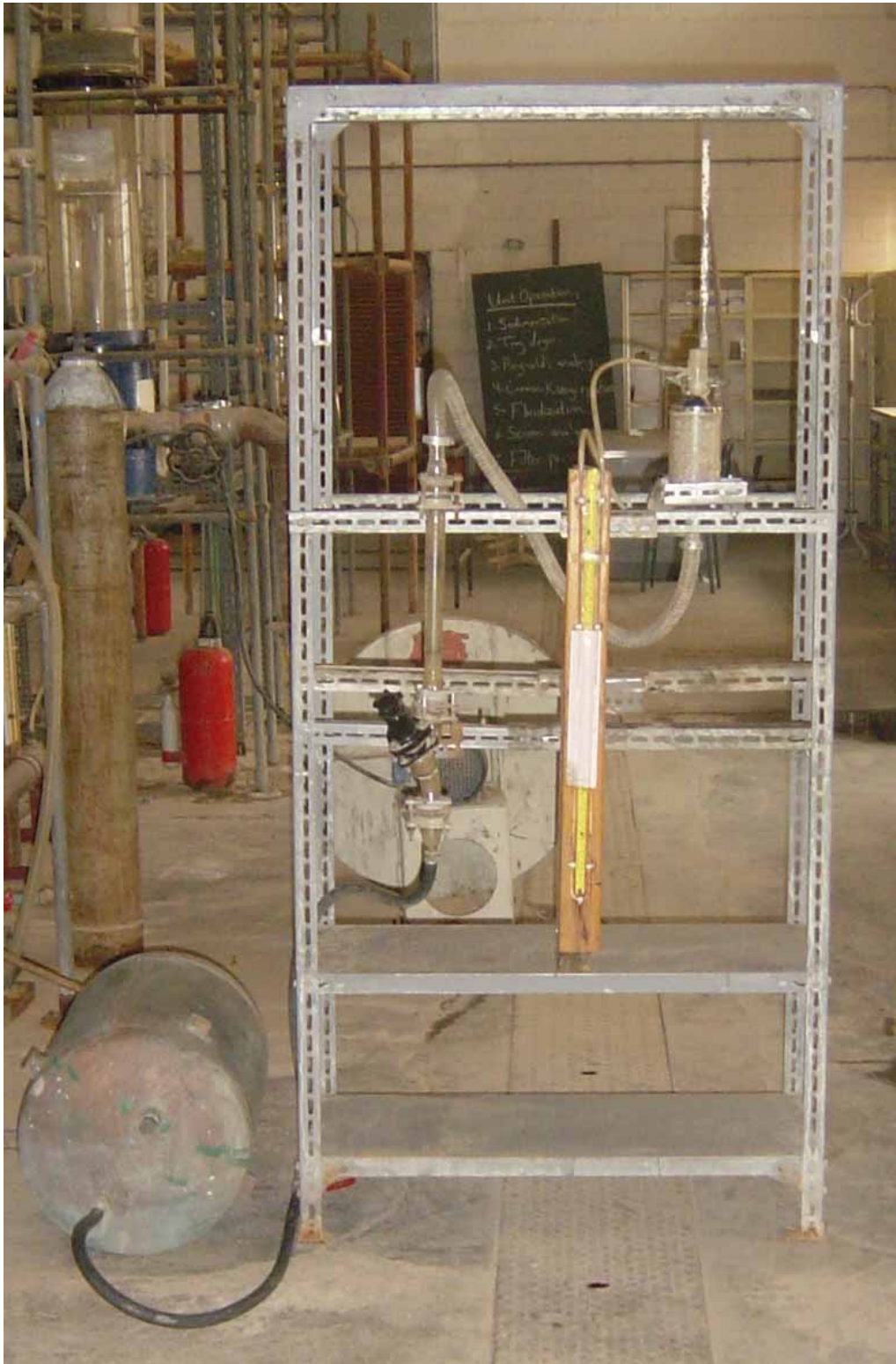


Figure 3-2 A photograph for air flow through packed bed



Figure 3-3 A photograph for water flow through packed bed

Chapter four

Results

The objective of the experimental results was to measure the friction factor for the flow of fluid (air and water) through a bed of sphere particles with the variation size distribution of packing (mono, binary and ternary), and comparing the results with results of Ergun, Carman and Sawistowski.

Tables 4-1 – 4-20 present the calculated values of friction factor of sphere particles using equation 2.45 and Reynolds number using equation 2.42.

The values of porosity, bulk density and specific surface area of the particles showed in table D.1 in appendix D.

4.1 Packing of mono size particles

4.1.1 Air flow

Table 4-1 Experiment results for spherical particles with $d_p = 0.9987$ cm and $\epsilon = 0.4508$

Q (m ³ /h)	u (m/s)	Re	Δp (Pa)	f
2	0.1211	22.5988	6.1813	0.6652
3	0.1817	33.9075	12.0938	0.5781
4	0.2424	45.2349	20.1564	0.5414
5	0.303	56.5437	29.5628	0.5082
6	0.3635	67.8338	40.3129	0.4815
7	0.4241	79.1425	55.0943	0.4834
8	0.4847	91.0111	67.1882	0.4513
9	0.5453	101.76	86.0009	0.4564
10	0.6059	113.0687	107.5012	0.4621
11	0.6665	124.3775	126.3139	0.4488
12	0.7271	135.6862	147.8141	0.4421
13	0.7877	146.995	172.0019	0.4375
14	0.8482	158.285	201.5647	0.4421
15	0.9088	169.5938	228.44	0.4365
16	0.9695	180.9212	258.0028	0.4331

Table 4-2 Experiment results for spherical particles with $d_p = 0.421$ cm and $\varepsilon = 0.3888$

Q (m ³ /h)	u (m/s)	Re	Δp (Pa)	f
2	0.1211	8.5648	33.5941	0.8808
3	0.1817	12.8507	60.4694	0.7042
4	0.2424	17.1437	92.7197	0.6067
5	0.303	21.4296	133.0327	0.5571
6	0.3635	25.7085	180.0645	0.524
7	0.4241	29.9944	231.1275	0.4941
8	0.4847	34.2804	292.9407	0.4794
9	0.5453	38.5663	354.7539	0.4587
10	0.6059	42.8523	430.0047	0.4504
11	0.6665	47.1382	510.6306	0.442
12	0.7271	51.4241	596.6315	0.4339
13	0.7877	55.7101	688.0075	0.4263
14	0.8482	59.9889	787.4461	0.4208
15	0.9088	64.2749	900.3223	0.4191
16	0.9695	68.5679	1010.511	0.4134

4.1.2 Water flow

Table 4-3 Experiment results for spherical particles with $d_p = 0.9987$ cm and $\varepsilon = 0.4508$

Q (m ³ /h)	u (m/s)	Re	Δp (kPa)	f
0.5	0.0303	114.2908	0.2056	0.4123
1	0.0606	228.5816	0.7092	0.3554
1.5	0.0909	342.8724	1.4184	0.3159
2	0.1211	456.786	2.4822	0.3115
2.5	0.1511	569.9452	3.8297	0.3087
3	0.1817	685.3676	5.2482	0.2926
3.5	0.2121	800.0356	7.0212	0.2875
4	0.2424	914.3256	9.0071	0.2821
4.5	0.2726	1028.2401	11.4184	0.2828
5	0.303	1142.908	13.9007	0.2701

Table 4-4 Experiment results for spherical particles with $d_p=0.509\text{cm}$ and $\varepsilon=0.3931$

Q (m ³ /h)	u (m/s)	Re	Δp (kPa)	f
0.5	0.0303	52.7117	0.7446	0.4565
1	0.0606	105.4235	2.5531	0.3913
1.5	0.0909	158.1353	5.3191	0.3623
2	0.1211	210.6731	8.5106	0.3266
2.5	0.1511	262.8631	12.907	0.3182
3	0.1817	316.0967	17.731	0.3023
3.5	0.2121	368.7521	23.901	0.2993
4	0.2424	421.6943	30.8511	0.2955
4.5	0.2726	474.2321	37.5886	0.2847
5	0.303	527.1179	46.0992	0.2826

4.2 Packing of binary size particles

In the packing of binary size particles the mixture contains two sizes of sphere particles. The percentage of each size is equal 1/2 from the total packing. The most noticeable effect from mixing two sizes of particle is the decrease in porosity with respect to mono size mixture, because the smaller spheres can fill the interstices of the larger spheres.

4.2.1 Air flow

Table 4-5 Experiment results for spherical particles with $d_p = 0.9987, 0.7955$ cm and $\varepsilon = 0.4232$

Q (m ³ /h)	u (m/s)	Re	Δp (Pa)	f
2	0.1211	33.3402	4.0312	0.5306
3	0.1817	50.0241	8.0625	0.4714
4	0.2424	66.7355	13.4376	0.4414
5	0.303	83.4194	20.1564	0.4238
6	0.3635	100.0758	28.2191	0.4122
7	0.4241	116.7596	37.6254	0.4038
8	0.4847	133.4435	48.3755	0.3974
9	05453	150.1274	61.8131	0.4012
10	0.6059	166.8113	75.2508	0.3956
11	0.6665	183.4952	90.0322	0.3912
12	0.7271	200.1791	106.1574	0.3876
13	0.7877	216.86302	122.2826	0.3804
14	0.8482	233.5193	142.4391	0.382
15	0.9088	250.2032	161.2518	0.3768
16	0.9695	266.9146	180.0645	0.3698

Table 4-6 Experiment results for spherical particles with $d_p = 0.9987, 0.421$ cm and $\varepsilon = 0.3822$

Q (m ³ /h)	u (m/s)	Re	Δp (Pa)	f
2	0.1211	19.5526	12.0938	0.6876
3	0.1817	29.33701	22.844	0.5769
4	0.2424	39.1375	38.9691	0.553
5	0.303	48.9219	53.7505	0.4882
6	0.3635	58.6901	75.2508	0.4749
7	0.4241	68.4745	99.4385	0.461
8	0.4847	78.2589	126.3139	0.4483
9	05453	88.0433	155.8767	0.4371
10	0.6059	97.8277	185.4395	0.4212
11	0.6665	107.6121	223.0649	0.4187
12	0.7271	117.3964	255.3153	0.4027
13	0.7877	127.1808	301.0033	0.4045
14	0.8482	136.9491	341.3162	0.3956
15	0.9088	146.733	389.6917	0.3934
16	0.9695	156.534	446.1299	0.3957

Table 4-7 Experiment results for spherical particles with $d_p = 0.7955, 0.421$ cm and $\varepsilon=0.3965$

Q (m ³ /h)	u (m/s)	Re	Δp (Pa)	f
2	0.1211	18.7976	10.7501	0.6561
3	0.1817	28.2042	21.5002	0.5829
4	0.2424	37.6264	34.9378	0.5322
5	0.303	47.033	52.4068	0.5109
6	0.3635	56.424	75.2508	0.5097
7	0.4241	65.8306	96.7511	0.4814
8	0.4847	75.2372	120.9388	0.4607
9	05453	84.6438	150.5016	0.4531
10	0.6059	94.0504	182.752	0.4455
11	0.6665	103.457	215.0023	0.4332
12	0.7271	112.8636	255.3153	0.4322
13	0.7877	122.2702	292.9407	0.4225
14	0.8482	131.6613	335.9412	0.4178
15	0.9088	141.0679	373.5666	0.4048
16	0.9695	150.49	432.6922	0.412

Table 4-8 Experiment results for spherical particles with $d_p = 0.509, 0.421$ cm and $\varepsilon=0.3933$

Q (m ³ /h)	u (m/s)	Re	Δp (Pa)	f
2	0.1211	16.1421	14.2439	0.7286
3	0.1817	24.2198	26.8752	0.6106
4	0.2424	32.3109	44.3442	0.5661
5	0.303	40.3887	64.5007	0.527
6	0.3635	48.4531	91.376	0.5187
7	0.4241	56.5308	119.5951	0.4988
8	0.4847	64.6085	150.5016	0.4805
9	05453	72.6863	188.1271	0.4746
10	0.6059	80.764	225.7525	0.4613
11	0.6665	88.8418	271.4405	0.4583
12	0.7271	96.9195	311.7534	0.4423
13	0.7877	104.9973	365.504	0.4419
14	0.8482	113.0617	419.2546	0.4371
15	0.9088	121.1394	475.6927	0.432
16	0.9695	129.2305	537.5059	0.4289

4.2.2 Water flow

Table 4-9 Experiment results for spherical particles with $d_p = 0.9987, 0.7955$ cm and $\varepsilon=0.4232$

Q (m ³ /h)	u (m/s)	Re	Δp (kPa)	f
0.5	0.0303	159.7724	0.1560	0.3816
1	0.0606	319.5449	0.5319	0.3252
1.5	0.0909	479.3174	1.1347	0.3083
2	0.1211	638.5625	1.8439	0.2823
2.5	0.1511	796.753	2.9787	0.2929
3	0.1817	958.1075	4.5390	0.3087
3.5	0.2121	1118.4072	5.6737	0.2834
4	0.2424	1277.6524	7.3049	0.2791
4.5	0.2726	1437.4249	9.2198	0.2786
5	0.303	1597.7246	10.992	0.2688

Table 4-10 Experiment results for spherical particles with $d_p = 0.9987, 0.421$ cm and $\varepsilon=0.3822$

Q (m ³ /h)	u (m/s)	Re	Δp (kPa)	f
0.5	0.0303	98.831	0.3971	0.4196
1	0.0606	197.662	1.3475	0.3559
1.5	0.0909	296.493	2.8368	0.333
2	0.1211	394.9978	4.7517	0.3143
2.5	0.1511	429.8503	7.4468	0.3163
3	0.1817	592.6598	10.5673	0.3104
3.5	0.2121	691.8171	13.8297	0.2984
4	0.2424	790.6481	17.7305	0.2927
4.5	0.2726	889.1529	21.9858	0.2869
5	0.303	988.3101	26.9503	0.2847

Table 4-11 Experiment results for spherical particles with $d_p = 0.7955, 0.421$ cm and $\varepsilon=0.3965$

Q (m ³ /h)	u (m/s)	Re	Δp (kPa)	f
0.5	0.0303	95.015	0.3829	0.4343
1	0.0606	1902.03	1.3120	0.3721
1.5	0.0909	285.0451	2.8368	0.3574
2	0.1211	379.7466	4.9645	0.3524
2.5	0.1511	473.8209	7.3049	0.3331
3	0.1817	569.776	10.2836	0.3243
3.5	0.2121	665.1053	13.6170	0.3154
4	0.2424	760.1203	17.3049	0.3066
4.5	0.2726	854.8218	21.6312	0.3030
5	0.303	950.1504	26.0283	0.2951

Table 4-12 Experiment results for spherical particles with $d_p = 0.509, 0.421$ cm and $\varepsilon=0.3933$

Q (m ³ /h)	u (m/s)	Re	Δp (kPa)	f
0.5	0.0303	81.5923	0.4255	0.4044
1	0.0606	163.1847	1.4184	0.3370
1.5	0.0909	244.7771	3.1914	0.3370
2	0.1211	326.1002	5.31914	0.3165
2.5	0.1511	406.8847	8.0851	0.3090
3	0.1817	489.285	11.4893	0.3036
3.5	0.2121	571.1466	14.8936	0.2891
4	0.2424	652.739	19.5035	0.2896
4.5	0.2726	734.0621	24.1134	0.2831
5	0.303	815.9238	28.3687	0.2696

4.3 Packing of ternary size particles

In the Packing of ternary size particles the mixture contains three sizes of sphere particle. The percentage of each size is equal 1/3 from the total packing.

4.3.1 Air flow

Table 4-13 Experiment results for spherical particles with $d_p = 0.9987, 0.509, 0.421$ cm and $\epsilon=0.3838$

Q (m ³ /h)	u (m/s)	Re	Δp (Pa)	f
2	0.1211	18.3931	13.1688	0.7132
3	0.1817	27.5972	25.5315	0.6142
4	0.2424	36.8165	41.6567	0.5631
5	0.303	46.0207	61.8131	0.5348
6	0.3635	55.0965	83.3134	0.5008
7	0.4241	64.4137	115.5637	0.5103
8	0.4847	73.6179	142.439	0.4815
9	0.5453	82.822	177.3769	0.4738
10	0.6059	92.0262	212.3148	0.4593
11	0.6665	101.2303	249.9402	0.4469
12	0.7271	110.4345	292.9407	0.4401
13	0.7877	119.6386	341.3162	0.4369
14	0.8482	128.8275	389.6917	0.4302
15	0.9088	138.0317	440.7548	0.4238
16	0.9695	147.251	499.8804	0.4224

Table 4-14 Experiment results for spherical particles with $d_p = 0.7955, 0.6015, 0.509$ cm and $\varepsilon=0.3985$

Q (m ³ /h)	u (m/s)	Re	Δp (Pa)	f
2	0.1211	21.1092	9.6751	0.6732
3	0.1817	31.6726	18.8127	0.5814
4	0.2424	42.2534	30.9065	0.5367
5	0.303	52.8167	47.0317	0.5227
6	0.3635	63.3627	65.3069	0.5043
7	0.4241	73.926	86.0009	0.4879
8	0.4847	84.489	108.8449	0.4727
9	05453	95.0527	134.3765	0.4611
10	0.6059	105.6161	161.2517	0.4482
11	0.6665	116.1795	190.8146	0.4383
12	0.7271	126.7428	223.0649	0.4305
13	0.7877	137.306	258.0028	0.4243
14	0.8482	147.852	292.9407	0.4154
15	0.9088	158.4155	333.2536	0.4117
16	0.9695	168.9963	381.6291	0.4143

Table 4-15 Experiment results for spherical particles with $d_p = 0.7955, 0.6015, 0.421$ cm and $\varepsilon=0.3984$

Q (m ³ /h)	u (m/s)	Re	Δp (Pa)	f
2	0.1211	19.2761	10.21261	0.6484
3	0.1817	28.922	20.15647	0.5684
4	0.2424	38.5839	32.25035	0.511
5	0.303	48.2299	48.37552	0.4906
6	0.3635	57.86	67.18823	0.4734
7	0.4241	67.506	86.00093	0.4452
8	0.4847	77.152	112.8762	0.4473
9	05453	86.798	139.7515	0.4376
10	0.6059	96.444	169.3143	0.4294
11	0.6665	106.09	201.5647	0.4225
12	0.7271	115.736	241.8776	0.426
13	0.7877	125.382	274.128	0.4113
14	0.8482	135.0121	314.4409	0.4069
15	0.9088	144.6581	357.4414	0.4029
16	0.9695	154.32	400.4418	0.3966

Table 4-16 Experiment results for spherical particles with $d_p = 0.7955, 0.509, 0.421\text{cm}$ and $\varepsilon=0.3836$

Q (m ³ /h)	u (m/s)	Re	Δp (Pa)	f
2	0.1211	17.544	13.43765	0.6934
3	0.1817	26.3233	26.87529	0.615
4	0.2424	35.117	44.34423	0.5711
5	0.303	43.8963	61.81317	0.5095
6	0.3635	52.661	88.68846	0.5079
7	0.4241	61.4403	115.5637	0.4862
8	0.4847	70.2195	147.8141	0.4761
9	0.5453	78.9988	182.752	0.4651
10	0.6059	87.7781	225.7524	0.4653
11	0.6665	96.5573	260.6903	0.4441
12	0.7271	105.3366	306.3783	0.4385
13	0.7877	114.1158	349.3788	0.4261
14	0.8482	122.8806	403.1294	0.424
15	0.9088	131.6599	454.1924	0.4161
16	0.9695	140.4536	510.6305	0.4111

4.3.2 Water flow

Table 4-17 Experiment results for spherical particles with $d_p = 0.9987, 0.509, 0.421\text{ cm}$ and $\varepsilon=0.3838$

Q (m ³ /h)	u (m/s)	Re	Δp (kPa)	f
0.5	0.0303	92.79002	0.4539	0.4568
1	0.0606	185.94	1.4893	0.3747
1.5	0.0909	278.91	3.1914	0.3569
2	0.1211	371.5732	5.6737	0.3574
2.5	0.1511	463.6227	8.5106	0.3444
3	0.1817	557.5133	12.0567	0.3374
3.5	0.2121	650.7901	16.3121	0.3353
4	0.2424	743.7602	20.5673	0.3234
4.5	0.2726	836.4233	25.6737	0.3192
5	0.303	929.7002	30.8511	0.3105

Table 4-18 Experiment results for spherical particles with $d_p = 0.7955, 0.6015, 0.509$ cm and $\varepsilon=0.3985$

Q (m ³ /h)	u (m/s)	Re	Δp (kPa)	f
0.5	0.0303	106.6993	0.319149	0.382385
1	0.0606	213.3986	1.053191	0.315467
1.5	0.0909	320.098	2.297872	0.305908
2	0.1211	426.4452	4.085106	0.306413
2.5	0.1511	532.0881	5.93617	0.286003
3	0.1817	639.8439	8.361701	0.278598
3.5	0.2121	746.8953	11.48936	0.280936
4	0.2424	853.5947	14.04255	0.193691
4.5	0.2726	959.9419	17.87234	0.264559
5	0.303	1066.9934	21.51064	0.257727

Table 4-19 Experiment results for spherical particles with $d_p = 0.7955, 0.6015, 0.421$ cm and $\varepsilon=0.3984$

Q (m ³ /h)	u (m/s)	Re	Δp (kPa)	f
0.5	0.0303	97.4331	0.3687	0.4351
1	0.0606	194.8663	1.2765	0.3764
1.5	0.0909	292.2994	2.6241	0.3439
2	0.1211	389.411	4.5390	0.3352
2.5	0.1511	485.8795	6.8085	0.3229
3	0.1817	584.2773	9.4326	0.3094
3.5	0.2121	682.032	12.7659	0.3076
4	0.2424	779.4652	16.3121	0.3006
4.5	0.2726	876.5768	20.2127	0.2945
5	0.303	974.3315	24.1134	0.2844

Table 4-20 Experiment results for spherical particles with
 $d_p = 0.7955, 0.509, 0.421$ cm and $\epsilon=0.3836$

Q (m ³ /h)	u (m/s)	Re	Δp (kPa)	f
0.5	0.0303	88.6783	0.4893	0.4691
1	0.0606	177.3566	1.7731	0.4248
1.5	0.0909	266.035	3.7588	0.4002
2	0.1211	354.4207	6.0283	0.3617
2.5	0.1511	442.221	9.21985	0.3553
3	0.1817	531.7774	13.1205	0.3496
3.5	0.2121	620.7484	17.5177	0.3429
4	0.2424	709.4267	22.5531	0.3377
4.5	0.2726	794.8124	28.0851	0.3325
5	0.303	886.7834	34.0425	0.3262

Chapter five

Discussion

5.1 Packing of mono size particles

5.1.1 Air flow

The values of friction factor for air flow are plotted versus Reynolds number as shown in figures 5-1 to 5-5

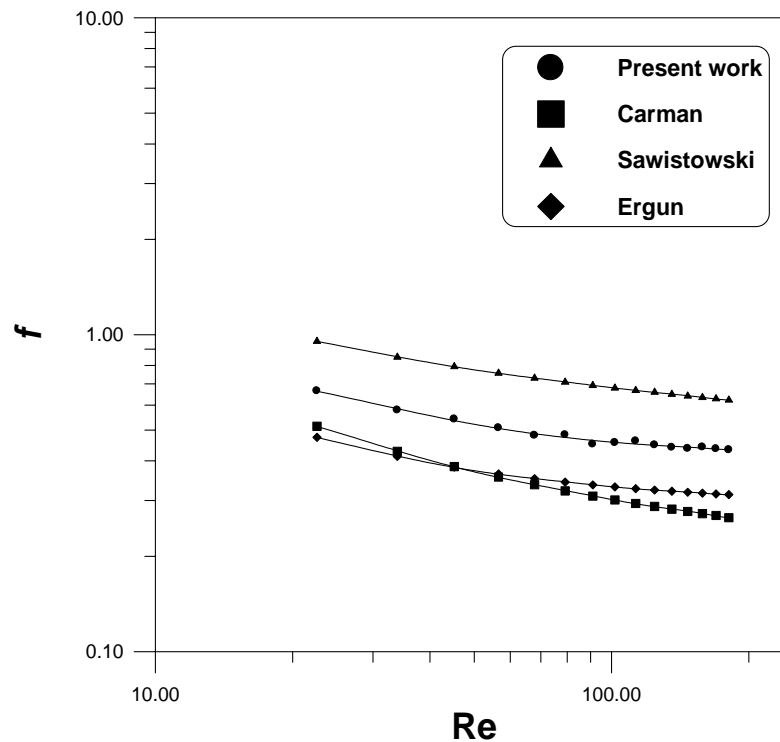


Figure 5-1 Friction factor versus Reynolds number for spherical particles with $d_p=0.9987$ cm and $\varepsilon=0.4505$ (Table 4-1)

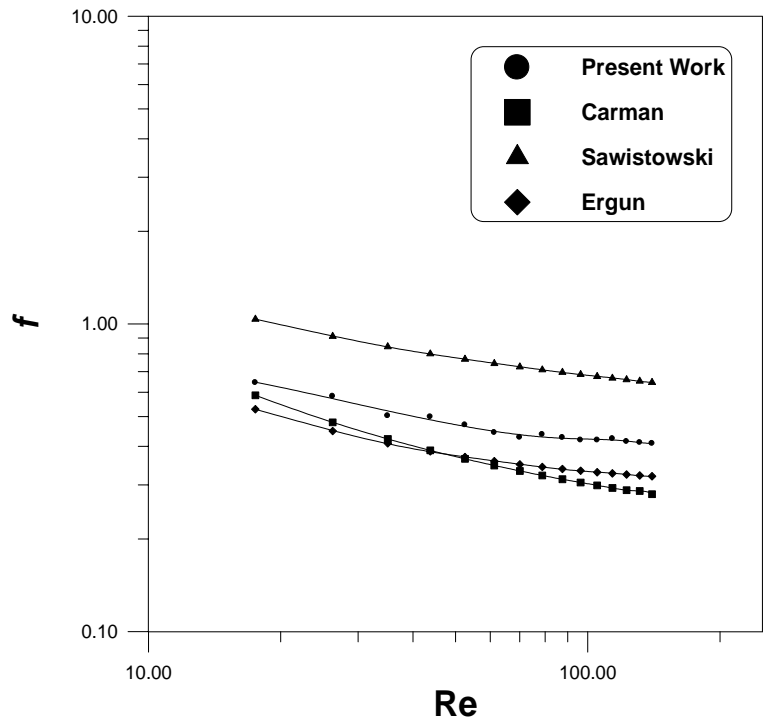


Figure 5-2 Friction factor versus Reynolds number for spherical particles with $d_p=0.7955$ cm and $\epsilon=0.4349$ (Appendix A-1)

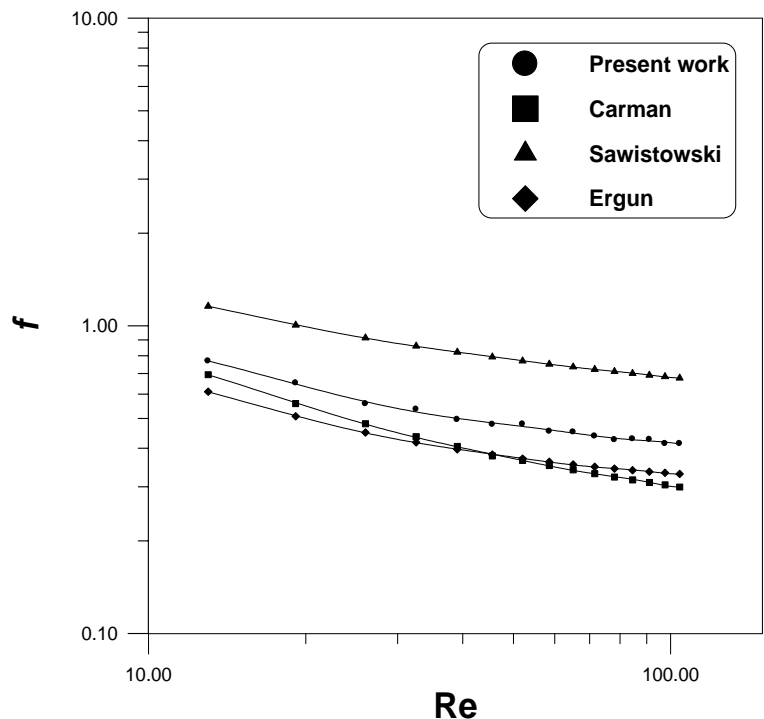


Figure 5-3 Friction factor versus Reynolds number for spherical particles with $d_p=0.6015$ cm and $\epsilon=0.4249$ (Appendix A-2)

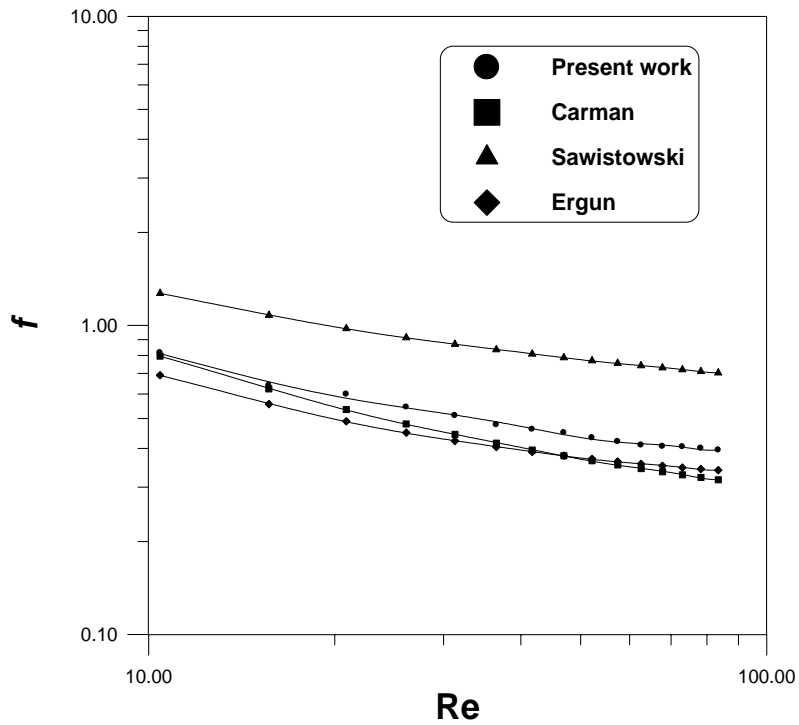


Figure 5-4 Friction factor versus Reynolds number for spherical particles with $d_p=0.509$ cm and $\epsilon=0.3931$ (Appendix A-3)

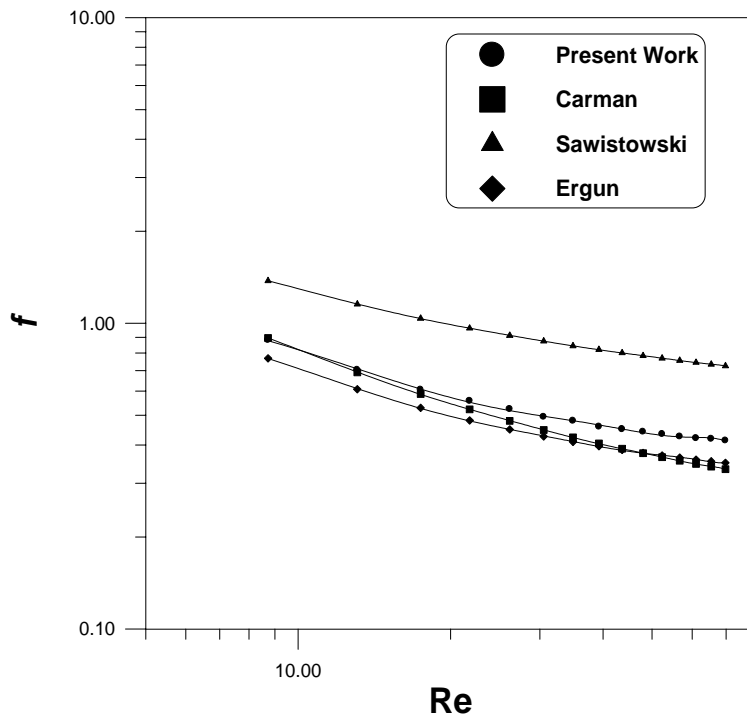


Figure 5-5 Friction factor versus Reynolds number for spherical particles with $d_p=0.421$ cm and $\epsilon=0.3888$ (Table 4-2)

The wall affect on the bed porosity and increase its value, this appears in Fig. 5-1 where the bed porosity increases to a value of 0.4505, this wall effect may be due to that the ratio of bed diameter (7.64 cm) to the particles diameter (0.9987 cm) is less than the supposed ratio ($\frac{D}{d_p} \geq 10$)[21].

Examining Figs. 5-1 to 5-5 show that the values of friction factor of Fig.5-1 decrease slightly with increasing Reynolds number values rather than that of Fig. 5-5 decrease sharply with increasing Reynolds numbers, because the Reynolds number of Fig. 5-1 is at the transition and turbulent regions (where the friction factor-Reynolds number curve become more linear) while the Reynolds number of Fig. 5-5 is at the laminar and transition regions

It can be noticed that the pressure drop values in table 4-1 range 6.1-25.8 Pa are less than those in table 4-2 range 33.6-1010.5 Pa, because of porosity in table 4-1(0.4505) is greater than in table 4-2 (0.3888), as the porosity decreased the pressure drop will be increased [8]. And the specific surface area in table 4-1 (600.781m^{-1}) is less than in table 4-2 (1425.1784m^{-1}), as the surface area of particles increased the resistance of fluid flow increased.

The best fitting for the experimental data for mono size systems for spherical particles are represented by the following equation.

$$\frac{R_1}{\rho u_1^2} = 3.21\text{Re}^{-1} + 0.61\text{Re}^{-0.1} \quad \dots (5.1)$$

with a correlation coefficient of 0.9419 and a percentage of average errors of 5.82341%.

5.1.2 Water flow

The values of friction factor for water flow are plotted versus Reynolds number as shown in figures 5-6 to 5-10

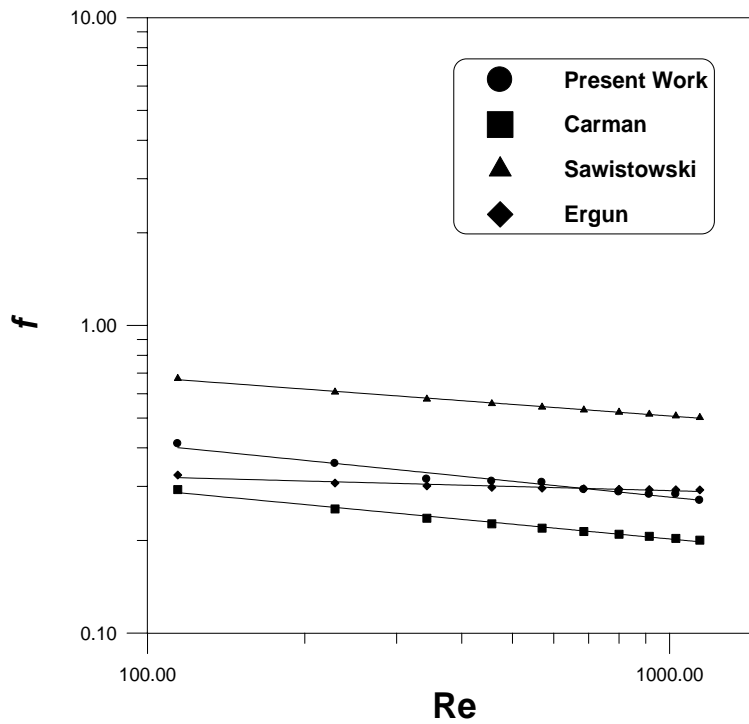


Figure 5-6 Friction factor versus Reynolds number for spherical particles with $d_p=0.9987$ cm and $\varepsilon=0.4505$ (Table 4-3)

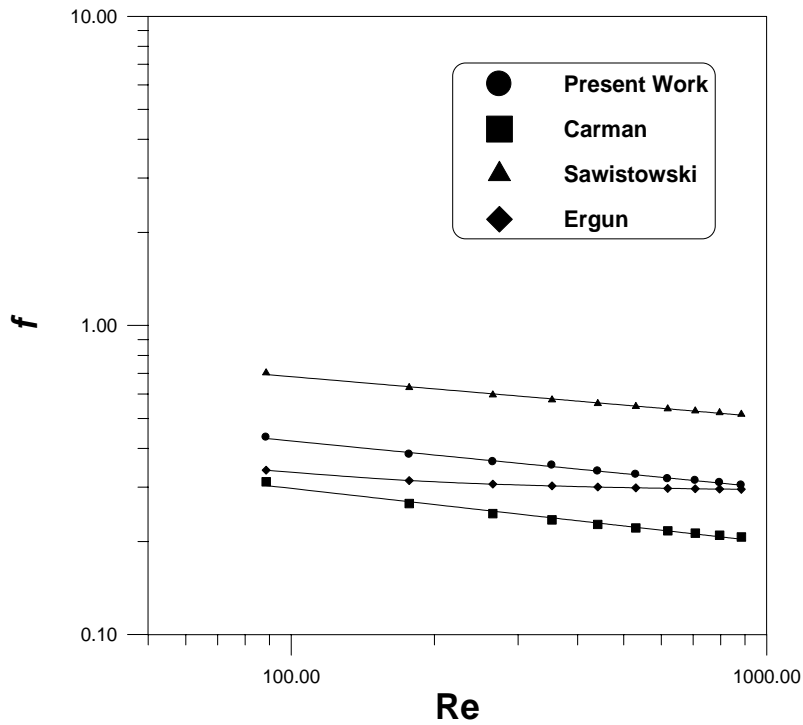


Figure 5-7 Friction factor versus Reynolds number for spherical particles with $d_p=0.7955$ cm and $\epsilon=0.4349$ (Appendix A-4)

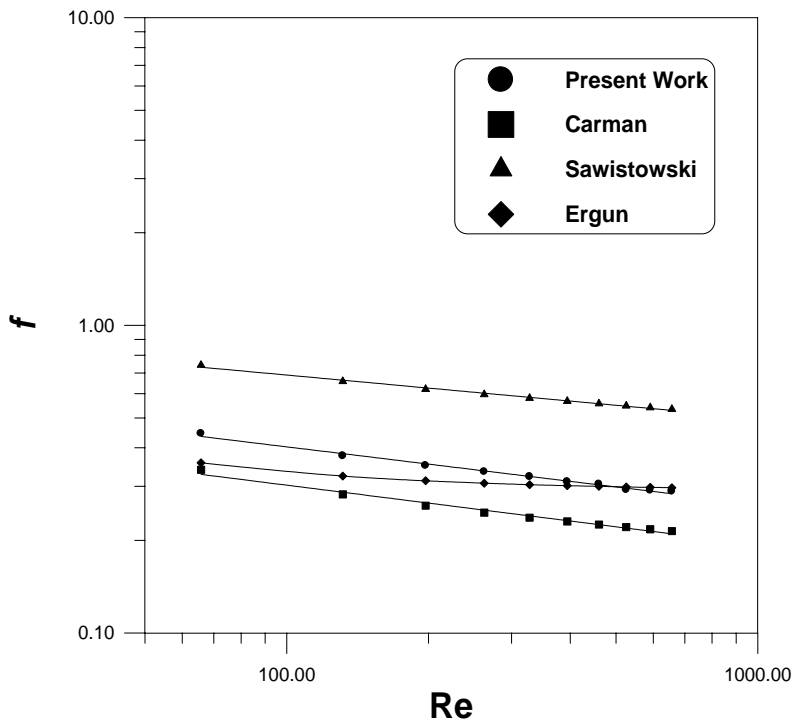


Figure 5-8 Friction factor versus Reynolds number for spherical particles with $d_p=0.6015$ cm and $\epsilon=0.4249$ (Appendix A-5)

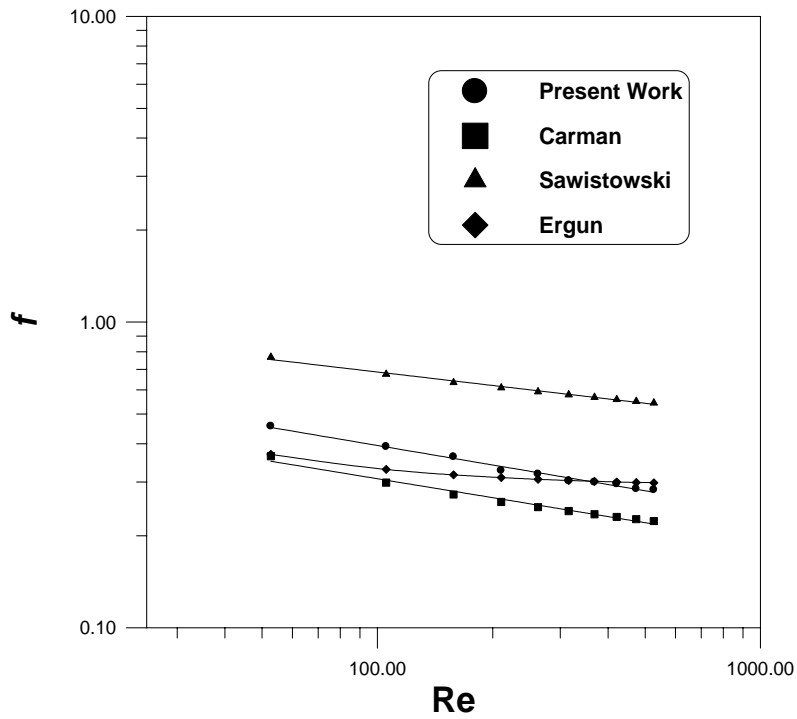


Figure 5-9 Friction factor versus Reynolds number for spherical particles with $d_p=0.509\text{cm}$ and $\varepsilon=0.3931$ (Table 4-4)

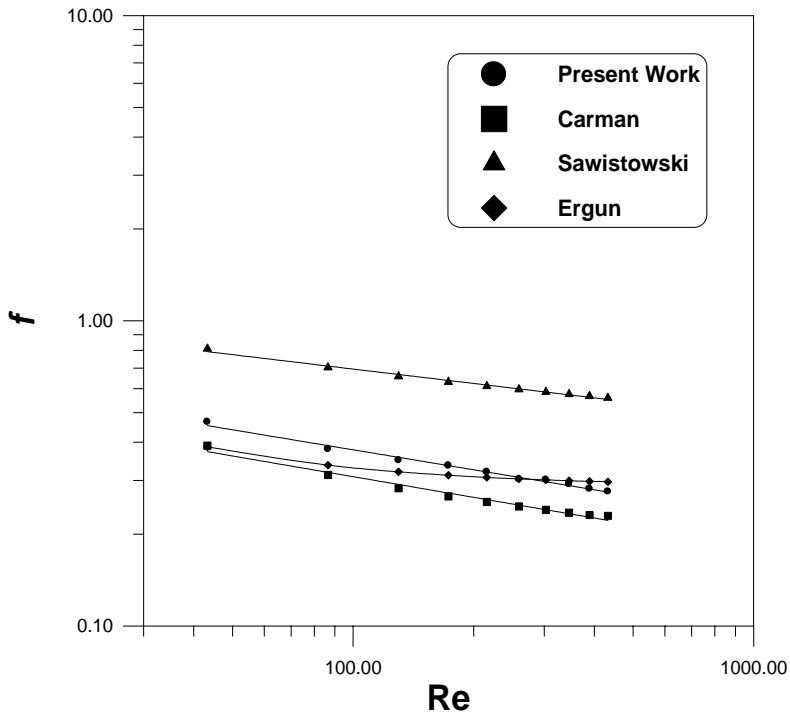


Figure 5-10 Friction factor versus Reynolds number for spherical particles with $d_p=0.421\text{cm}$ and $\varepsilon=0.3888$ (Appendix A)

These figures showed that the values of friction factor decreased as Reynolds number increased.

Figures 5-6 to 5-10 show that as the particle size decreases from 0.99 to 0.42 cm, the bed porosity decreases from 0.4508 to 0.3888 and the Reynolds number values decrease from the range of 114- 1142 (Fig 5.6) to the range of 43-432 (Fig 5.10) which lead to increase the friction factor values from the range of 0.41-0.27 (Fig. 5-6) to the range of 0.46-0.28 (Fig. 5-10).

It can be noticed that for the same flow rate the water pressure drop is greater than air pressure drop, in table 4-3 (for water for $\epsilon=0.4508$) at superficial velocity 0.1211 m/s the value of pressure drop 2801.4 Pa is greater than in table 4-1 (for air for $\epsilon=0.4508$) 6.2 Pa, this is due to the physical properties of fluid.

The best fitting for the experimental data for mono size systems for spherical particles are represented by the following equation.

$$\frac{R_1}{\rho u_1^2} = 3.88 \text{Re}^{-1} + 0.56 \text{Re}^{-0.1} \quad \dots (5.2)$$

with a correlation coefficient of 0.8488 and a percentage of average errors of 6.6766%.

Comparison of the results of air and water flow show that the values of water flow friction factor are close to those of air flow for approximately near value of Reynolds number, e.g., at near values of Reynolds number 65.06 (Fig. 5-3) and 65.73 (Fig. 5-8), the friction factor values are 0.4518 (Fig 5-3) and 0.4451 (Fig. 5-8) approximately near each other.

5.2 Packing of binary size particles

5.2.1 Air flow

The values of air flow friction factor for binary size particles are plotted versus Reynolds number as shown in figures 5-11 to 5-20

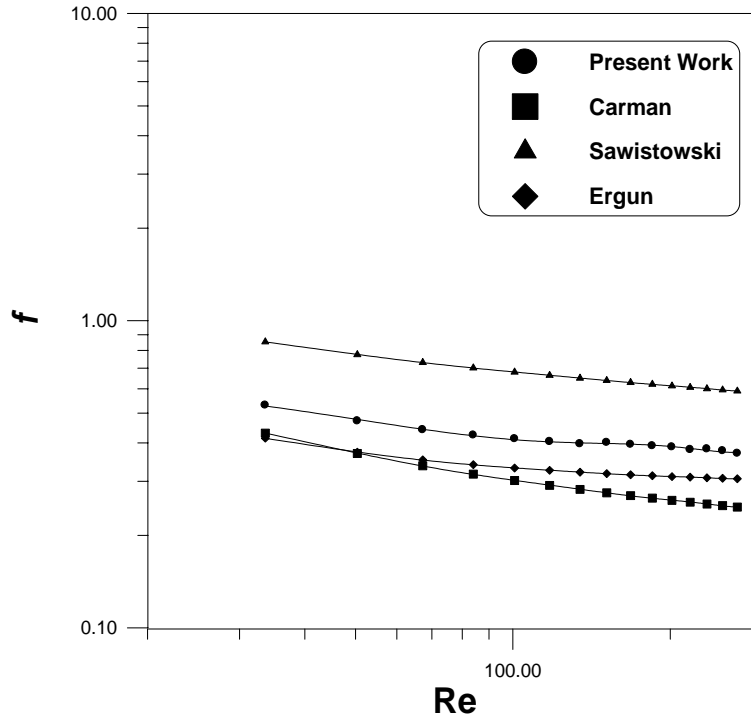


Figure 5-11 Friction factor versus Reynolds number for spherical particles with $d_p = 0.9987, 0.7955$ cm and $\epsilon = 0.4232$ (Table 4-5)

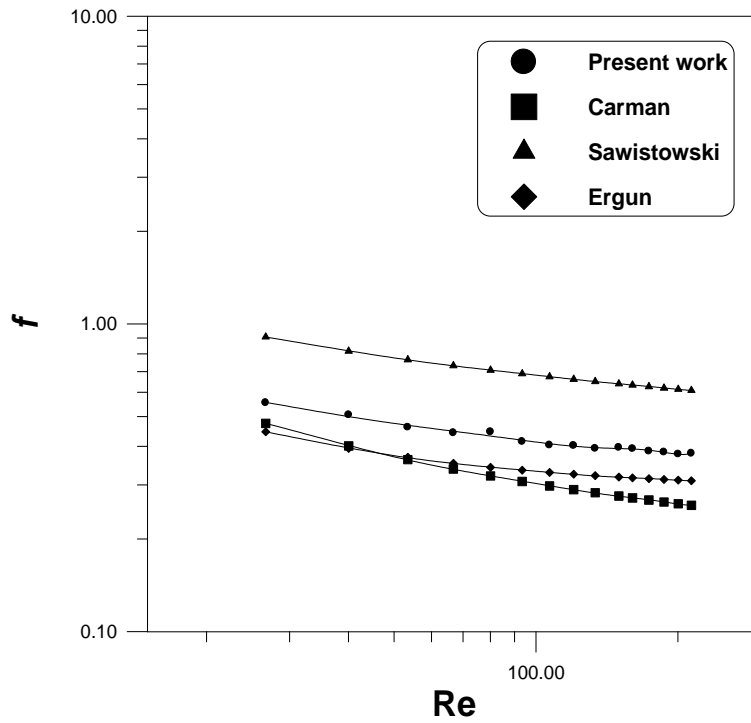


Figure 5-12 Friction factor versus Reynolds number for spherical particles with $d_p = 0.9987, 0.6015$ cm and $\epsilon = 0.4186$ (Appendix B-1)

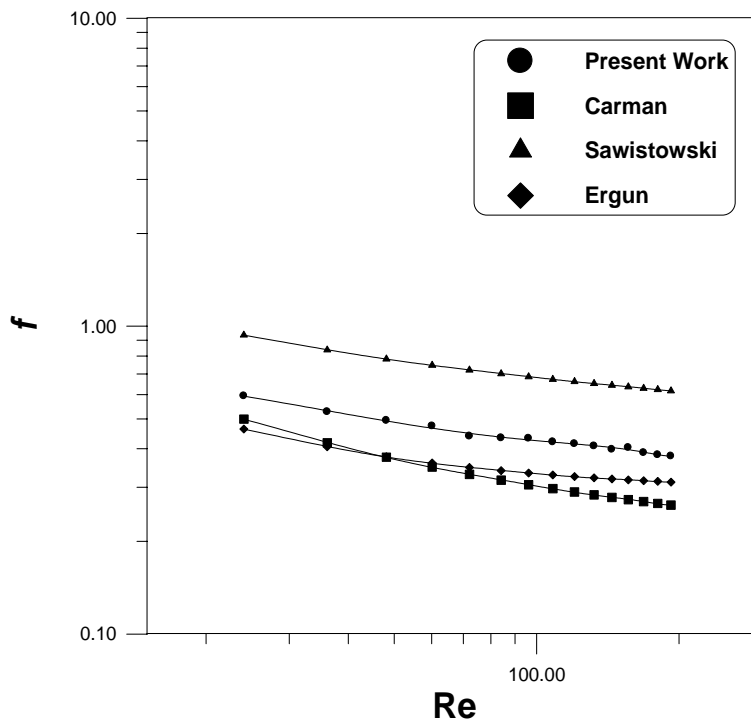


Figure 5-13 Friction factor versus Reynolds number for spherical particles with $d_p = 0.9987, 0.509$ cm and $\epsilon = 0.4171$ (Appendix B-2)

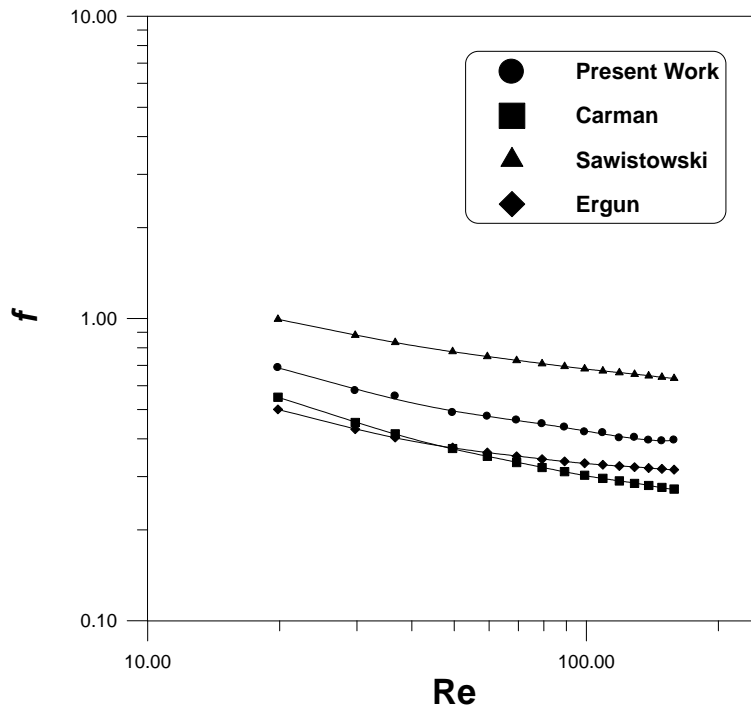


Figure 5-14 Friction factor versus Reynolds number for spherical particles with $d_p = 0.9987, 0.421$ cm and $\epsilon = 0.3822$ (Table 4-6)

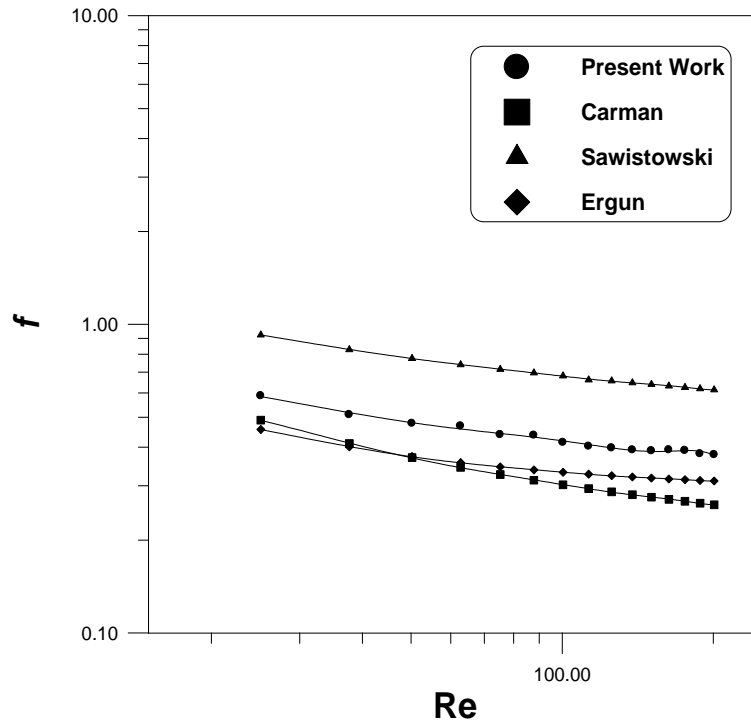


Figure 5-15 Friction factor versus Reynolds number for spherical particles with $d_p = 0.7955, 0.6015$ cm and $\epsilon = 0.4173$ (Appendix B-3)

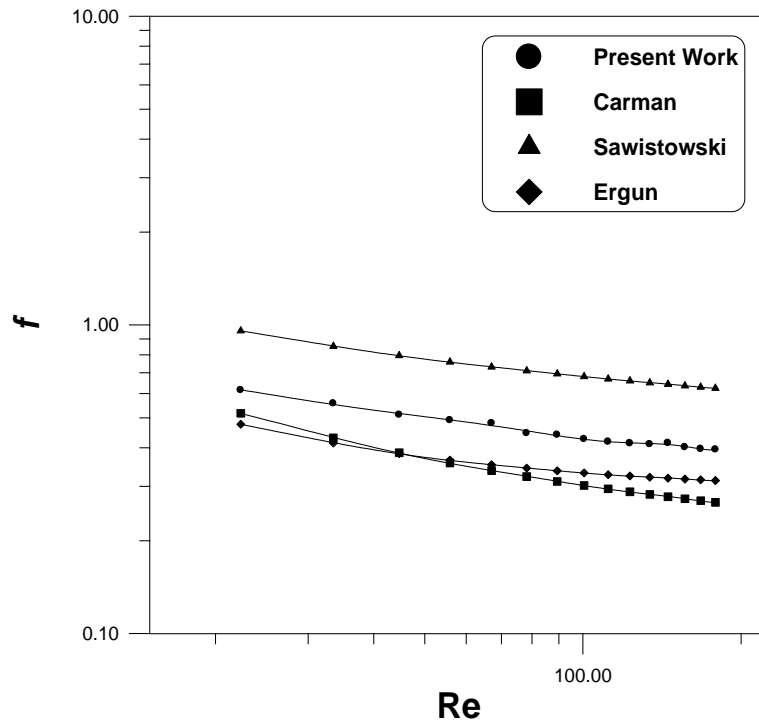


Figure 5-16 Friction factor versus Reynolds number for spherical particles with $d_p = 0.7955, 0.509$ cm and $\epsilon = 0.4166$ (Appendix B-4)

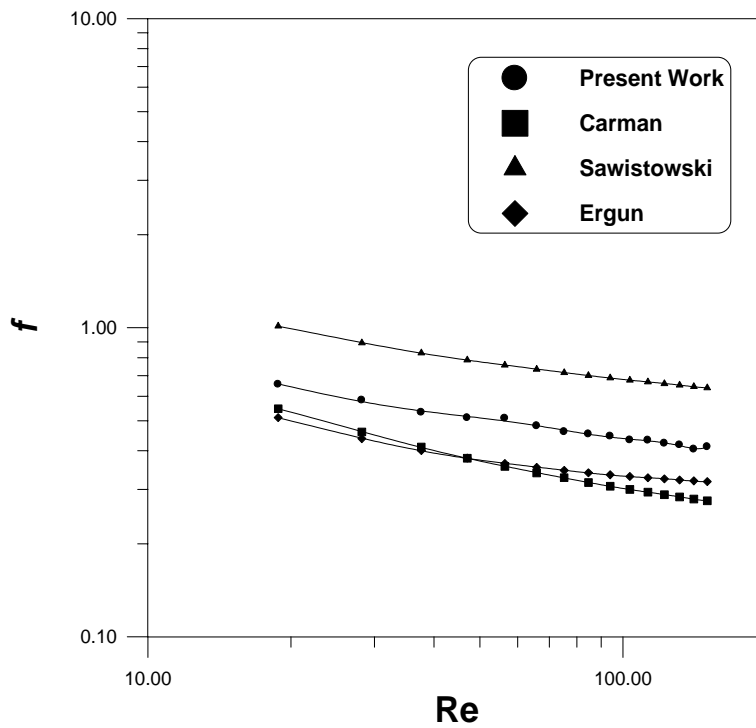


Figure 5-17 Friction factor versus Reynolds number for spherical particles with $d_p = 0.7955, 0.421$ cm and $\epsilon = 0.3965$ (Table 4-7)

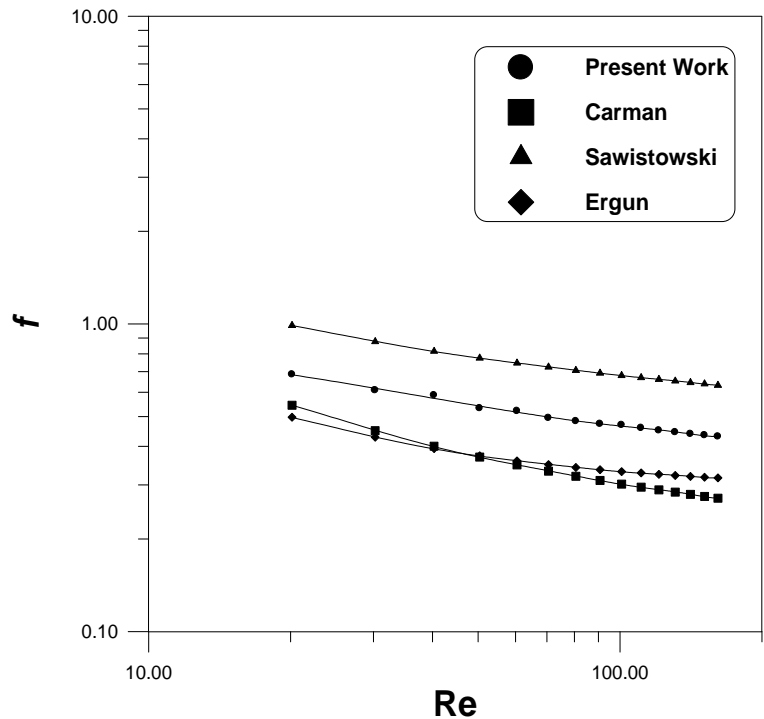


Figure 5-18 Friction factor versus Reynolds number for spherical particles with $d_p = 0.6015, 0.509$ cm and $\epsilon = 0.4186$ (Appendix B-5)

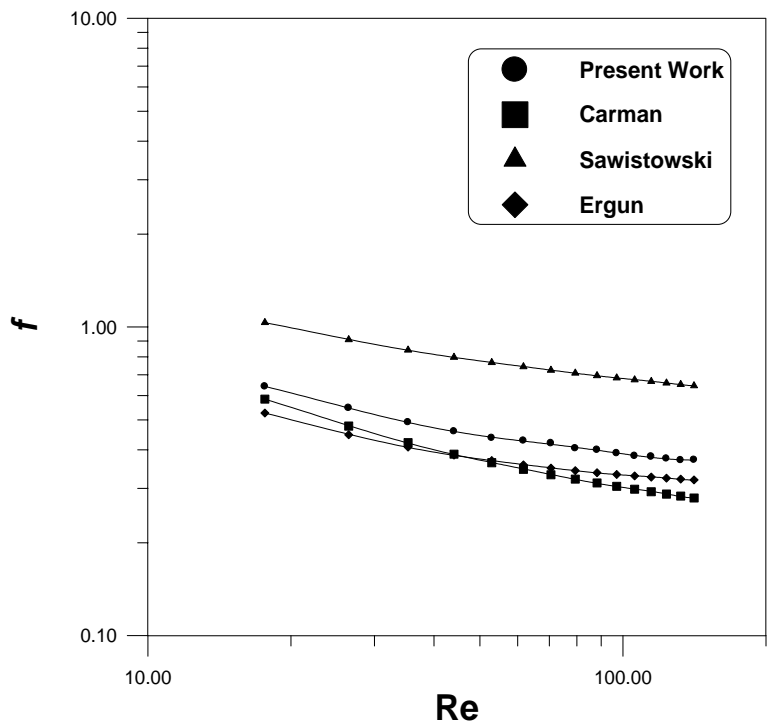


Figure 5-19 Friction factor versus Reynolds number for spherical particles with $d_p = 0.6015, 0.421$ cm and $\epsilon = 0.409$ (Appendix B-6)

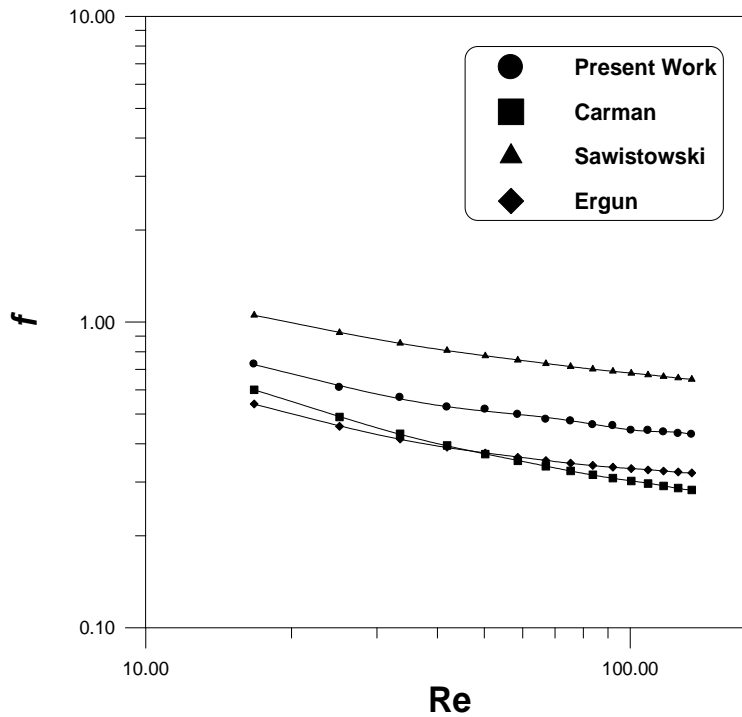


Figure 5-20 Friction factor versus Reynolds number for spherical particles with $d_p = 0.509, 0.421\text{cm}$ and $\epsilon = 0.3933$ (Table 4-8)

The most noticeable effect from mixing two sizes of particle is the decrease in porosity with respect to mono size mixture, because the smaller spheres can fill the interstices of the larger spheres [42].

It can be noticed the values of air friction factor for binary size particles is less than those for mono size particles for the approximately near values of porosity. e.g., in Fig. 5-20 (binary size particles) and 5-4 (mono size particles) which have porosity 0.3933, 0.3931 respectively, the values of friction factor in Fig. 5-20 range 0.72-0.42 are less than those in Fig. 5-4 range 0.81-0.39, because the surface area of binary size particles (761.7m^{-1}) is less than it for mono size particles (1178.7m^{-1}). As the surface area increases the values of Reynolds

number decreases ($Re_1 = \frac{\rho u}{S(1-\varepsilon)\mu}$) which lead to increases the values of friction factor.

The following equation is the best fitting for experimental data in binary system for spherical particles.

$$\frac{R_1}{\rho u_1^2} = 3.81Re^{-1} + 0.61Re^{-0.1} \quad \dots (5.3)$$

with a correlation coefficient of 0.9525 and a percentage of average errors of 3.52771%.

5.2.1 Water flow

The values of friction factor for water flow are plotted versus Reynolds number as shown in figures 5-21 to 5-30

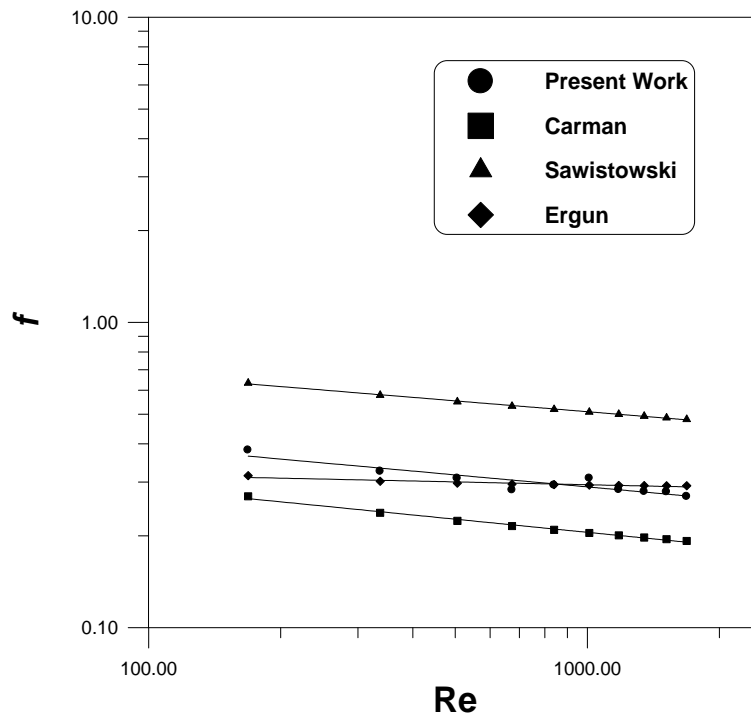


Figure 5-21 Friction factor versus Reynolds number for spherical particles with $d_p = 0.9987, 0.7955\text{cm}$ and $\varepsilon = 0.4232$ (Table 4-9)

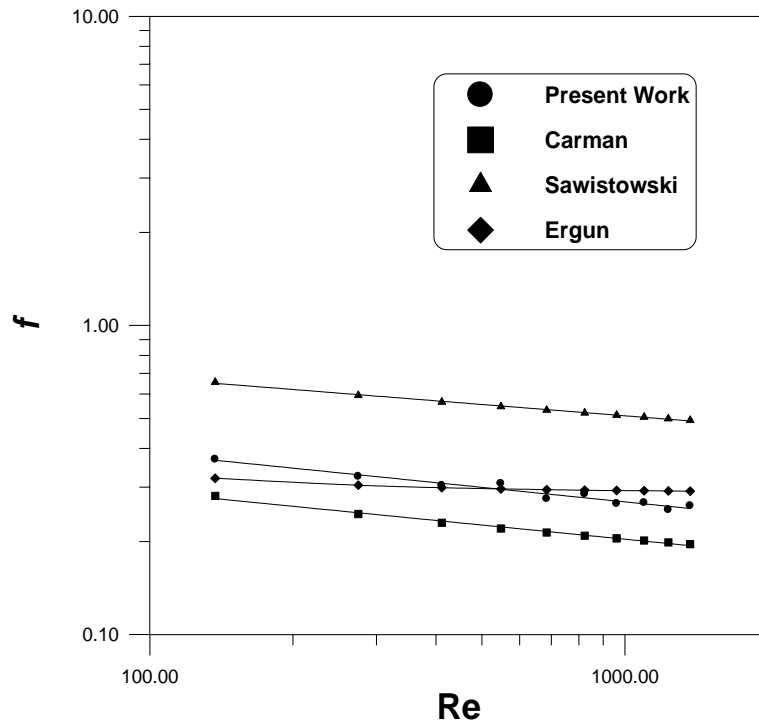


Figure 5-22 Friction factor versus Reynolds number for spherical particles with $d_p = 0.9987, 0.6015$ cm and $\epsilon = 0.4186$ (Appendix B-7)

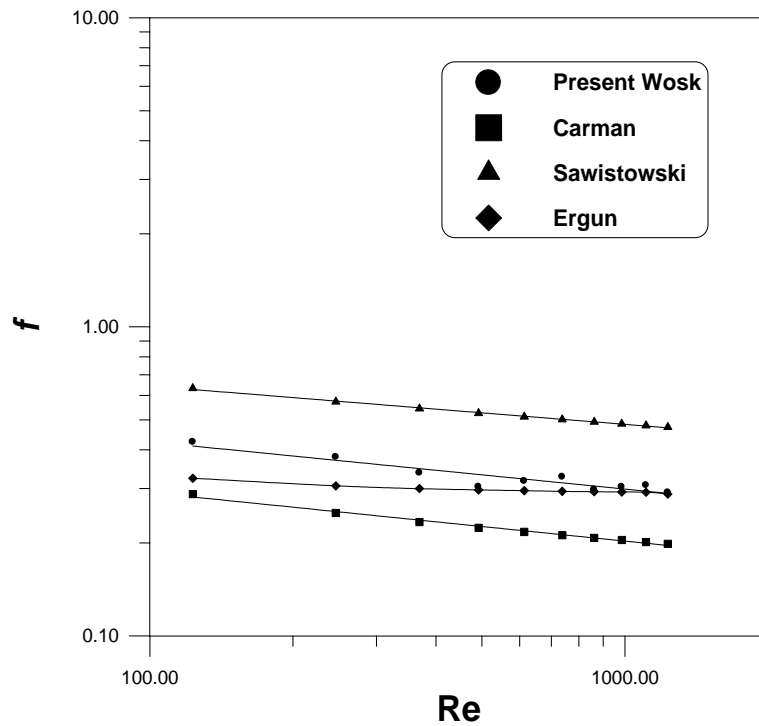


Figure 5-23 Friction factor versus Reynolds number for spherical particles with $d_p = 0.9987, 0.509$ cm and $\epsilon = 0.4171$ (Appendix B-8)

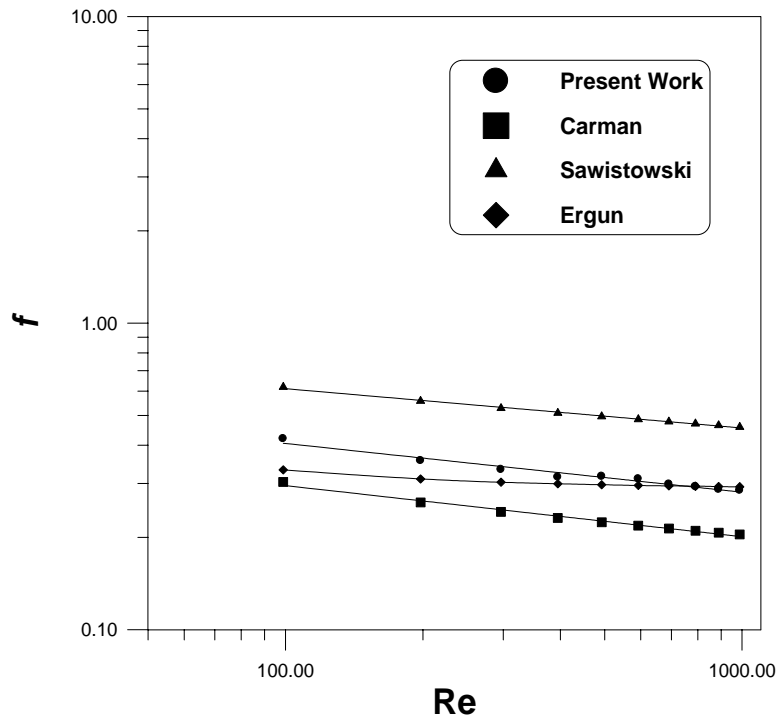


Figure 5-24 Friction factor versus Reynolds number for spherical particles with $d_p = 0.9987, 0.421$ cm and $\epsilon = 0.3822$ (Table 4-10)

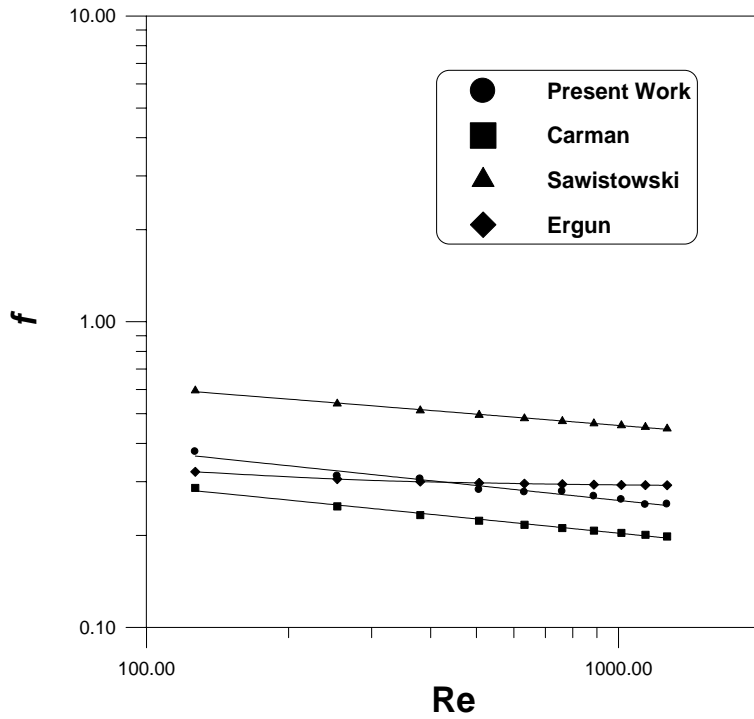


Figure 5-25 Friction factor versus Reynolds number for spherical particles with $d_p = 0.7955, 0.6015$ cm and $\epsilon = 0.4173$ (Appendix B-9)

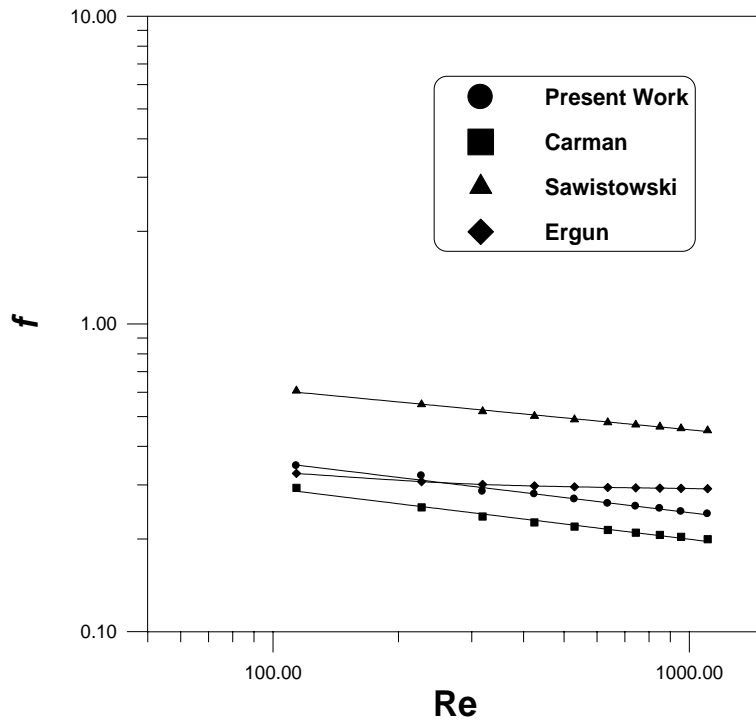


Figure 5-26 Friction factor versus Reynolds number for spherical particles with $d_p = 0.7955, 0.509$ cm and $\epsilon=0.4166$ (Appendix B-10)

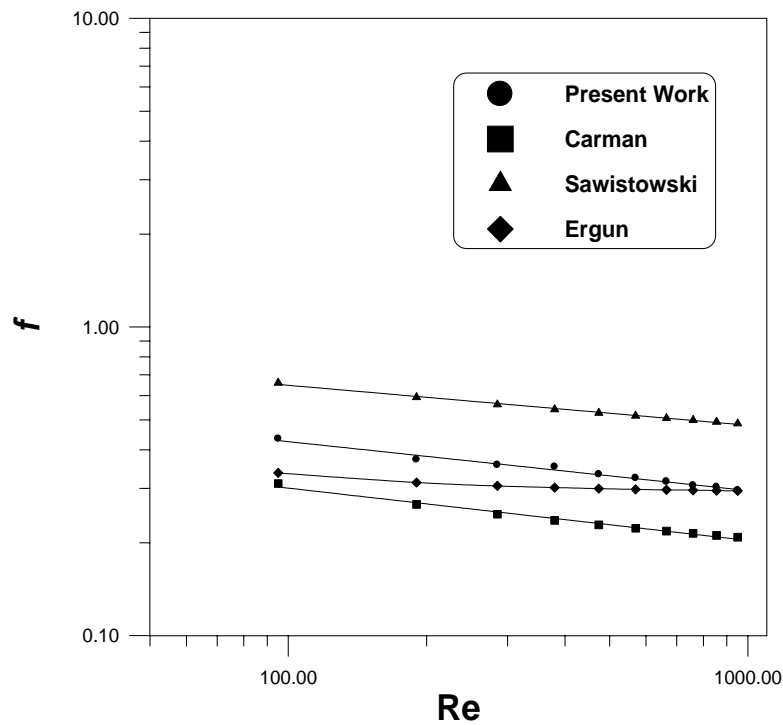


Figure 5-27 Friction factor versus Reynolds number for spherical particles with $d_p = 0.7955, 0.421$ cm and $\epsilon=0.3965$ (Table 4-11)

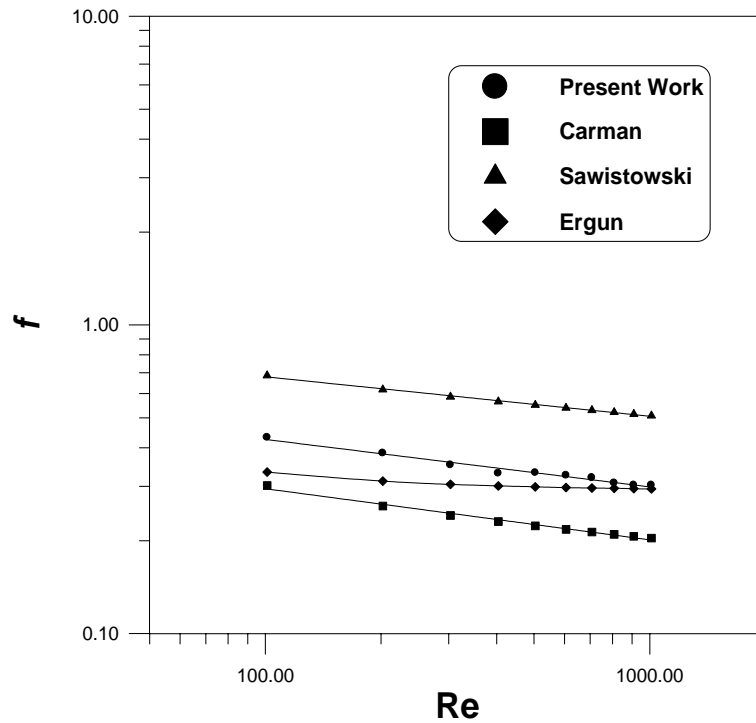


Figure 5-28 Friction factor versus Reynolds number for spherical particles with $d_p = 0.6015, 0.509$ cm and $\epsilon = 0.4121$ (Appendix B-11)

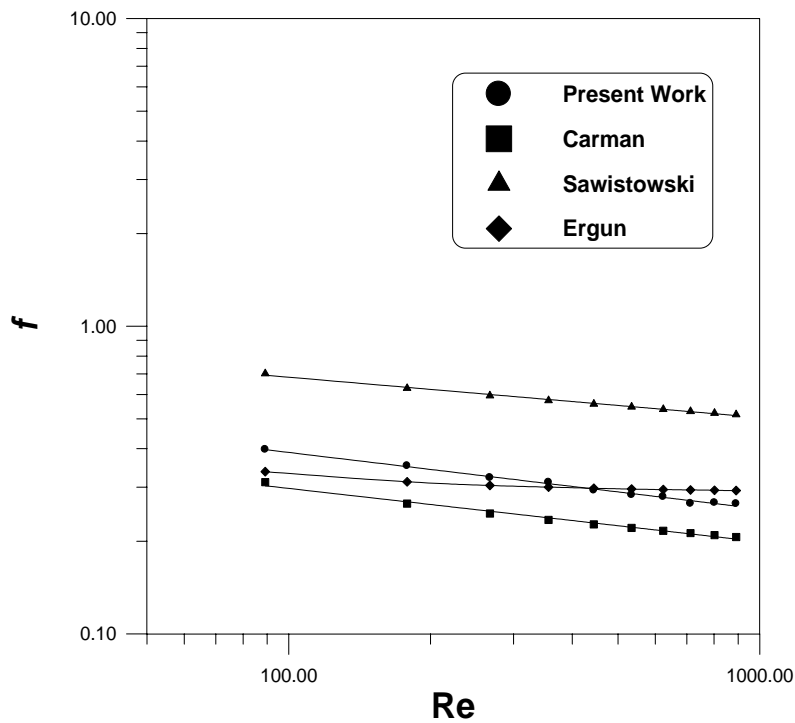


Figure 5-29 Friction factor versus Reynolds number for spherical particles with $d_p = 0.6015, 0.421$ cm and $\epsilon = 0.409$ (Appendix B-12)

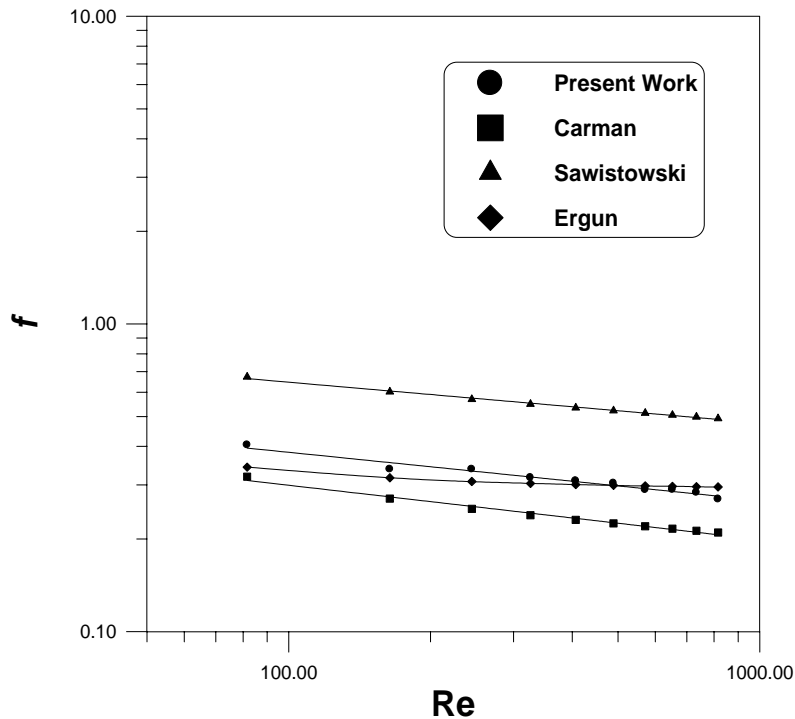


Figure5-30 Friction factor versus Reynolds number for spherical particles with $d_p = 0.509, 0.421$ cm and $\varepsilon = 0.3933$ (Table 4-12)

From these figures it can be noticed that the experimental curves behave as a linear curves whilst, the Ergun curves behaviors approximately as horizontal line, these differences may lie in the differences of the variables which were used such as; sphericity, void fraction, particle diameter, bed dimensions, fluid density, or fluid viscosity.

The values of air pressure drop for binary size particles is less than those for mono size particles for approximately the same porosity. e.g., It can be seen from in table 4-12 (binary size particles) which have porosity 0.3933 the values of pressure drop range 425-28368 Pa are less than in table 4-4 (mono size particles) which have porosity 0.3931 and the values of pressure drop range 744-46099 Pa, this may be due to the surface area of binary size particles (761.7m^{-1}) is less than it for mono size particles (1178.7m^{-1}). As the surface area decreases

the resistance of fluid flow decreases and the pressure drop through bed decreases.

The best fitting for the experimental data for mono size systems for spherical particles are represented by the following equation.

$$\frac{R_1}{\rho u_1^2} = 6.21 \text{Re}^{-1} + 0.54 \text{Re}^{-0.1} \quad \dots (5.4)$$

with a correlation coefficient of 0.8722 and a percentage of average errors of 5.7897%.

5.3 Packing of ternary size particles

5.3.1 Air flow

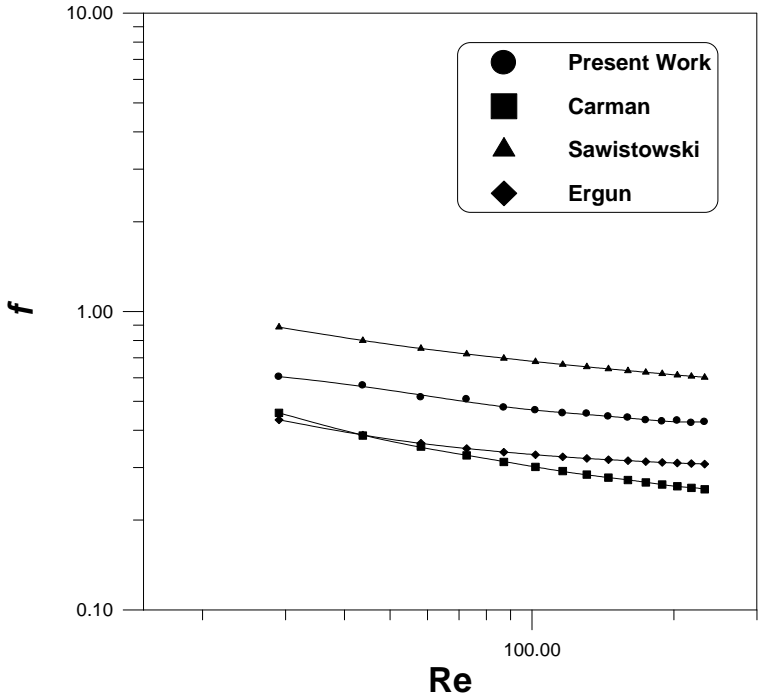


Figure 5-31 Friction factor versus Reynolds number for spherical particles with $d_p = 0.9987, 0.7955, 0.6015$ cm and $\epsilon = 0.427$ (Appendix C-1)

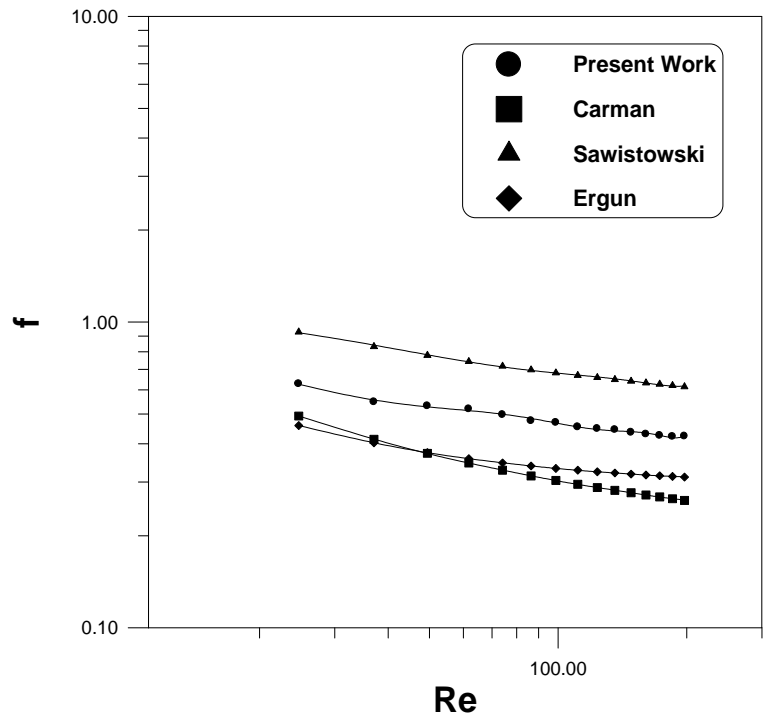


Figure 5-32 Friction factor versus Reynolds number for spherical particles with $d_p = 0.9987, 0.7955, 0.509$ cm and $\epsilon = 0.4019$ (Appendix C-4)

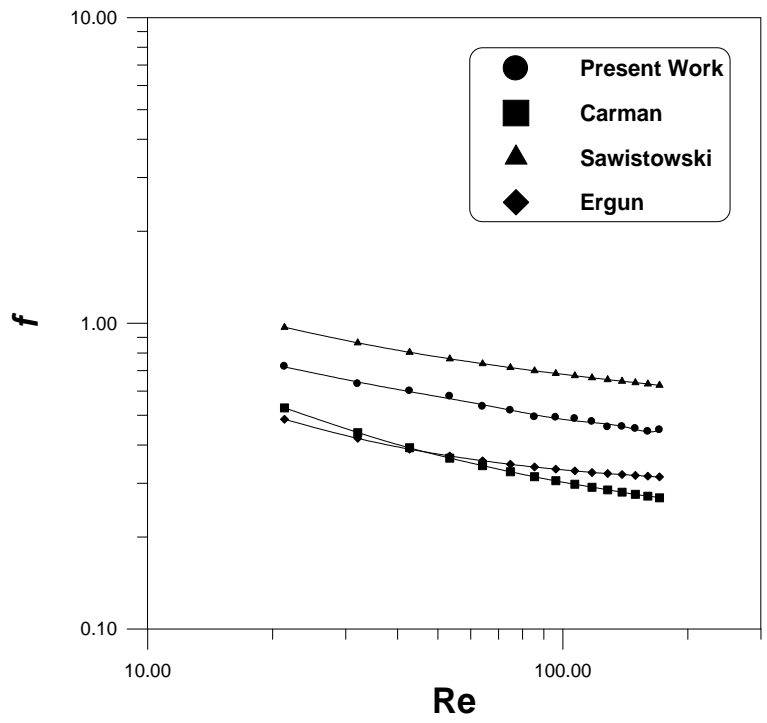


Figure 5-33 Friction factor versus Reynolds number for spherical particles with $d_p = 0.9987, 0.7955, 0.421$ cm and $\epsilon = 0.386$ (Appendix C-3)

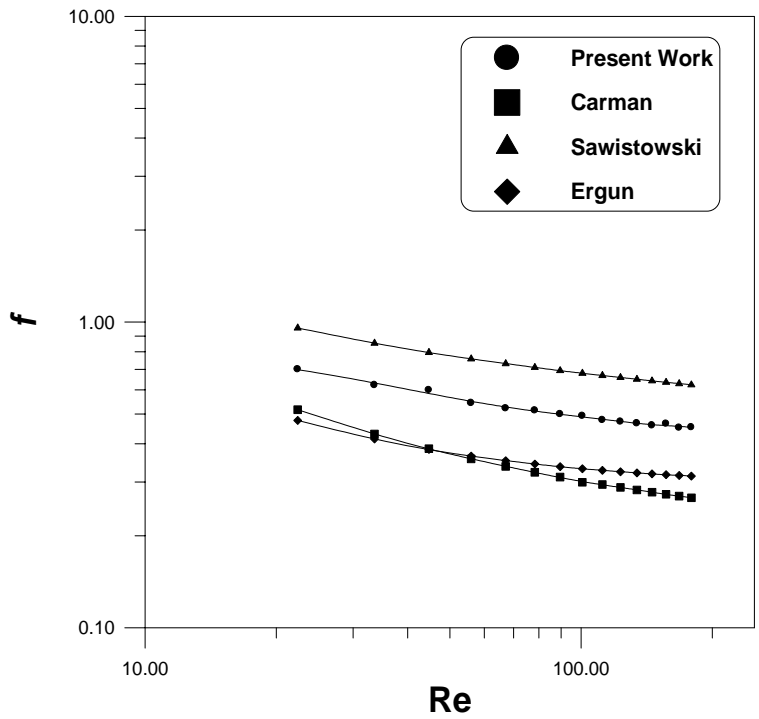


Figure 5-34 Friction factor versus Reynolds number for spherical particles with $d_p = 0.9987, 0.6015, 0.509$ cm and $\epsilon = 0.3998$ (Appendix C-4)

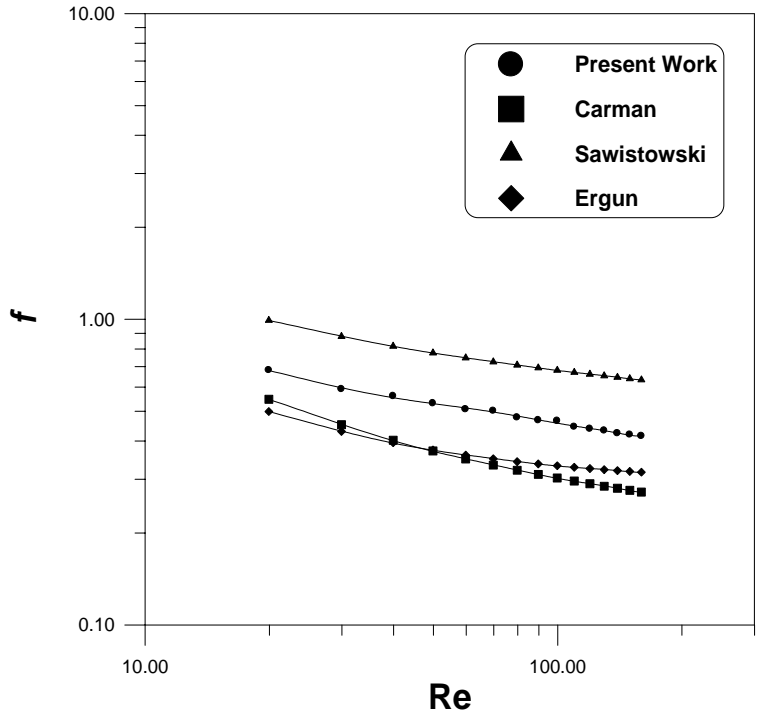


Figure 5-35 Friction factor versus Reynolds number for spherical particles with $d_p = 0.9987, 0.6015, 0.421$ cm and $\epsilon = 0.3906$ (Appendix C-5)

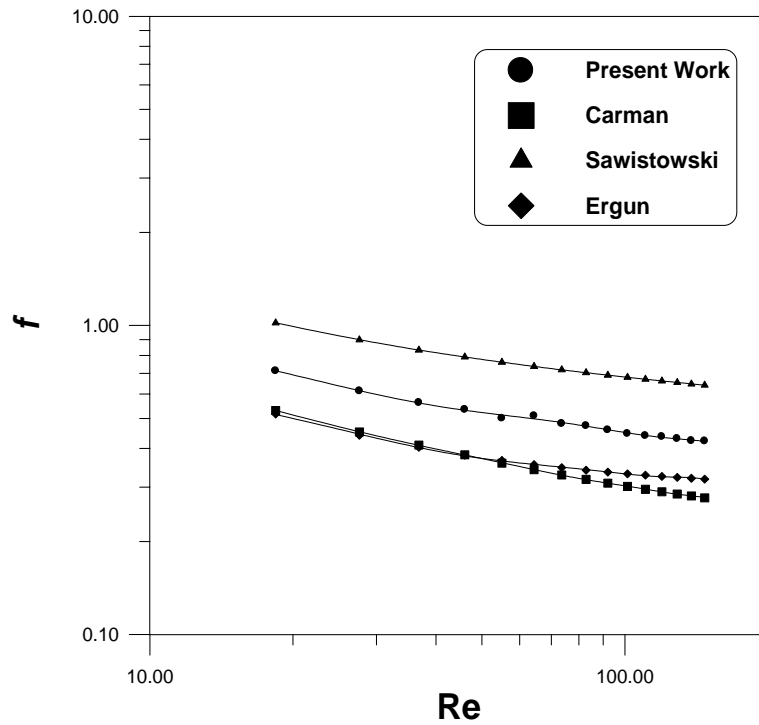


Figure 5-36 Friction factor versus Reynolds number for spherical particles with $d_p = 0.9987, 0.509, 0.421$ cm and $\epsilon = 0.3838$ (Table 4-13)

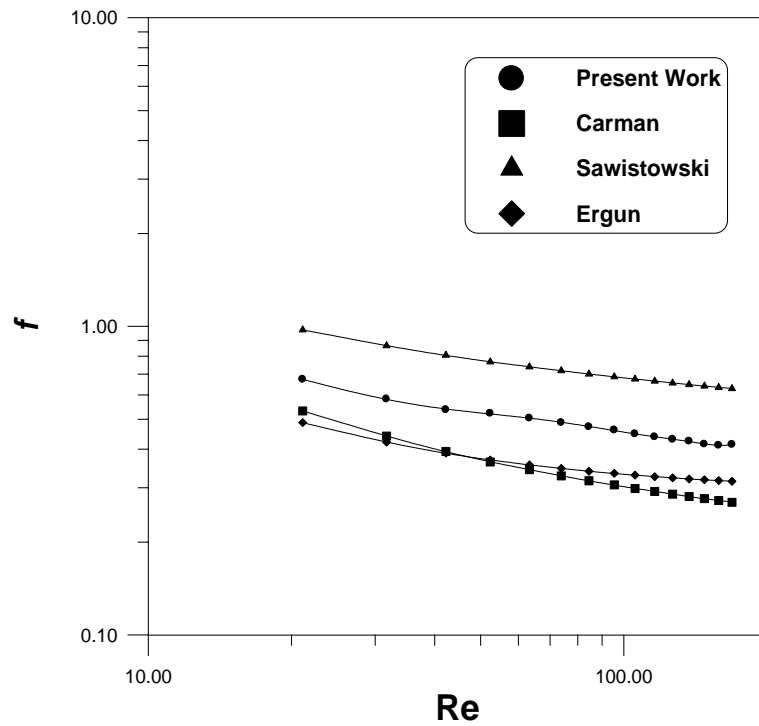


Figure 5-37 Friction factor versus Reynolds number for spherical particles with $d_p = 0.7955, 0.6015, 0.509$ cm and $\epsilon = 0.3985$ (Table 4-14)

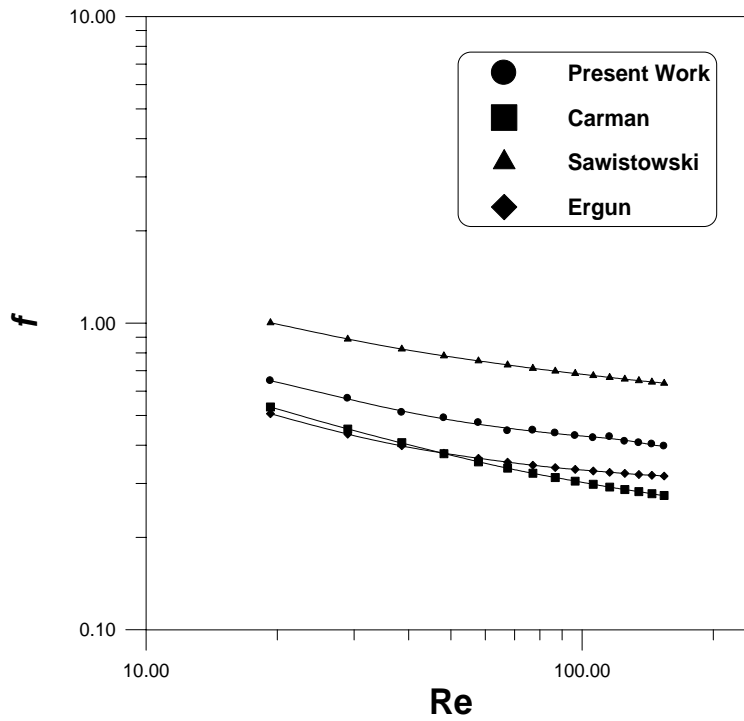


Figure 5-38 Friction factor versus Reynolds number for spherical particles with $d_p = 0.7955, 0.6015, 0.421$ cm and $\varepsilon = 0.3984$ (Table 4-15)

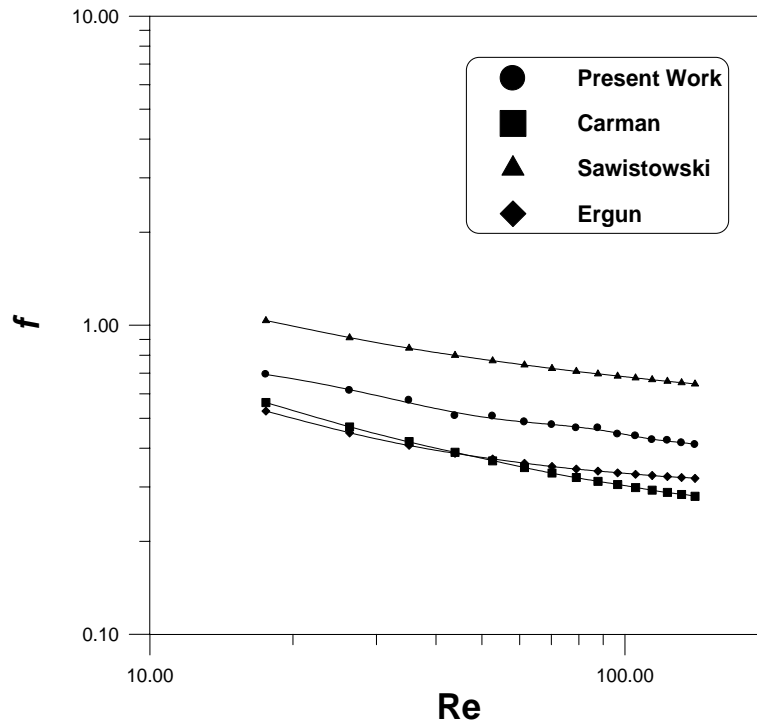


Fig. 5-39 Friction factor versus Reynolds number for spherical particles with $d_p = 0.7955, 0.509, 0.421$ cm and $\varepsilon = 0.3836$ (Table 4-16)

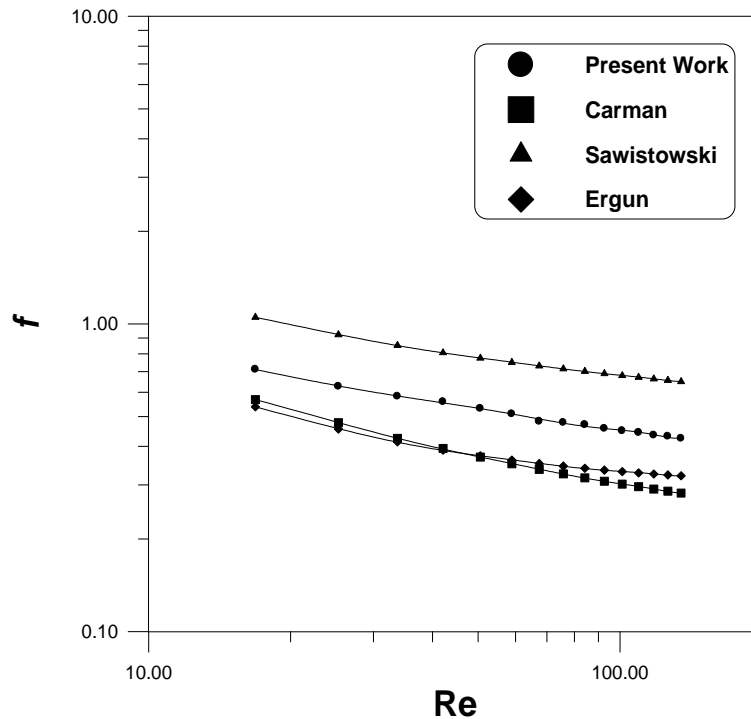


Figure 5-40 Friction factor versus Reynolds number for spherical particles with $d_p = 0.6015, 0.509, 0.421$ cm and $\varepsilon = 0.3766$ (Appendix C-6)

In all figures, it can be noticed the divergence values of friction factor at low values of Reynolds number (transition region) but its convergence at high values of Reynolds number (turbulent region), because in the turbulent region where the high rate velocity of fluid behaves as a slip velocity and has insignificant effect on the friction values.

Examining the experimental results it can be seen that the pressure drop in the bed is inversely proportional with porosity for the same velocity of fluid entering the bed, where it is found for the same porosity of mixtures the values of pressure drop are nearly the same e.g., as shown in tables 4-16 and 4-13 which have porosity 0.3836, 0.3838 the pressure drop range values 16.4-626 Pa and 15.3-576.4 Pa respectively. Also in table 4-15 and 4-14 which have porosity

0.3984, 0.3985 the pressure drop range values 12.3-456.8 Pa and 10.75- 424.6 Pa respectively.

The following equation is the best fitting for experimental data in ternary system.

$$\frac{R_1}{\rho u_1^2} = 3.66 \text{Re}^{-1} + 0.67 \text{Re}^{-0.1} \quad \dots (5.5)$$

with a correlation coefficients of 0.9545 a percentage of average errors of 3.5093%.

5.3.2 Water flow

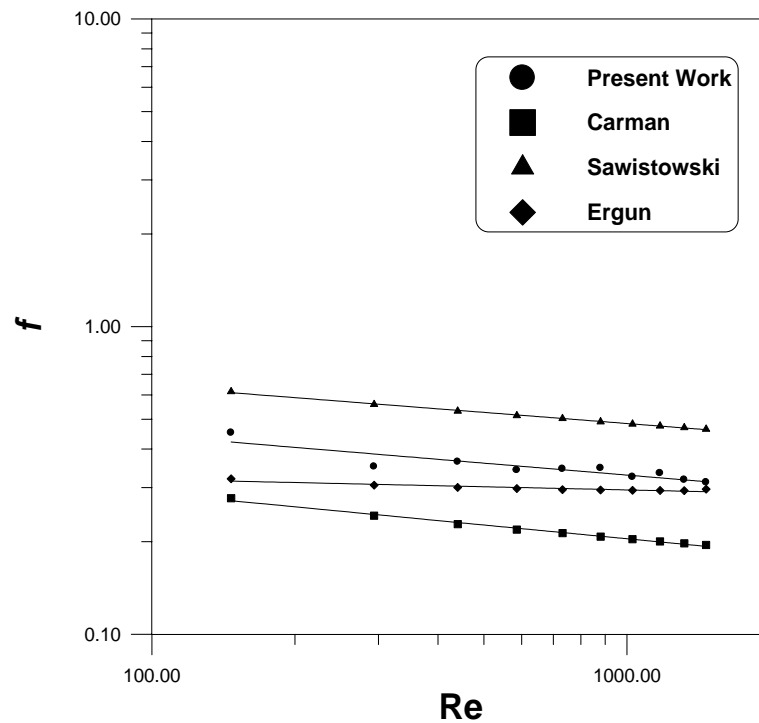


Figure 5-41 Friction factor versus Reynolds number for spherical particles with $d_p = 0.998, 0.7955, 0.6015$ cm and $\epsilon = 0.4276$ (Appendix C-7)

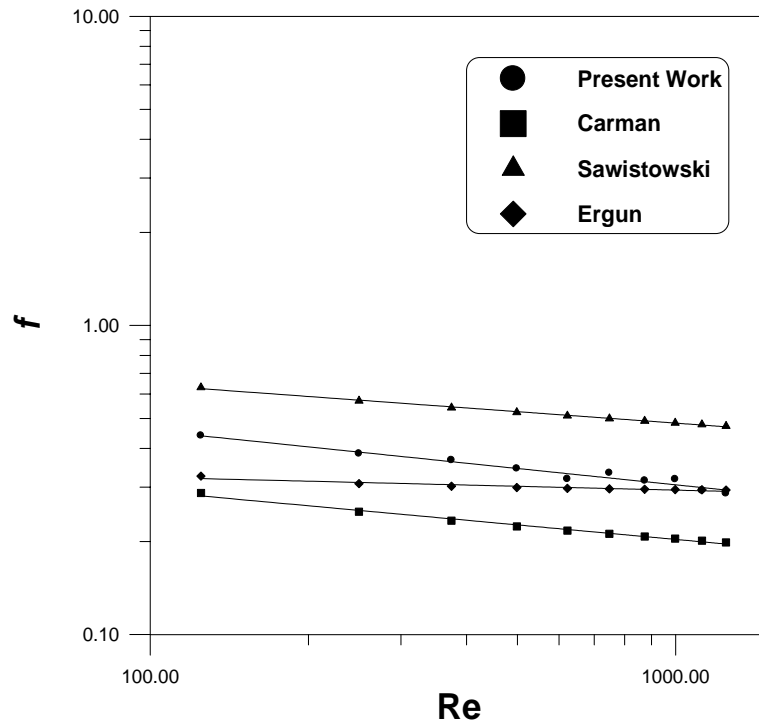


Figure 5-42 Friction factor versus Reynolds number for spherical particles with $d_p = 0.9987, 0.7955, 0.509 \text{ cm}$ and $\epsilon = 0.4019$ (Appendix C-8)

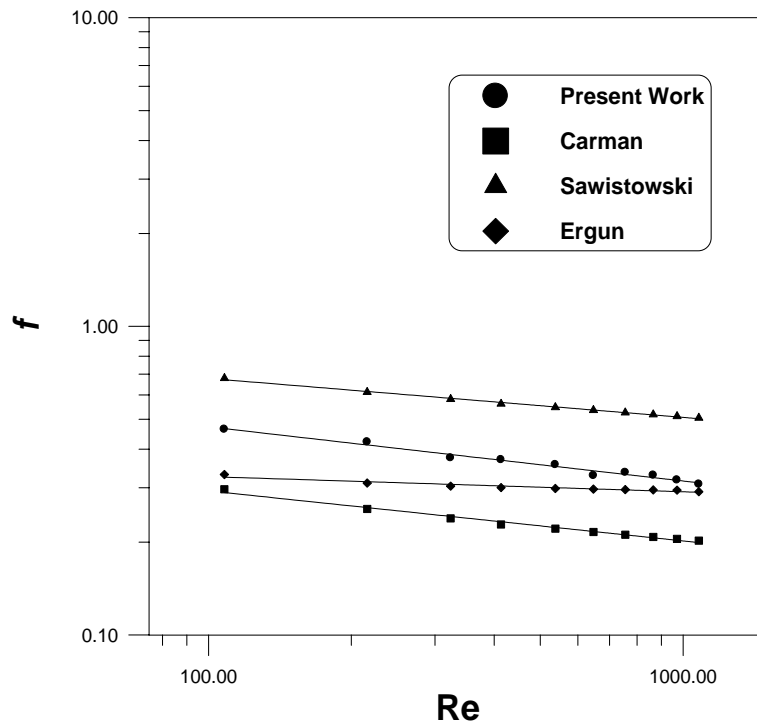


Figure 5-43 Friction factor versus Reynolds number for spherical particles with $d_p = 0.9987, 0.7955, 0.421 \text{ cm}$ and $\epsilon = 0.386$ (Appendix C-9)

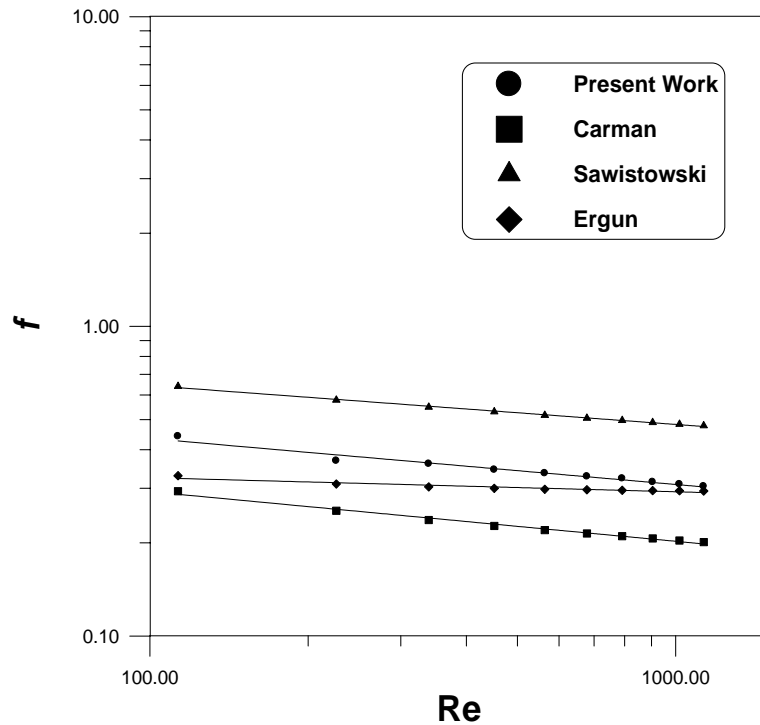


Fig. 5-44 Friction factor versus Reynolds number for spherical particles with $d_p = 0.9987, 0.6015, 0.509\text{cm}$ and $\varepsilon = 0.3998$ (Appendix C-10)

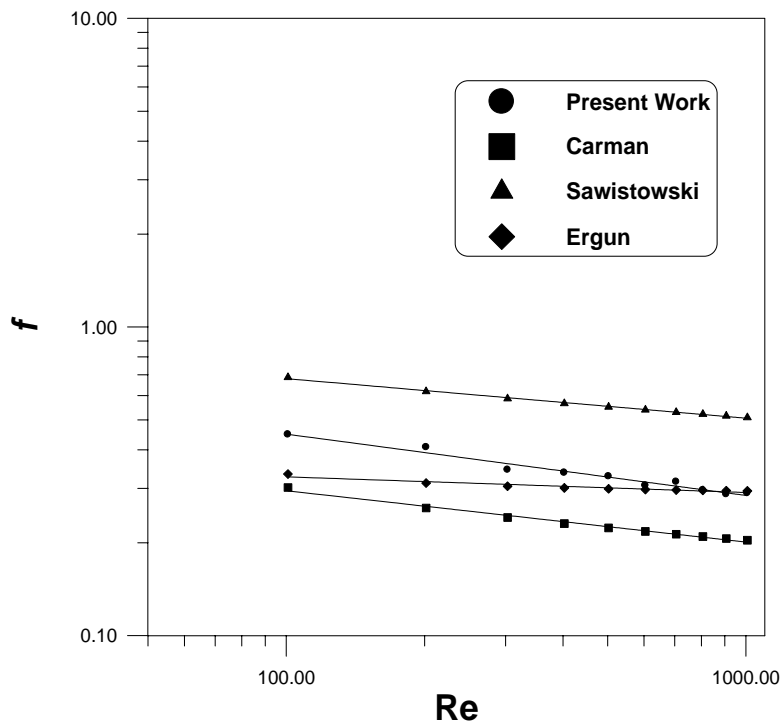


Figure 5-45 Friction factor versus Reynolds number for spherical particles with $d_p = 0.9987, 0.6015, 0.421\text{ cm}$ and $\varepsilon = 0.3906$ (Appendix C-11)

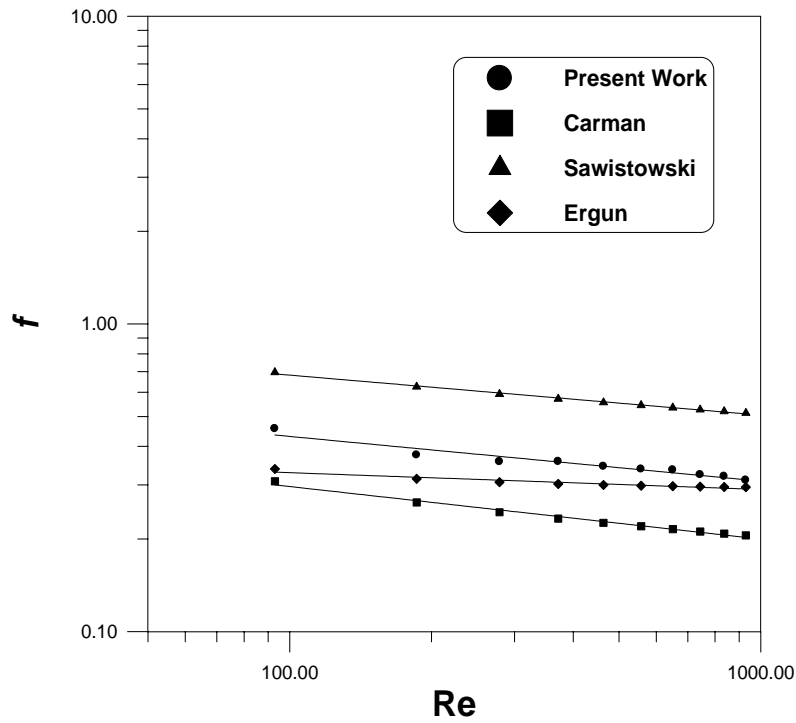


Figure 5-46 Friction factor versus Reynolds number for spherical particles with $d_p = 0.9987, 0.509, 0.421$ cm and $\epsilon = 0.3838$ (Table 4-17)

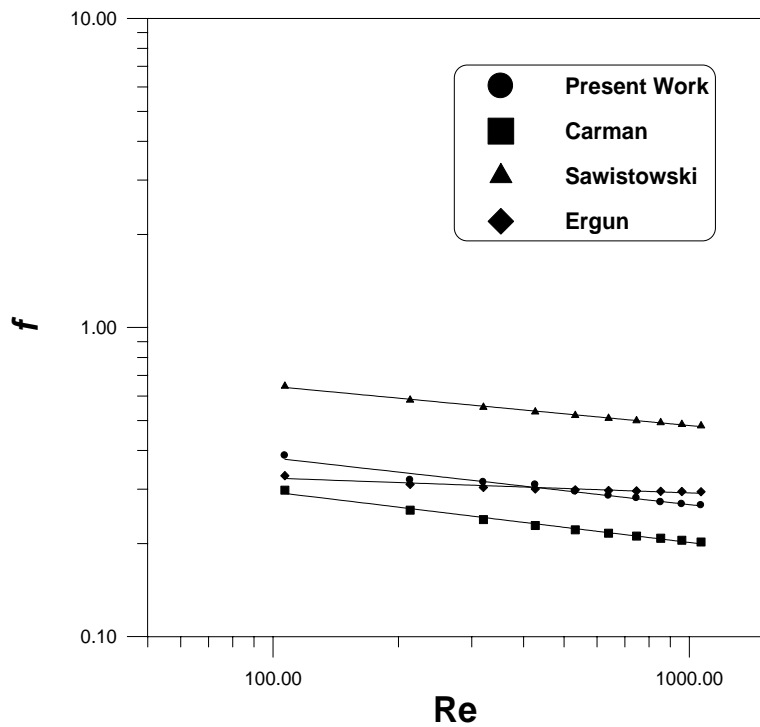


Figure 5-47 Friction factor versus Reynolds number for spherical particles with $d_p = 0.7955, 0.6015, 0.509$ cm and $\epsilon = 0.3985$ (Table 4-18)

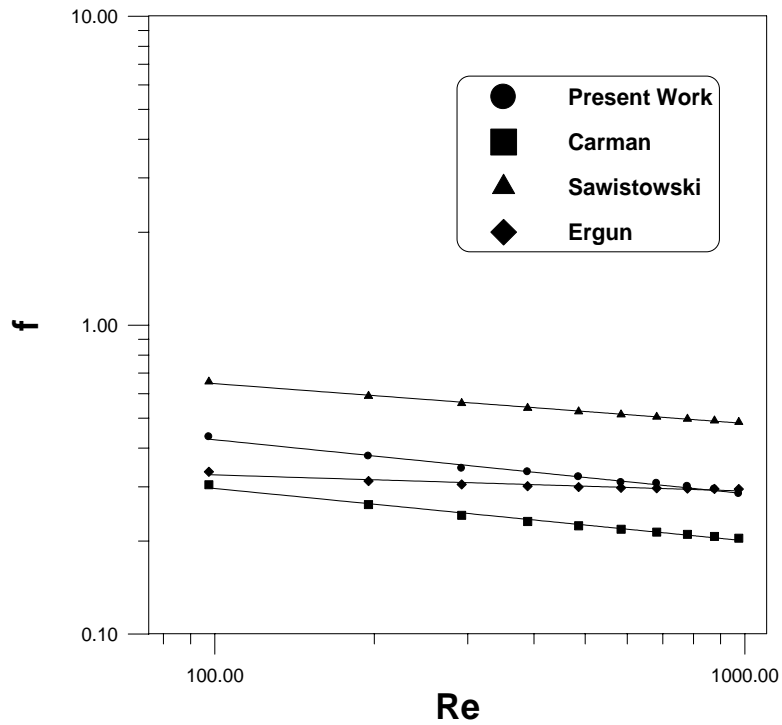


Figure 5-48 Friction factor versus Reynolds number for spherical particles with $d_p = 0.7955, 0.6015, 0.421$ cm and $\epsilon = 0.3983$ (Table 4-19)

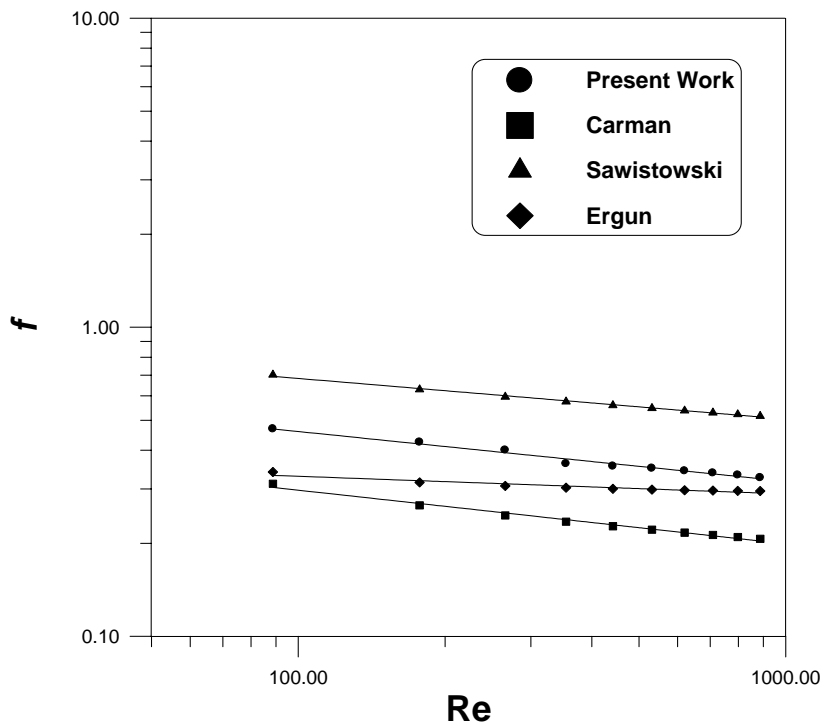


Figure 5-49 Friction factor versus Reynolds number for spherical particles with $d_p = 0.7955, 0.509, 0.421$ cm and $\epsilon = 0.3836$ (Table 4-20)

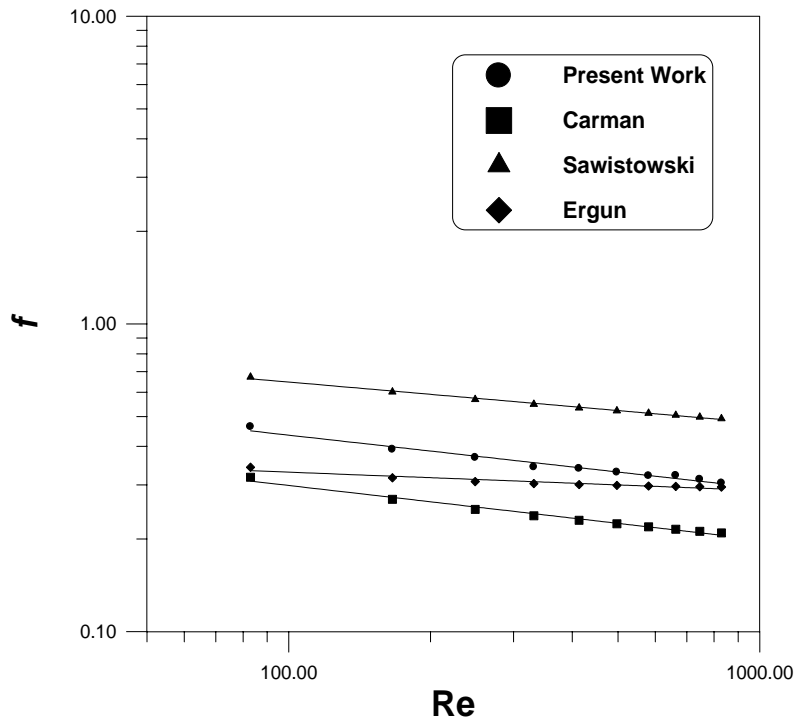


Figure 5-50 Friction factor versus Reynolds number for spherical particles with $d_p = 0.6015, 0.509, 0.421$ cm and $\varepsilon = 0.3766$ (Appendix C-12)

It can be noticed in Fig. 5-36 (for air for $\varepsilon = 0.3838$) show that at $Re.No = 92.02$ the value of friction factor is 0.4593 and in Fig. 5-46 (for water for $\varepsilon = 0.3838$) at $Re.No = 92.97$ the value of friction factor is 0.4611, for approximately near value of Reynolds number, the values of water friction factor are close to those of air.

The curves representing experimental results of friction factor for water flow are straighter than those of air flow where the curvatures of the curves indicate that the air flow was intermediate between the turbulent and laminar regions while water flow was at turbulent region (at turbulent region the Reynolds number have insignificant effect on friction factor values).

The best fitting for the experimental data for ternary size systems for spherical particles are represented by the following equation.

$$\frac{R_1}{\rho u_1^2} = 7.13 \text{Re}^{-1} + 0.61 \text{Re}^{-0.1} \quad \dots (5.6)$$

with a correlation coefficient of 0.9419 and a percentage of average errors of 5.82341%.

The experimental results of friction factor-Reynolds number curves lie among the result of Sawistowski, Carman and Ergun (above the result of Carman and Ergun and below those of Sawistowski, this may be due to :

1. The difference of bed dimensions(diameter and height of bed)
2. The difference of void fraction (difference of packing shape and size).
Ergun and Sawistowski used hollow packing which has a certain values of sphericity and porosity while Carman used sphere packing [4,8].

The main sources of errors can be attributed to:

1. Human error reading
2. Calibration of the experimental device.
3. Fluctuation in float of rotameter.

Chapter Six

Conclusions and Recommendations

6.1 Conclusions

For the single phase of fluid flow through a packed bed, the following conclusions can be drawn:

1. The size distribution of particle highly affected the bed porosity. It was found that the porosity of binary and ternary size particles are generally less than those of mono size particles, because the smaller particles can filled the interstices of the larger particles.
2. Increasing the Re. no. leads to decrease in the values of friction factor for all size distributions. For near values of Reynolds number the air and water flow show near values of friction factor.
3. The friction factor values for water flow decrease slightly with increasing Reynolds number values, because the water flow is at the turbulent region where the high rate velocity of fluid behaves as a slip velocity and has insignificant effect on the friction values.
4. Comparing the results of present work with those of Sawistowski, Carman and Ergun; it was noticed that the curves of the present work lie among the results of Sawistowski, Carman and Ergun; this is due to the differences of parameters, these parameters included void fraction, packing diameter, and bed height.
5. The bed porosity is greatly influences the pressure drop which also depends on several parameters as bed height, fluid velocity, average particle diameter and the physical properties of fluid. Water flow shows high values of pressure drop compared with air flow for the same bed porosity and volumetric flow rates.

6.2 Recommendations for future work

The following suggestions are to be considered or to be examined in greater detail for future work:

1. Study the effect of the geometry and material (such as rashing rings) of packing on the pressure drop and friction factor through packing bed
2. Study the possibility of developing a large scale of packing.
3. Study the possible effect of large Reynolds number.
4. Study the flow of two phases through the packed bed.
5. Study the effect of the temperature on pressure drop and friction factor.

References

1. Fluid flow in packed bed. Article given on the internet at the web site <http://www.chee.nus.edu.sg/pdf/EXPF7.pdf>.
2. Flow through packed beds and fluidized beds. Article given on the internet at the web site <http://www.clarkson.edu/subramanian/ch301/notes/packfluidbed.pdf>
3. R.B. Bird, W.E. Stewart, and E.N. Lightfoot, "Transport Phenomena", John Wiley and Sons, New York, 1960.
4. A.S. Foust, L.A. Wenzel, C.W. Clump, L. Maus, and L.B. Anderson, "Principles of Unit Operations", 2nd edition, John Wiley and Sons, New York, 1980.
5. M. R. Al-ubaidi, "pressure drop and flow distribution in a bed of uniform particles", M.Sc., Thesis, Nuclear Engineering Department, Bradford University, 1973.
6. L.oger, J.P. Troadec, D. Bideau, powder technology, 46 (1986) 121.
7. Fluid Distribution in Shallow Packed Beds. Article given on the internet at the web site <http://www.che.lsu.edu/courses/3101/summer00/ln7.pdf>
8. J.M. Coulson and J.F. Richardson, "chemical engineering", volume II Third Edition, Pergama press, Oxford, 1985.
9. Hydraulics of packed column. Article given on the internet at the web site [http://www.unb.ca/che/undergrad/lab/hydraulics .pdf](http://www.unb.ca/che/undergrad/lab/hydraulics.pdf)
10. J.M. Coulson, Inst. Chem. Eng, 13 (1949) 237.
11. J. Kozeny, Ber, Wien Akad, 136a (1927) 271.

12. P.C. Carman, Soc. Chem. Ind, 27 (1938) 1403.
13. F.C. Blank, Trans. Amer.Inst.chem.14 (1962) 415.
14. J. Green and Ampt, J. Agric. Sci, 13 (1962) 5.
15. Fluid flow through packed bed and fluidized systems. Article given on the internet at the web site
www.che.lsu.edu/courses/3101/summer00/ln7.pdf
16. Fluid flow analysis types: flow through porous media. Article given on the internet at the web site
http://www.algor.com/products/analysis_types/fluid_flow/porous_media.asp
17. Flow through porous media. Article given on the internet at the web site
<http://www.arunn.net/scienceblog/2006/10/23/flow-through-porous-media-summary>
18. A. Marmur, powder technology, 44 (1985) 249.
19. D.B. Shukla, P.M. 03a and V.P. Pandya, powder technology, 47 (1986) 233.
20. N.M. Norio Ouchlyama, Ind. Eng. Chem, 23 (1984) 490.
21. C.C. Furnas, Ind. Eng. Chem. 23 (1931) 1052.
22. A.E.R. Westman and M.R.Hugill, J. Am.ceram.soc, 13 (1930) 767.
23. C.E. Schwartz and J. M. smith, Ind. Eng. Chem., 45 (1953) 1209.
24. L.C. Graton and H.j. Fraser,J. Geol,73(1947) 785.
25. W.B. Fuller and A. E. Thompson, Trans. Am, Soci, Eng, 59 (1987) 67.
26. Packed column. Article given on the internet at the web site
<http://www.chromatograph/-online.org/topics/packedcolumn.html>
- 27.W.K. Lewis and W.C. Bauer, Ind. chem. Eng, 42(1949)1111.

28. M. X. Max Leva, chem. Eng, 13 (1949)115.
29. N. Y. Saied, " the effect of particle surface roughness on hydraulic flow through granular media", M.Sc.,Civil Engineering Department, Bradford University, 1977.
30. Geankoplis, Christie J.," Transport Processes and Unit perations",3rd ed., New Jersey: Prentice Hall, 1993.
31. O. B. Al-Dulami, "Porosity of particle mixture using RRSB size distribution", M.Sc., Thesis, Chemical Engineering Department, Al-Nahrain University,1998.
32. R. H. Perry and D. W. Green, Eds, "Perry's Chemical Engineer's Handbook", 7th ed., McGraw-Hill, 1997.
33. V. M. H. Govindaro and G.F. Froment, Chem. Eng. Sic, 43 (1988) 1403.
34. M. H. Vennti, Covindarao and G.F. Froment, chem. Eng. Sic, 14 (1986) 533.
35. M.J. Mattesson, C. Orr, "fitration", 2nd edition, New York and Basel, 1987.
36. Soil & Aquifer Properties and Their Effect on Groundwater. Article given on the internet at the web site <http://www.co.portage.wi.us/groundwater/undrstnd/soil.htm>
37. K. J. IVES, "the scientific basis of filtration", Lyden Noordholf International puplishing, 1975.
38. L.H.S, Robble and Tiennary, J.W, A.I. Ch. E.J, 4 (1658) 460.
39. R.F. Benenati, and Brosilow, A.I. Ch. E.J, 8 (1682) 359.
40. J.J. Lerou and Froment, Chem. Eng. Sic, 32(1986) 861.

41. The prediction of pressure drop and flow distribution in packed bed filter. Article given on the internet at the web site
http://www.cfd.com.au/cfd_conf99/papers/071TAYL.PDF
42. W. A. Gary, " the packing of solid particles", Chapman and Hall, first edition, London, 1968.
43. R. E. Acosta, A.I. Ch. E.J, 31 (1985) 478.
44. A. A. Orning, Ind. Eng. Chem, 41 (1949) 1179.
45. Pressure Drop for Flow in Packed Beds: An analysis using Ergun's Article given on the internet at the web site
http://rothfus.cheme.cmu.edu/tlab/pbeds/projects/t3_s04/t3_s04.pdf
46. Packed Beds: Pressure Drop versus Fluid Velocity and the Ergun. Article given on the internet at the web site
http://rothfus.cheme.cmu.edu/tlab/pbeds/projects/t10_s02/t10_s02.pdf
47. Warren L. McCabe, Julian C. Smith, Peter Harriott "unit operations of chemical engineering", Sixth Edition, 2001.
48. N. Standish and A.B. Yu, powder technology, 49 (1987) 249.
49. J.M. Coulson , " chemical engineering", volume I, first published, Pergama press, london,1998.
50. H. Sawistowaski, chem.. Eng. Sci, 6 (1957) 138.
51. S. Ergun, chem.. Eng.Prog,48(1952)89.
52. W. A. Gary, " the packing of solid particles", Chapman and Hall, first edition, London, 1968.
53. G. Meyer and Lincolnt, A.I.Ch.E.J,13(1936)11.

Appendix A

Packing of mono size particles

I. Air flow

Table A.1 Experimental results for spherical particles with
 $d_p = 0.7955\text{cm}$ and $\varepsilon = 0.4349$

Q (m ³ /h)	u (m/s)	Re	Δp (Pa)	f
2	0.1211	17.5038	8.6001	0.6449
3	0.1817	26.2629	17.4689	0.5819
4	0.2424	35.0365	26.8752	0.503
5	0.303	43.7957	41.6567	0.499
6	0.3635	52.5404	56.4381	0.4697
7	0.4241	61.2995	72.5632	0.4437
8	0.4847	70.0587	91.3759	0.4277
9	0.5453	78.8178	118.251	0.4373
10	0.6059	87.577	142.439	0.4273
11	0.6665	96.3361	169.3143	0.4192
12	0.7271	105.095	201.5647	0.4193
13	0.7877	113.8544	239.1901	0.4239
14	0.8482	122.5991	271.4404	0.4148
15	0.9088	131.3583	309.0658	0.4115
16	0.9695	140.1319	349.3788	0.4088

Table A.2 Experimental results for spherical particles with
 $d_p = 0.6015\text{cm}$ and $\varepsilon = 0.4249$

Q (m ³ /h)	u (m/s)	Re	Δp (Pa)	f
2	0.1211	13.005	14.78141	0.7681
3	0.1817	19.1289	28.21905	0.6513
4	0.2424	26.0315	43.0004	0.5577
5	0.303	32.5393	64.5007	0.5354
6	0.3635	39.0365	86.0009	0.496
7	0.4241	45.5444	112.8762	0.4782
8	0.4847	52.0522	147.8141	0.4794
9	0.5453	58.5601	177.3769	0.4546
10	0.6059	65.068	217.6898	0.4518
11	0.6665	71.5759	255.3153	0.438
12	0.7271	78.0837	295.6282	0.4261
13	0.7877	84.5916	349.3788	0.4291
14	0.8482	91.088	403.1294	0.427
15	0.9088	97.5966	448.8173	0.4141
16	0.9695	104.1152	510.6305	0.414

Table A.3 Experimental results for spherical particles with $d_p=0.509\text{cm}$ and $\varepsilon=0.3931$

Q (m ³ /h)	u (m/s)	Re	Δp (Pa)	f
2	0.1211	10.4284	24.72527	0.8156
3	0.1817	15.6469	43.53797	0.6394
4	0.2424	20.8741	72.56329	0.5987
5	0.303	26.0926	103.2011	0.5441
6	0.3635	31.3025	139.7515	0.5112
7	0.4241	36.521	177.3769	0.4773
8	0.4847	41.7396	223.0649	0.4612
9	0.5453	46.9581	274.128	0.4496
10	0.6059	52.1766	327.8786	0.4331
11	0.6665	57.3952	384.3167	0.4213
12	0.7271	62.6137	446.1299	0.4099
13	0.7877	67.8322	518.6932	0.406
14	0.8482	73.0421	602.0066	0.4049
15	0.9088	78.2607	682.6324	0.4004
16	0.9695	83.4878	767.8271	0.3952

II. Water flow

Table A.4 Experimental results for spherical particles with $d_p=0.7955\text{cm}$ and $\varepsilon=0.4349$

Q (m ³ /h)	u (m/s)	Re	Δp (kPa)	f
0.5	0.0303	88.4752	0.3121	0.4348
1	0.0606	176.9504	1.0992	0.3829
1.5	0.0909	265.4256	2.3404	0.3623
2	0.1211	353.6088	4.0425	0.3526
2.5	0.1511	441.2081	6.0283	0.3378
3	0.1817	530.5593	8.5106	0.3298
3.5	0.2121	619.3265	11.2056	0.3189
4	0.2424	707.8017	14.4680	0.3151
4.5	0.2726	795.9849	18.0141	0.3101
5	0.303	884.7522	21.8439	0.3044

Table A.5 Experimental results for spherical particles with $d_p=0.6015\text{cm}$ and $\varepsilon=0.4249$

Q (m ³ /h)	u (m/s)	Re	Δp (kPa)	f
0.5	0.0303	65.7353	0.3156	0.4451
1	0.0606	131.4707	0.2671	0.3766
1.5	0.0909	197.206	0.2482	0.35
2	0.1211	262.7244	0.2371	0.3344
2.5	0.1511	347.809	0.2285	0.3221
3	0.1817	327.809	0.2201	0.3104
3.5	0.2121	460.1475	0.2162	0.3049
4	0.2424	525.8828	0.2071	0.2921
4.5	0.2726	591.4012	0.2064	0.2911
5	0.303	657.3535	0.2049	0.2889

Table A.6 Experimental results for spherical particles with $d_p = 0.421 \text{ cm}$ and $\varepsilon = 0.3888$

Q (m ³ /h)	u (m/s)	Re	Δp (kPa)	f
0.5	0.0303	43.2917	0.9574	0.4664
1	0.0606	86.5835	3.1205	0.3801
1.5	0.0909	129.8753	6.4539	0.3493
2	0.1211	173.0242	10.9929	0.3352
2.5	0.1511	215.8874	16.3121	0.3195
3	0.1817	259.6078	22.3404	0.3026
3.5	0.2121	303.0425	30.2836	0.3014
4	0.2424	346.3343	38.2978	0.2915
4.5	0.2726	389.4832	46.8085	0.2817
5	0.303	432.6478	56.5957	0.2757

Appendix B

Packing of binary size particles

I. Air flow

Table B.1 Experimental results for spherical particles with
 $d_p = 0.9987, 0.6015$ cm and $\varepsilon = 0.4186$

O (m ³ /h)	u (m/s)	Re	Δp (Pa)	f
2	0.1211	27.1511	5.375059	0.5546
3	0.1817	40.7379	11.01887	0.5064
4	0.2424	54.3472	17.73769	0.4614
5	0.303	67.934	26.60654	0.4429
6	0.3635	81.4983	37.62541	0.4459
7	0.4241	95.0851	48.37553	0.4145
8	0.4847	108.6719	61.81317	0.4039
9	0.5453	122.2587	77.93835	0.4027
10	0.6059	135.8455	94.06353	0.3938
11	0.6665	149.4323	115.5638	0.3967
12	0.7271	163.0191	137.064	0.3931
13	0.7877	176.6059	155.8767	0.3859
14	0.8482	190.1703	180.0645	0.383
15	0.9088	185.1745	204.2522	0.3775
16	0.9695	217.3663	233.815	0.3798

Table B.2 Experimental results for spherical particles with
 $d_p = 0.9987, 0.509$ cm and $\varepsilon = 0.4171$

O (m ³ /h)	u (m/s)	Re	Δp (Pa)	f
2	0.1211	24.3556	6.4500	0.5937
3	0.1817	36.5434	12.9001	0.5275
4	0.2424	48.7514	21.5002	0.494
5	0.303	60.9393	32.2503	0.4742
6	0.3635	73.107	43.0004	0.4393
7	0.4241	85.2949	57.7818	0.4337
8	0.4847	97.4827	75.2508	0.4324
9	0.5453	109.6706	92.7197	0.4209
10	0.6059	121.8585	112.8762	0.4151
11	0.6665	134.0463	134.3765	0.4083
12	0.7271	146.2342	155.8767	0.398
13	0.7877	158.422	185.4395	0.4034
14	0.8482	170.5898	206.9397	0.3882
15	0.9088	182.7776	233.815	0.3821
16	0.9695	194.9856	263.3778	0.3782

Table B.3 Experimental results for spherical particles with $d_p = 0.7955, 0.6015\text{cm}$, and $\varepsilon = 0.4173$

Q (m ³ /h)	u (m/s)	Re	Δp (Pa)	f
2	0.1211	25.0863	6.1813	0.5869
3	0.1817	37.6399	12.0938	0.5101
4	0.2424	50.2141	20.1564	0.4777
5	0.303	62.7677	30.9065	0.4687
6	0.3635	75.3005	41.6567	0.439
7	0.4241	87.8541	56.4381	0.4369
8	0.4847	100.4076	69.8757	0.4141
9	0.5453	112.9612	86.0009	0.4027
10	0.6059	125.5147	104.8136	0.3975
11	0.6665	138.068	124.9701	0.3917
12	0.7271	150.6218	147.8141	0.3893
13	0.7877	163.1753	174.6894	0.392
14	0.8482	175.708	201.5647	0.39
15	0.9088	188.2617	225.7525	0.3806
16	0.9695	200.836	255.3153	0.3782

Table B.4 Experimental results for spherical particles with $d_p = 0.7955, 0.509\text{ cm}$ and $\varepsilon = 0.4166$

Q (m ³ /h)	u (m/s)	Re	Δp (Pa)	f
2	0.1211	22.5049	7.2563	0.615
3	0.1817	33.7666	14.7814	0.5565
4	0.2424	45.047	24.1877	0.5116
5	0.303	56.3088	36.2816	0.4912
6	0.3635	67.5519	51.0631	0.4803
7	0.4241	78.8137	64.5007	0.4457
8	0.4847	90.0755	83.3134	0.4407
9	0.5453	101.3372	102.1261	0.4269
10	0.6059	112.599	123.6263	0.4185
11	0.6665	123.8607	147.8141	0.4136
12	0.7271	135.1225	174.6894	0.4107
13	0.7877	146.3843	206.9398	0.4145
14	0.8482	157.6274	232.4713	0.4015
15	0.9088	168.8892	263.3779	0.3963
16	0.9695	180.1695	298.3158	0.3945

Table B.5 Experimental results for spherical particles with
 $d_p = 0.6015, 0.509\text{cm}$ and $\varepsilon = 0.41208$

Q (m ³ /h)	u (m/s)	Re	Δp (Pa)	f
2	0.1211	19.9893	9.4063	0.6853
3	0.1817	29.9922	18.8127	0.6088
4	0.2424	40.0117	32.2503	0.5864
5	0.303	50.0146	45.688	0.5317
6	0.3635	60.0011	64.5007	0.5215
7	0.4241	70.004	83.31341	0.4949
8	0.4847	80.0069	106.1574	0.4828
9	0.5453	90.0098	131.6889	0.4732
10	0.6059	100.0128	161.2518	0.4693
11	0.6665	110.0157	190.8146	0.4589
12	0.7271	120.0186	223.0649	0.4508
13	0.7877	130.0215	258.0028	0.4443
14	0.8482	140.008	295.6282	0.439
15	0.9088	150.0109	335.9412	0.4346
16	0.9695	160.0303	378.9416	0.4307

Table B.6 Experimental results of sphere particles
 $d_p = 0.6015, 0.421\text{ cm}$ and $\varepsilon = 0.409$

Q (m ³ /h)	u (m/s)	Re	Δp (Pa)	f
2	0.1211	17.633	10.2126	0.6417
3	0.1817	26.4568	20.1564	0.5464
4	0.2424	35.2952	32.2503	0.4912
5	0.303	44.119	47.0317	0.4585
6	0.3635	52.9429	64.5007	0.4369
7	0.4241	61.7521	86.0009	0.4279
8	0.4847	70.5759	110.1887	0.4198
9	0.5453	79.3997	134.3765	0.4045
10	0.6059	88.2236	163.9393	0.3997
11	0.6665	97.0474	193.5021	0.3898
12	0.7271	105.871	225.7525	0.3822
13	0.7877	114.695	263.3779	0.3799
14	0.8482	123.5043	301.0033	0.3744
15	0.9088	132.328	341.3162	0.3699
16	0.9695	141.1665	389.6917	0.3711

II. Water flow

Table B.7 Experimental results for spherical particles with $d_p = 0.9987, 0.6015$ cm and $\varepsilon = 0.4186$

Q (m ³ /h)	u (m/s)	Re	Δp (kPa)	f
0.5	0.0303	137.2382	0.1914	0.3691
1	0.0606	274.4765	0.6737	0.3246
1.5	0.0909	411.7148	1.4184	0.3037
2	0.1211	548.5001	2.5531	0.3081
2.5	0.1511	684.3796	3.5461	0.2748
3	0.1817	822.9766	5.3191	0.2851
3.5	0.2121	960.6678	6.7375	0.2652
4	0.2424	1097.9061	8.8652	0.2671
4.5	0.2726	1234.6914	10.6383	0.2533
5	0.303	1372.3826	13.5461	0.2611

Table B.8 Experimental results for spherical particles with $d_p = 0.9987, 0.509$ cm and $\varepsilon = 0.4171$

Q (m ³ /h)	u (m/s)	Re	Δp (kPa)	f
0.5	0.0303	123.1082	0.2482	0.4246
1	0.0606	246.2165	0.8865	0.3791
1.5	0.0909	369.3247	1.7731	0.3369
2	0.1211	429.0267	2.8368	0.3037
2.5	0.1511	613.9161	4.6099	0.3171
3	0.1817	738.2432	6.8794	0.3272
3.5	0.2121	861.7578	8.5106	0.2973
4	0.2424	984.8661	11.3475	0.3032
4.5	0.2726	1107.568	14.539	0.3072
5	0.303	1231.0826	17.0212	0.2911

Table B.9 Experimental results for spherical particles with
 $d_p = 0.7955, 0.6015$ cm and $\varepsilon = 0.4173$

Q (m ³ /h)	u (m/s)	Re	Δp (kPa)	f
0.5	0.0303	126.802	0.2127	0.3754
1	0.0606	253.604	0.7092	0.3128
1.5	0.0909	380.406	1.5602	0.3058
2	0.1211	506.7895	2.5531	0.282
2.5	0.1511	632.3361	3.9007	0.2767
3	0.1817	760.3936	5.6737	0.2783
3.5	0.2121	887.9141	7.4468	0.2684
4	0.2424	1014.4161	9.5035	0.262
4.5	0.2726	1140.7996	11.5602	0.252
5	0.303	1268.0201	14.3262	0.2527

Table B.10 Experimental results for spherical particles with
 $d_p = 0.7955, 0.509$ cm and $\varepsilon = 0.4166$

Q (m ³ /h)	u (m/s)	Re	Δp (kPa)	f
0.5	0.0303	113.7538	0.2198	0.3462
1	0.0606	227.5076	0.8156	0.3211
1.5	0.0909	341.2614	1.6312	0.2854
2	0.1211	454.6398	2.8368	0.2797
2.5	0.1511	567.2674	4.2553	0.2694
3	0.1817	682.1475	5.9574	0.2609
3.5	0.2121	796.2767	7.9432	0.2553
4	0.2424	910.0305	10.2127	0.2513
4.5	0.2726	1023.4089	12.6241	0.2456
5	0.303	1137.5382	15.3191	0.2412

Table B.11 Experimental results for spherical particles with
 $d_p = 0.6015, 0.509$ cm and $\varepsilon = 0.41208$

Q (m ³ /h)	u (m/s)	Re	Δp (kPa)	f
0.5	0.0303	101.0385	0.3191	0.4321
1	0.0606	202.077	1.1347	0.3841
1.5	0.0909	303.1155	2.3404	0.3521
2	0.1211	403.8206	3.9007	0.3306
2.5	0.1511	503.8587	6.0992	0.332
3	0.1817	605.8976	8.6524	0.3257
3.5	0.2121	707.2696	11.5602	0.3197
4	0.2424	808.3081	14.539	0.3075
4.5	0.2726	909.0132	18.0851	0.3024
5	0.303	1010.385	22.3404	0.3024

Table B.12 Experimental results for spherical particles with
 $d_p = 0.6015, 0.421$ cm and $\varepsilon = 0.409$

Q (m ³ /h)	u (m/s)	Re	Δp (kPa)	f
0.5	0.0303	89.1284	0.3404	0.3975
1	0.0606	178.2568	1.2056	0.3519
1.5	0.0909	267.3852	2.4822	0.3221
2	0.1211	356.2195	4.2553	0.3111
2.5	0.1511	444.4655	6.2411	0.2931
3	0.1817	534.4763	8.7234	0.2832
3.5	0.2121	623.8989	11.7021	0.2791
4	0.2424	713.0273	14.539	0.2652
4.5	0.2726	801.8616	18.5106	0.267
5	0.303	891.2842	22.695	0.265

Appendix c

Packing of ternary size particles

I. Air flow

Table C.1 Experimental results for spherical particles with
 $d_p = 0.9987, 0.7955, 0.6015$ cm and $\varepsilon = 0.42763$

Q (m ³ /h)	u (m/s)	Re	Δp (Pa)	f
2	0.1211	29.041	5.1063	0.6038
3	0.1817	43.7362	10.7501	0.5647
4	0.2424	58.1301	17.4689	0.5156
5	0.303	72.6626	26.8752	0.5076
6	0.3635	87.1712	36.2816	0.4762
7	0.4241	101.7037	48.3755	0.4664
8	0.4847	116.2362	61.8131	0.4563
9	0.5453	130.7688	77.9383	0.4545
10	0.6059	145.3013	94.0635	0.4443
11	0.6665	159.8338	112.876	0.4406
12	0.7271	174.3664	131.6889	0.432
13	0.7877	188.8989	153.1892	0.4281
14	0.8482	203.4075	178.7207	0.4308
15	0.9088	217.94	201.5647	0.4232
16	0.9695	232.4965	231.1275	0.4264

Table C.2 Experimental results for spherical particles with
 $d_p = 0.9987, 0.7955, 0.509$ cm and $\varepsilon = 0.4019$

Q (m ³ /h)	u (m/s)	Re	Δp (Pa)	f
2	0.1211	24.6927	7.5251	0.6283
3	0.1817	37.0493	14.7814	0.5482
4	0.2424	49.4263	25.5315	0.5321
5	0.303	61.7829	38.9691	0.5197
6	0.3635	74.1191	53.7505	0.4981
7	0.4241	86.4757	69.8757	0.4757
8	0.4847	98.8323	90.0322	0.4692
9	0.5453	111.1889	110.1887	0.4537
10	0.6059	123.5455	134.3765	0.4482
11	0.6665	135.8001	161.2517	0.4444
12	0.7271	148.2587	188.127	0.4357
13	0.7877	160.6153	217.6898	0.4296
14	0.8482	172.9515	249.9402	0.4253
15	0.9088	185.308	284.8781	0.4223
16	0.9695	197.685	325.191	0.4236

Table C.3 Experimental results for spherical particles with $d_p = 0.9987, 0.7955, 0.421$ cm and $\varepsilon = 0.38606$

Q (m ³ /h)	u (m/s)	Re	Δp (Pa)	f
2	0.1211	21.3586	11.2876	0.7225
3	0.1817	32.0467	22.3064	0.6342
4	0.2424	42.7524	36.2816	0.6011
5	0.303	53.4405	56.4381	0.5771
6	0.3635	64.111	75.2508	0.5346
7	0.4241	74.7992	99.4385	0.519
8	0.4847	85.4873	123.6263	0.494
9	0.5453	96.1754	155.8767	0.4921
10	0.6059	106.8635	190.8146	0.4879
11	0.6665	117.5516	225.7524	0.4771
12	0.7271	128.2398	258.0028	0.4581
13	0.7877	138.9279	303.6908	0.4594
14	0.8482	149.5984	346.6912	0.4523
15	0.9088	160.2865	389.6917	0.4429
16	0.9695	170.9922	448.8173	0.4482

Table C.4 Experimental results for spherical particles with $d_p = 0.9987, 0.6015, 0.509$ cm and $\varepsilon = 0.39983$

Q (m ³ /h)	u (m/s)	Re	Δp (Pa)	f
2	0.1211	22.3746	9.4063	0.7005
3	0.1817	33.5711	18.8127	0.6223
4	0.2424	44.7862	32.2503	0.5994
5	0.303	55.9827	45.6879	0.5435
6	0.3635	67.1608	63.1569	0.5221
7	0.4241	78.3573	84.6571	0.514
8	0.4847	89.5539	107.5011	0.4997
9	0.5453	100.7504	134.3764	0.4935
10	0.6059	111.947	161.2517	0.4792
11	0.6665	123.1436	192.1583	0.4724
12	0.7271	134.3401	225.7524	0.4664
13	0.7877	145.5367	260.6903	0.4589
14	0.8482	156.7147	306.3783	0.4651
15	0.9088	167.9113	341.3162	0.4513
16	0.9695	179.1263	389.6917	0.4528

Table C.5 Experimental results for spherical particles with $d_p = 0.9987, 0.6015, 0.421$ cm and $\varepsilon = 0.39063$

Q (m ³ /h)	u (m/s)	Re	Δp (Pa)	f
2	0.1211	19.9353	11.0188	0.6818
3	0.1817	29.9112	21.5002	0.5909
4	0.2424	39.9036	36.2816	0.5603
5	0.303	49.8795	53.7505	0.5312
6	0.3635	59.8389	73.907	0.5075
7	0.4241	69.8148	99.4385	0.5017
8	0.4847	79.7908	123.6263	0.4775
9	0.5453	89.7667	153.1892	0.4675
10	0.6059	99.7426	188.127	0.465
11	0.6665	109.7185	217.6898	0.4447
12	0.7271	119.6944	255.3153	0.4382
13	0.7877	129.6703	295.6282	0.4323
14	0.8482	139.6297	335.9411	0.4237
15	0.9088	149.605	381.6291	0.4193
16	0.9695	159.598	430.0046	0.4151

Table C.6 Experimental results for spherical particles with $d_p = 0.6015, 0.509, 0.421$ cm and $\varepsilon = 0.3766$

Q (m ³ /h)	u (m/s)	Re	Δp (Pa)	f
2	0.1211	16.4096	15.5876	0.7116
3	0.1817	132.5132	30.9065	0.6267
4	0.2424	176.7815	51.0631	0.5818
5	0.303	220.9769	76.5945	0.5585
6	0.3635	265.0994	104.8136	0.5311
7	0.4241	309.2948	137.064	0.5102
8	0.4847	353.4902	169.3143	0.4825
9	0.5453	397.6856	212.3148	0.478
10	0.6059	441.881	258.0028	0.4705
11	0.6665	486.0764	303.6908	0.4577
12	0.7271	530.2719	354.7538	0.4492
13	0.7877	574.467	411.1919	0.4437
14	0.8482	618.5896	467.63	0.4351
15	0.9088	662.785	532.1307	0.4313
16	0.9695	707.0533	596.6314	0.4249

II. Water flow

Table C.7 Experimental results for spherical particles with $d_p = 0.9987, 0.7955, 0.6015$ cm and $\varepsilon = 0.42763$

Q (m ³ /h)	u (m/s)	Re	Δp (kPa)	f
0.5	0.0303	146.782	0.2056	0.4521
1	0.0606	293.5641	0.6382	0.3507
1.5	0.0909	440.3461	1.4893	0.3637
2	0.1211	586.6437	2.4822	0.3415
2.5	0.1511	731.9725	3.9007	0.3447
3	0.1817	880.2079	5.6737	0.3467
3.5	0.2121	1027.4743	7.234	0.3247
4	0.2424	1174.2564	9.7163	0.3336
4.5	0.2726	1320.554	11.7021	0.3177
5	0.303	1467.8205	14.18439	0.3117

Table C.8 Experimental results for spherical particles with $d_p = 0.9987, 0.7955, 0.509$ cm and $\varepsilon = 0.4019$

Q (m ³ /h)	u (m/s)	Re	Δp (kPa)	f
0.5	0.0303	124.8125	0.2836	0.4401
1	0.0606	249.6251	0.9929	0.3851
1.5	0.0909	374.4377	2.1276	0.3667
2	0.1211	498.8384	3.5461	0.3444
2.5	0.1511	622.4152	5.1063	0.3185
3	0.1817	748.4636	7.73049	0.3335
3.5	0.2121	873.6881	9.92907	0.3146
4	0.2424	998.5007	13.1205	0.318
4.5	0.2726	1122.9013	15.2482	0.2922
5	0.303	1248.1259	18.4397	0.2861

Table C.9 Experimental results for spherical particles with $d_p = 0.9987, 0.7955, 0.421$ cm and $\varepsilon = 0.38606$

Q (m ³ /h)	u (m/s)	Re	Δp (kPa)	f
0.5	0.0303	107.9583	0.3901	0.4639
1	0.0606	215.9166	1.4184	0.4218
1.5	0.0909	323.8749	2.8368	0.3749
2	0.1211	431.469	4.9645	0.3696
2.5	0.1511	538.3663	7.4468	0.3561
3	0.1817	647.3935	9.92907	0.3284
3.5	0.2121	755.7081	13.8297	0.336
4	0.2424	865.6664	17.7304	0.3295
4.5	0.2726	971.2684	21.6312	0.3178
5	0.303	1079.583	25.8865	0.3079

Table C.10 Experimental results for spherical particles with $d_p = 0.9987, 0.6015, 0.509$ cm and $\varepsilon = 0.39983$

Q (m ³ /h)	u (m/s)	Re	Δp (kPa)	f
0.5	0.0303	113.0895	0.3191	0.4416
1	0.0606	226.179	1.0638	0.368
1.5	0.0909	339.2685	2.34042	0.3598
2	0.1211	451.9847	3.9716	0.3441
2.5	0.1511	563.9546	6.0283	0.3354
3	0.1817	678.1638	8.5106	0.3275
3.5	0.2121	791.6265	11.4184	0.3227
4	0.2424	904.716	14.539	0.3143
4.5	0.2726	1017.4323	18.0851	0.3092
5	0.303	1130.8951	21.9858	0.3042

Table C.11 Experimental results for spherical particles with $d_p = 0.9987, 0.6015, 0.421$ cm and $\varepsilon = 0.39063$

Q (m ³ /h)	u (m/s)	Re	Δp (kPa)	f
0.5	0.0303	100.7655	0.3901	0.4486
1	0.0606	201.5311	1.4184	0.4078
1.5	0.0909	302.2966	2.695	0.3444
2	0.1211	402.7297	4.6808	0.337
2.5	0.1511	502.4975	7.0921	0.328
3	0.1817	604.2608	9.5744	0.3062
3.5	0.2121	705.3589	13.4042	0.3149
4	0.2424	806.1245	16.4538	0.2956
4.5	0.2726	906.5575	20.2127	0.2872
5	0.303	1007.6556	25.1773	0.2895

Table C.12 Experimental results for spherical particles with $d_p = 0.6015, 0.509, 0.421$ cm and $\varepsilon = 0.3766$

Q (m ³ /h)	u (m/s)	Re	Δp (kPa)	f
0.5	0.0303	82.9443	0.5461	0.4635
1	0.0606	165.8887	1.8439	0.3913
1.5	0.0909	248.833	3.9007	0.3679
2	0.1211	331.5036	6.4539	0.3429
2.5	0.1511	413.6268	9.9291	0.3389
3	0.1817	497.3924	13.9716	0.3298
3.5	0.2121	580.6105	18.5106	0.3209
4	0.2424	663.5548	24.2553	0.3217
4.5	0.2726	746.2254	29.7872	0.3123
5	0.303	829.4435	35.8156	0.304

Appendix D

Table D.1 The porosity, bulk density and specific surface area of the particles

d_p (m)	ϵ	ρ_b (g/cm ³)	S (m ² /m ³)
0.9987	0.4508	1.4057	600.781
0.7955	0.4349	1.4211	754.4226
0.6015	0.4249	1.4694	997.5062
0.509	0.3931	1.5252	1178.781
0.421	0.3888	1.5118	1425.1784
0.9987,0.7955	0.4232	1.4633	387.95004
0.9987,0.6015	0.4186	1.4869	472.6153
0.9987,0.509	0.4171	1.4784	525.5049
0.9987,0.421	0.3822	1.5754	617.6136
0.7955,0.6015	0.4173	1.4771	510.37202
0.7955,0.509	0.4166	1.4667	568.2318
0.7955,0.421	0.3965	1.5253	657.6042
0.6015,0.509	0.4121	1.4897	634.8232
0.6015,0.421	0.409	1.5057	715.9032
0.509,0.421	0.3933	1.5333	761.7885
0.9987,0.7955,0.6015	0.4276	1.4556	448.8336
0.9987,0.7955,0.509	0.4019	1.5208	505.1563
0.9987,0.7955,0.421	0.3861	1.5583	568.9525
0.9987,0.6015,0.509	0.3998	1.5261	555.5712
0.9987,0.6015,0.421	0.3906	1.555	614.1363
0.9987,0.509,0.421	0.3838	1.5636	658.2538
0.7955,0.6015,0.509	0.3985	1.5204	587.5714
0.7955,0.6015,0.421	0.3984	1.5262	643.3335
0.7955,0.509,0.421	0.3836	1.555	689.9427
0.6015,0.509,0.421	0.3766	1.4685	729.2969

D.2 Calibration of rotameters

A. for air flow

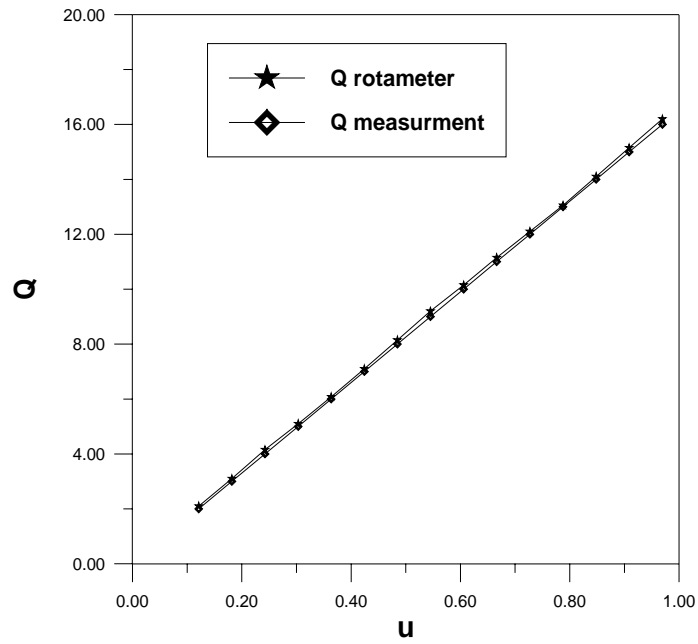


Figure D-1 show the calibration of air rotameter

B. for water flow

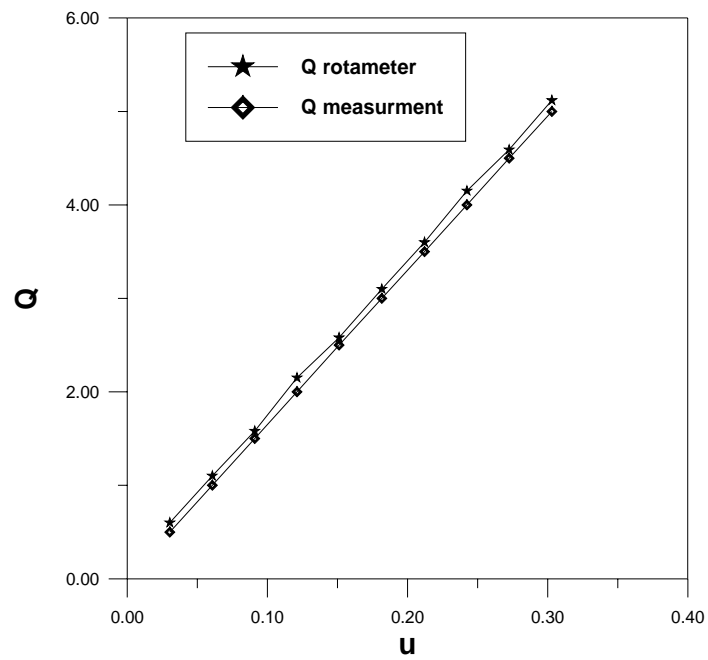


Figure D-2 show the calibration of water rotameter

الخلاصة

يتضمن البحث دراسة جريان أحادي للمائع خلال عمود حشوي، حيث استخدم نوعان من المائع (هواء و ماء). كما استخدمت جسيمات زجاجية كروية لتمثيل الطور الصلب. وقد كان أقطار الجسيمات الكروية ٤٢١،٥٠٩،٥٠،٦٠١٥،٥٠،٧٧٩٥،٥٠،٩٩٨٧،٥٠ سم

كان قطر البرج المحشو ٧،٦٤ سم وطوله ١٥،١٥ سم. يعمل العمود الحشوي تحت ظروف ثابتة من ضغط وحرارة. لقد تم دراسة عوامل رئيسيه في العمود الحشوي هذه العوامل تمثل تغير مسامية الحشوه (أحاديه، ثنائيه وثلاثيه)، نوع المائع و سرعه الجريان المائع الممثل بعدد رينولد لمعرفة تأثير هذه العوامل على هبوط الضغط ومعامل الاحتكاك.

لقد كان معدل عدد رينولد المستخدم في الهواء هو ٧٠٧-٨،٥ وفي الماء ١٤٦٧-٤٣ أثبتت النتائج إن مسامية تؤثر بشكل كبير على هبوط الضغط ووجد أن هبوط الضغط يتناسب عكسيا مع مسامية حيث وجد عند أعلى قيمه للمسامية (٠،٤٥٠٨) كان هبوط الضغط (٢٥،٨ - ٦،١ Pa) للهواء و (١٣٦٠٠-٢٠٥،٦ Pa) للماء اقل من أدنا قيمه للمسامية (٠،٣٧٦٦) حيث كان هبوط الضغط (١٥،٥- ٥٩٦،٩ Pa) للهواء و (٣٥٨١٥،٦ Pa - ٥٤٦) للماء.

معامل الاحتكاك للحشوات الثنائية الحجم اقل من الحشوات الاحاديه الحجم للحشوات المتقاربة المسامية ، لان المساحة السطحية للحشوات الثنائية اقل من الاحاديه ، عندما تزداد المساحة السطحية للجزيئات يقل عدد رينولد مما يؤدي إلى زيادة معامل الاحتكاك.

في السرعة العالية (الجريان المضطرب) يكون المنحني بين عدد رينولد ومعامل الاحتكاك مستقيما (عند الجريان المضطرب يكون تأثير عدد رينولد غير ملموس على معامل الاحتكاك)

وقد تم التعبير عن معامل الاحتكاك بدلاله عدد رينولد وجدد أن المعادلة العامة التي تمثل النظام

الأحادي، ثنائي و ثلاثي هي :

١. لجريان الهواء.

$$\frac{R_1}{\rho u_1^2} = 3.21Re^{-1} + 0.65Re^{-0.1}$$

وكان معامل التصحيح ٠,٩١٧٢ ونسبه الخطى ٥,٣٩٦٤%

ب. لجريان الماء.

$$\frac{R_1}{\rho u_1^2} = 4.97 \text{Re}^{-1} + 0.57 \text{Re}^{-0.1}$$

وكان معامل التصحيح ٠,٨٢٨٦ ونسبه الخطى ٦,٧٦١%

وصف لخصائص الحشوات المكونة من حبيبات كروية أحادية، ثنائية ،
وثلاثية الحجم

رسالة

مقدمة إلى كلية الهندسة في جامعة نهرين
وهي جزء من متطلبات نيل درجه ماجستير علوم
في الهندسة الكيماوية

من قبل

هناء رياض صالح

(بكالوريوس علوم في الهندسة الكيماوية ٢٠٠٤)

١٤٢٨

٢٠٠٧

ربيع الأول

نيسان